QC
1
.U56
LH.64A
74.8

Volume 64A
Number 3
May-June 1960

OF MICHIGAN
JUL 8 1960
LIBRARY

Journal of Research

of the

NATIONAL BUREAU OF STANDARDS

A. PHYSICS AND CHEMISTRY

Journal of Research

of the

National Bureau of Standards

A. Physics and Chemistry

MAY–JUNE • 1960

VOLUME • 64A

NUMBER • 3

Editor: U. Fano

Associate Editors: L. M. Kushner
J. M. Richardson

Publication dates:
Feb. 1, Apr. 1, June 1, Aug. 1, Oct. 1, Dec. 1, 1960.

JOURNAL OF RESEARCH

The National Bureau of Standards Journal of Research reports research and development in the fields of activity shown at right. Also included from time to time are survey articles on topics closely related to the Bureau's scientific and technical program.

The Journal is published in four separate sections as follows:

A. Physics and Chemistry

Contains papers of interest primarily to scientists working in these fields. Issued six times a year. Annual subscription: domestic, $4.00; foreign, $4.75.

B. Mathematics and Mathematical Physics

Presents studies and compilations designed mainly for the mathematician and the theoretical physicist. Issued quarterly. Annual subscription: domestic, $2.25; foreign, $2.75.

C. Engineering and Instrumentation

Reports research and development results of interest chiefly to the engineer and the applied scientist. Issued quarterly. Annual subscription: domestic, $2.25; foreign, $2.75.

D. Radio Propagation

Reports work in radio propagation, upper atmospheric physics, and communications. Issued six times a year. Annual subscription: domestic, $4.00; foreign, $4.75.

Functions and Activities

The functions of the National Bureau of Standards are set forth in the Act of Congress, March 3, 1901, as amended. These include the development and maintenance of the national standards of measurement and the provision of means and methods for making measurements consistent with these standards; the determination of physical constants and properties of materials; the development of methods and instruments for testing materials, devices, and structures; advisory services to government agencies on scientific and technical problems; invention and development of devices to serve special needs of the Government; and the development of standard practices, codes, and specifications. The work includes basic and applied research, development, engineering, instrumentation, testing, evaluation, calibration services, and various consultation and information services. The Bureau also serves as the Federal technical research center in a number of specialized fields. The scope of activities of the National Bureau of Standards is suggested in the following listing of the divisions and sections engaged in technical work.

Washington, D.C.

Electricity and Electronics. Resistance and Reactance. Electron Devices. Electrical Instruments. Magnetic Measurements. Dielectrics. Engineering Electronics. Electronic Instrumentation. Electrochemistry.

Optics and Metrology. Photometry and Colorimetry. Optical Instruments. Photographic Technology. Length. Engineering Metrology.

Heat. Temperature Physics. Thermodynamics. Cryogenic Physics. Rheology. Molecular Kinetics. Free Radicals Research.

Atomic and Radiation Physics. Spectroscopy. Radiometry. Mass Spectrometry. Solid State Physics. Electron Physics. Atomic Physics. Neutron Physics. Radiation Theory. Radioactivity. X-ray. High Energy Radiation. Nucleonic Instrumentation. Radiological Equipment.

Chemistry. Organic Coatings. Surface Chemistry. Organic Chemistry. Analytical Chemistry. Inorganic Chemistry. Electrodeposition. Molecular Structure and Properties of Gases. Physical Chemistry. Thermochemistry. Spectrochemistry. Pure Substances.

Mechanics. Sound. Mechanical Instruments. Fluid Mechanics. Engineering Mechanics. Mass and Scale. Capacity, Density, and Fluid Meters. Combustion Controls.

Organic and Fibrous Materials. Rubber. Textiles. Paper. Leather. Testing and Specifications. Polymer Structure. Plastics. Dental Research.

Metallurgy. Thermal Metallurgy. Chemical Metallurgy. Mechanical Metallurgy. Corrosion. Metal Physics.

Mineral Products. Engineering Ceramics. Glass. Refractories. Enameled Metals. Constitution and Microstructure.

Building Technology. Structural Engineering. Fire Protection. Air Conditioning, Heating, and Refrigeration. Floor, Roof, and Wall Coverings. Codes and Safety Standards. Heat Transfer. Concreting Materials.

Applied Mathematics. Numerical Analysis. Computation. Statistical Engineering. Mathematical Physics.

Data Processing Systems. SEAC Engineering Group. Components and Techniques. Digital Circuitry. Digital Systems. Analog Systems. Applications Engineering.

• Office of Basic Instrumentation. • Office of Weights and Measures.

Boulder, Colorado

Cryogenic Engineering. Cryogenic Equipment. Cryogenic Processes. Properties of Materials. Gas Liquefaction.

Radio Propagation Physics. Upper Atmosphere Research. Ionosphere Research. Regular Prediction Services. Sun-Earth Relationships. VHF Research. Radio Warning Services. Airglow and Aurora. Radio Astronomy and Arctic Propagation.

Radio Propagation Engineering. Data Reduction Instrumentation. Radio Noise. Tropospheric Measurements. Tropospheric Analysis. Propagation-Terrain Effects. Radio-Meteorology. Lower Atmosphere Physics.

Radio Standards. High-Frequency Electrical Standards. Radio Broadcast Service. Radio and Microwave Materials. Electronic Calibration Center. Microwave Circuit Standards.

Radio Communication and Systems. Low Frequency and Very Low Frequency Research. High Frequency and Very High Frequency Research. Modulation Systems. Antenna Research. Navigation Systems. Systems Analysis. Field Operations.

U.S. DEPARTMENT OF COMMERCE
Frederick H. Mueller, Secretary

NATIONAL BUREAU OF STANDARDS
A. V. Astin, Director

Order all publications from the Superintendent of Documents, U.S. Government Printing Office, Washington 25, D.C.

The funds for printing this publication approved by the Director of the Bureau of the Budget (June 24, 1958).

DEPOSITED BY THE
UNITED STATES OF AMERICA

JOURNAL OF RESEARCH of the National Bureau of Standards—A. Physics and Chemistry

Vol. 64A, No. 3, May–June 1960

Phase Shift Effects in Fabry-Perot Interferometry

Charles J. Koester [1]

(January 14, 1960)

A method is demonstrated for utilizing in Fabry-Perot interferometry the data on reflection phase shift dispersion obtained from fringes of equal chromatic order. Unknown wavelengths can be calculated from the Fabry-Perot patterns obtained with a large etalon spacing, even without prior knowledge of the phase shift of the reflecting surfaces. When the theoretical phase shift as a function of wavelength is known approximately, then the correct orders of interference can be determined for both the Fabry-Perot fringes and fringes of equal chromatic order. From the wavelengths of the latter the phase shift dispersion can be measured to an accuracy of about 10 A. The method is especially useful for reflectors with large dispersion of phase shift, such as multilayers. Results in the visible spectrum are reported for aluminum films and a pair of dielectric 15-layer broadband reflectors.

1. Introduction

In the field of interferometric length and wavelength measurement it has long been recognized that the dispersion of phase shift on reflection must be considered. In Fabry-Perot interferometry, procedures for determining and/or correcting for phase shift dispersion have been described by Fabry and Buisson [1],[2] Eversheim [2], Meggers [3], Bauer [4], Jackson [5], Meissner [6], Barrell and Teasdale-Buckell [7], and by Rank and Bennett [8].

In wavelength intercomparison, the phase shift dispersion enters the calculations at two points: (1) The determination of the etalon spacing, and (2) the calculation of the unknown wavelength.

The purpose of this paper is to describe how the accurate measurement of phase shift dispersion by fringes of equal chromatic order (*feco*) [9, 10, 11] can be used with Fabry-Perot interferometry in the determination of the etalon spacing and in precise measurement of unknown wavelengths.

1.1. Determination of Etalon Spacing

The method of exact fractions [12, 13] is generally used to determine the etalon spacing from the observed interference pattern. For three known wavelengths, λ_a, λ_b, λ_c, the fractional orders f_a, f_b, and f_c, are calculated [6, 14] from the diameters of the circular fringes. Then the integral order numbers, m_a, m_b, m_c, and the exact etalon spacing, t, are found by trying many different integers for m_a, m_b, and m_c until the products $(m_a+f_a)\lambda_a$, $(m_b+f_b)\lambda_b$, and $(m_c+f_c)\lambda_c$ are all essentially equal. The etalon spacing is then set equal to

$$\tfrac{1}{2}(m_a+f_a)\lambda_a=\tfrac{1}{2}(m_b+f_b)\lambda_b=\tfrac{1}{2}(m_c+f_c)\lambda_c. \quad (1)$$

This method obviously ignores the phase shift. The quantity $\frac{1}{2}(m+f)\lambda$ really represents the optical spacing of the etalon plates, which is the physical separation plus the phase shift on reflection for the particular wavelength. Since in general the phase shift is a function of wavelength, the quantity $\frac{1}{2}(m+f)\lambda$ is not constant as implied in eq (1) but is a function of wavelength. It is fortunate that for the metals aluminum and silver which are commonly used on Fabry-Perot mirrors, the phase shift dispersion is such that it is possible to find integers m_a, m_b, and m_c which satisfy eq (1). When two different etalon spacings are determined by this method correct wavelengths values can be calculated.

Multilayer reflectors [15, 16, 17, 18] are finding considerable application in interferometry because of their low absorbance and high reflectance. For the common type of high reflection coating consisting of alternate high and low index layers, each of quarter-wave thickness for wavelength λ, the phase shift dispersion is small in the wavelength region near λ. Outside this spectral region the phase shift dispersion is much larger than for silver and aluminum mirrors. A 15-layer broadband high reflectance multilayer described by Baumeister and Stone [19] has a very large phase shift dispersion [20]. In such cases of high phase shift dispersion it is possible that integers cannot be found which will satisfy eq (1), or wrong integers may be selected.

Rank and Bennett [8] have described a method for using calculated values of the phase shift to correct the order number of interference in a Fabry-Perot etalon. Baumeister and Jenkins [20] have described another method for employing calculated phase shifts and have applied it to a nine-layer coating. The latter authors have also made measurements of the phase shift produced by the 15-layer broadband multilayer using Fizeau fringes [1]. The precision of this method was limited by the broad two-beam fringes used for comparison.

1.2. Calculation of the Unknown Wavelength

For work of highest accuracy, the above method of exact fractions is used only to determine the

[1] Now with American Optical Company, Southbridge, Mass.; work performed under a National Research Council Postdoctoral Research Associateship.

[2] Figures in brackets indicate the literature references on page. 199.

correct order numbers. The etalon spacing and the unknown wavelength are computed from a standard wavelength λ_s as follows. The method eliminates phase shift dispersion errors.

The fractional orders of interference, f_x and f_s are obtained for the unknown wavelength, λ_x, and for the standard wavelength, which can be one of the wavelengths used to determine the etalon spacing. The equations for interference at normal incidence are

$$(m_x+f_x)\lambda_x=2t+2\phi(\lambda_x) \tag{2}$$

and

$$(m_s+f_s)\lambda_s=2t+2\phi(\lambda_s). \tag{3}$$

Here $\phi(\lambda)$ is the phase shift in units of length; it is the additional optical path introduced on reflection. There are as many as four unknowns in these equations: λ_x, t, $\phi(\lambda_x)$, and $\phi(\lambda_s)$. (The unknown wavelength, λ_x, must be known in advance with sufficient accuracy to determine the order number, m_x.)

If another etalon spacing, t', is used, two more equations are obtained

$$(m'_x+f'_x)\lambda_x=2t'+2\phi(\lambda_x), \tag{4}$$

$$(m'_s+f'_s)\lambda_s=2t'+2\phi(\lambda_s). \tag{5}$$

The order number m'_s can be determined by the method of exact fractions described above. Again m'_x is determined from the approximate value of λ_x. The four equations can be solved [6] for λ_x by forming the difference between the two equations involving λ_x, also between the two equations involving λ_s, and equating the differences.

$$\lambda_x=\lambda_s\frac{m_s+f_s-m'_s-f'_s}{m_x+f_x-m'_x-f'_x}. \tag{6}$$

The phase shift terms are thereby eliminated. The difference in etalon spacing, $t-t'$, is obtained by subtracting eq (5) from eq (3)

$$t-t'=\tfrac{1}{2}\lambda_s(m_s+f_s-m'_s-f'_s).$$

Variations of the above method of analysis have been used by Meggers [3], Jackson [5], and Meissner [6]. The variations make analysis of an extended series of data more convenient, but fundamentally they depend on the measured quantities, f_s, f'_s, f_x, and f'_x in the manner shown in eq (6).

The order numbers m_s, m'_s, m_x, and m'_x are integers which can be determined without ambiguity in cases where $\phi(\lambda_s)$ and $\phi(\lambda_x)$ can be adequately approximated. The accuracy with which λ_x can be calculated from eq (6) therefore depends on the accuracy with which the fractions, f, can be measured. In particular, the error in λ_x is given approximately by

$$\left(\frac{\Delta\lambda_x}{\lambda_x}\right)^2$$

$$=\left(\frac{\Delta f_s}{m_s-m'_s}\right)^2+\left(\frac{\Delta f'_s}{m_s-m'_s}\right)^2+\left(\frac{\Delta f_x}{m_x-m'_x}\right)^2+\left(\frac{\Delta f'_x}{m_x-m'_x}\right)^2 \tag{7}$$

where $\Delta\lambda_x$, Δf_s, $\Delta f'_s$, Δf_x, and $\Delta f'_x$ represent the standard deviations in the values of λ_x, f_s, f'_s, f_x, and f'_x, respectively.

If the phase shift dispersion can be determined by independent measurements, then the unknown wavelength can be calculated from eqs (2) and (3)

$$\lambda_x=\frac{(m_s+f_s)\lambda_s+2\phi(\lambda_x)-2\phi(\lambda_s)}{m_x+f_x}. \tag{8}$$

The error in λ_x is given approximately by

$$\left(\frac{\Delta\lambda_x}{\lambda_x}\right)^2$$

$$=\left(\frac{\Delta f_s}{m_s}\right)^2+\left(\frac{\Delta f_x}{m_x}\right)^2+\left(\frac{2\Delta\phi(\lambda_x)}{m_s\lambda_s}\right)^2+\left(\frac{2\Delta\phi(\lambda_s)}{m_s\lambda_s}\right)^2. \tag{9}$$

Comparison of eqs (7) and (9) shows under what conditions the second method (eq 8) gives more accurate results than the first method (eq 6). For a given value of Δf_s, the value of $\Delta f_s/m_s$ in eq (9) will be smaller than $\Delta f_s/(m_s-m'_s)$ in eq (7). However, the difference need not be great if m'_s is small compared to m_s (that is, if the smaller etalon spacing, t', is small compared to the large etalon spacing, t).

The greatest gain is realized if $2\Delta\phi(\lambda_s)/m_s\lambda_s$ can be made significantly smaller than $\Delta f'_s/(m_s-m'_s)$, similarly for the quantities involving the unknown wavelength, λ_x. Since it is possible to have $m_s-m'_s\approx m_s$, this requirement can be written as $2\Delta\phi/\lambda<\Delta f'$. The limit on determination of the fraction f' from the diameters of the circular fringes is about $\Delta f'=0.01$ [21,22]. It will be shown that when fringes of equal chromatic order are used to determine the phase shift dispersion, the quantity $2\Delta\phi/\lambda$ can be considerably less than 0.01.

2. Theoretical Calculation of Phase Shift on Reflection

The convention used in this paper is that the phase shift on reflection, ϕ, represents an increase in optical path. The angular phase shift, $\epsilon=2\pi\phi/\lambda$, enters the expressions for the reflected waves as follows ($\theta=0$; see fig. 1)

$E_1=$(wave incident on surface 2)

$$=A_1e^{i(\omega T-\kappa x_2)}, \tag{10}$$

$E_2=$(reflected wave)

$$=A_2e^{i(\omega T-\kappa x_2-\epsilon_2)}, \tag{11}$$

E_3=(E_2 incident on surface 1 from inside)

$$=A_2 e^{i(\omega T-\kappa x_2-\epsilon_2-\kappa t)}, \tag{12}$$

E_4=(reflected component of E_3)

$$=A_4 e^{i(\omega T-\kappa x_2-\epsilon_2-\epsilon_1-\kappa t)}, \tag{13}$$

E_5=(wave E_4 incident on surface 2)

$$=A_4 e^{i(\omega T-\kappa x_2-\epsilon_2-\epsilon_1-2\kappa t)}. \tag{14}$$

Here ω is the angular frequency, T the time, $\kappa=2\pi/\lambda$.

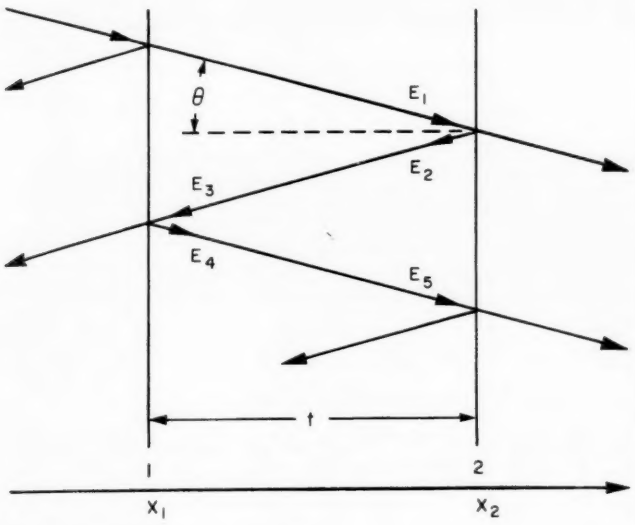

FIGURE 1. *Schematic diagram of interferometer.*

The reflecting surfaces are denoted by 1 and 2. For *feco* and for the center of the Fabry-Perot interference pattern the angle of incidence, θ, is zero.

The condition for constructive interference in transmission is that the optical path difference between two successive rays should be an integral number of wavelengths.

$$2\pi n=\arg E_1-\arg E_5=\omega T-\kappa x_2-(\omega T-\kappa x_2-\epsilon_2-\epsilon_1-2\kappa t)$$

$$=\epsilon_2+\epsilon_1+2\kappa t$$

$$n\lambda=\phi_2+\phi_1+2t. \tag{15}$$

From eqs (10) and (11) we have

$$\frac{E_2}{E_1}=\frac{A_2}{A_1}e^{-i\epsilon_2}.$$

For metals or for dielectric multilayers, theory can be used to calculate the quantity

$$\frac{E_2}{E_1}=\frac{A_2}{A_1}e^{i\delta_2}.$$

Therefore the relation between the desired angular phase shift, ϵ, and the calculated value, δ, is

$$\epsilon=\nu 2\pi-\delta \tag{16}$$

where ν is an integer.

For a metal reflector the angular phase shift, δ, is calculated from the index of the incident medium, μ_0, and the optical constants, μ and k, of the metal. The expression for the complex amplitude reflectance is [23]

$$\rho e^{i\delta}=\frac{\mu_0-\mu+ik}{\mu_0+\mu-ik}=\frac{\mu_0^2-\mu^2-k^2+i2\mu_0 k}{\mu_0^2+\mu^2+k^2+2\mu_0\mu}. \tag{17}$$

The tangent of the phase shift δ is then found by taking the ratio of imaginary part to real part:

$$\tan\delta=\frac{2\,\mu_0 k}{\mu_0^2-\mu^2-k^2}. \tag{18}$$

The quadrant for δ is determined by taking into account the signs of the real and imaginary parts of eq (17). Thus for $\mu^2+k^2>\mu_0^2$ (the case for all metals commonly employed in interferometry, when the separation medium is air or vacuum) the real part is negative and the imaginary part is positive, which means that δ is in the second quadrant. The phase shift $\phi=\epsilon\lambda/2\pi=(\nu 2\pi-\delta)\lambda/2\pi$ therefore represents an increase of optical path of between $\lambda/2$ and $3\lambda/4$.[3] Figure 2 shows the phase shift for aluminum calculated from the optical constants [24, 25].

For a multilayer the phase shift can be calculated from electromagnetic theory by one of several methods. An accurate method employs multiplication of matrices, each matrix representing a single layer [26, 27]. An exhaustive treatment of the subject has been given by Abelès [28], but the outline given by Koehler [29] is adequate for many problems.

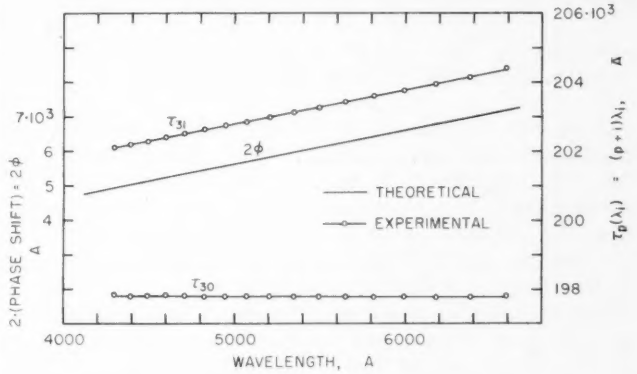

FIGURE 2. *Dispersion of phase shift on reflection for aluminum films.*

The theoretical values were calculated from the optical constants as given by Schulz [24, 25]. For the upper experimental curve the data from table 1 and the integer $q=31$ were used. Since this curve is parallel to the theoretical curve, it follows that $q=31$ is the correct order number for the fringe at $\lambda_0=6593.7$A. For the lower experimental curve the integer $q=30$ was used.

[3] The integer $\nu=1$ was selected for simplicity. Some other authors select $\nu=0$, which makes ϕ represent a *decrease* of optical path of between $\lambda/4$ and $\lambda/2$. For an infinite wave train the two interpretations are physically identical. They do lead to different order numbers of interference.

In dealing with phase shifts on reflection from multilayers the concept of nodes is very useful [20]. For light reflected from a plane interface between air and a high index dielectric, the phase shift is $\phi=\lambda/2$, and there is a node at the surface. For $\phi>\lambda/2$, as with a metal, the node is inside the metal. For $\phi<\lambda/2$, the node is on the air side of the surface. With multilayers of the common type, having a high index layer on the outside, a node for the tuned wavelength, λ, falls at the outer surface. For the broadband multilayer it has been shown [20] that there is one wavelength for which a node falls at the outer surface. At longer wavelengths the node is outside of this surface, and vice versa. Figure 3 shows the dependence of phase shift on wavelength.

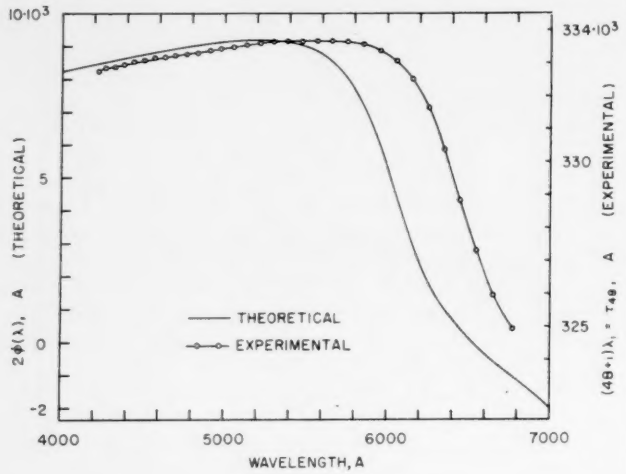

FIGURE 3. *Dispersion of phase shift on reflection for 15 layer broadband reflecting films.*

The angular phase shift, δ, as given by Baumeister and Jenkins [20] was converted to linear phase shift ϕ by means of eq (16) in which $\nu=1$ and the relation $\phi=\epsilon\lambda/2\pi$. The experimental curve has the same general shape except that it is shifted to longer wavelengths. Wavelengths from table 2 were used.

3. Experimental Procedure

Data on the phase shift dispersion were obtained by means of fringes of equal chromatic order [9, 10, 11, 30]. As shown in figure 4 collimated white light illuminated the interferometer. The very small spacing, 10 to 30μ, was accomplished by means of aluminum foil. The transmitted light entered a spectrograph, with the image of the interferometer surface being focused on the slit. As illustrated in figure 5, bright fringes appeared in the focal plane of the spectrograph for those wavelengths at which constructive interference occurred. After photographing the fringes along with an iron arc reference spectrum, the wavelengths of the fringes were measured. The method of calculating the phase shift dispersion is given below.

Fabry-Perot interference patterns were obtained using invar spacers of 2 and 5 mm, also fused quartz spacers of 20-mm length. The light source was a natural krypton lamp, krypton being selected because of its relatively sharp and well-distributed lines. The etalons were used in air maintained near 20° C and 10-mm water vapor pressure, and corrections to the wavelengths were made by the method described by Bruce [31].

From the photograph of the interference pattern the ring diameters were measured for several wavelengths. For the 2-mm spacer, two rings were measured at each wavelength; for the others, four rings were measured. The fractional orders, f, of interference at the center of the patterns were calculated with a least squares procedure described by Meissner [6].

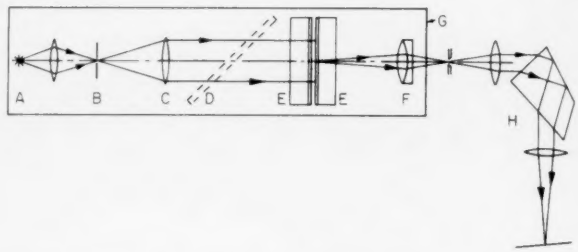

FIGURE 4. *Interferometer for fringes of equal chromatic order.*

A. White light source. B. pinhole, C. collimator, D. beam-divider (for reflected fringes), E. flats with metal or multilayer reflecting films, F. achromatic doublet, G. interferometer base, and H. spectrograph.

For Fabry-Perot interferometry the setup is changed as follows: The line source is placed at the focal point of the collimator, C. A larger spacer is introduced between the flats, E. A lens with longer focal length than F is used to focus the fringe pattern on the spectrograph slit, which in this case is wide.

4. Equations for Fringes of Equal Chromatic Order and Fabry-Perot Fringes

For the wavelengths λ_0, λ_1, etc., at which *feco* occur in the spectrograph, the normal incidence interference eq (15) can be written as

$$n\lambda_0=2t'+2\phi(\lambda_0), \tag{19}$$

$$(n+1)\lambda_1=2t'+2\phi(\lambda_1), \quad \text{etc.}, \tag{20}$$

λ_0 and λ_1 are the wavelengths of adjacent fringes, $\lambda_0>\lambda_1$. The order number for the fringe at λ_0 is n, and for each successive fringe the order number is increased by one. t' is the physical separation of the reflecting surfaces, and $\phi(\lambda)$ is the phase shift in units of length at each surface.

In these equations the left sides can be evaluated only at the wavelengths λ_0, λ_1, etc., at which there are fringes. However the quantity on the right side is a continuous function of λ which is conveniently denoted as $\tau_n(\lambda)$,

$$\tau_n(\lambda)\equiv 2t'+2\phi(\lambda). \tag{21}$$

The function $\tau_n(\lambda)$ is then evaluated by plotting $n\lambda_0$ versus λ_0, $(n+1)\,\lambda_1$ versus λ_1, etc., and connecting the points by a smooth curve. This curve has the same shape as the $2\phi(\lambda)$ curve but is displaced vertically by $2t'$.

With the Fabry-Perot etalon the interference equa-

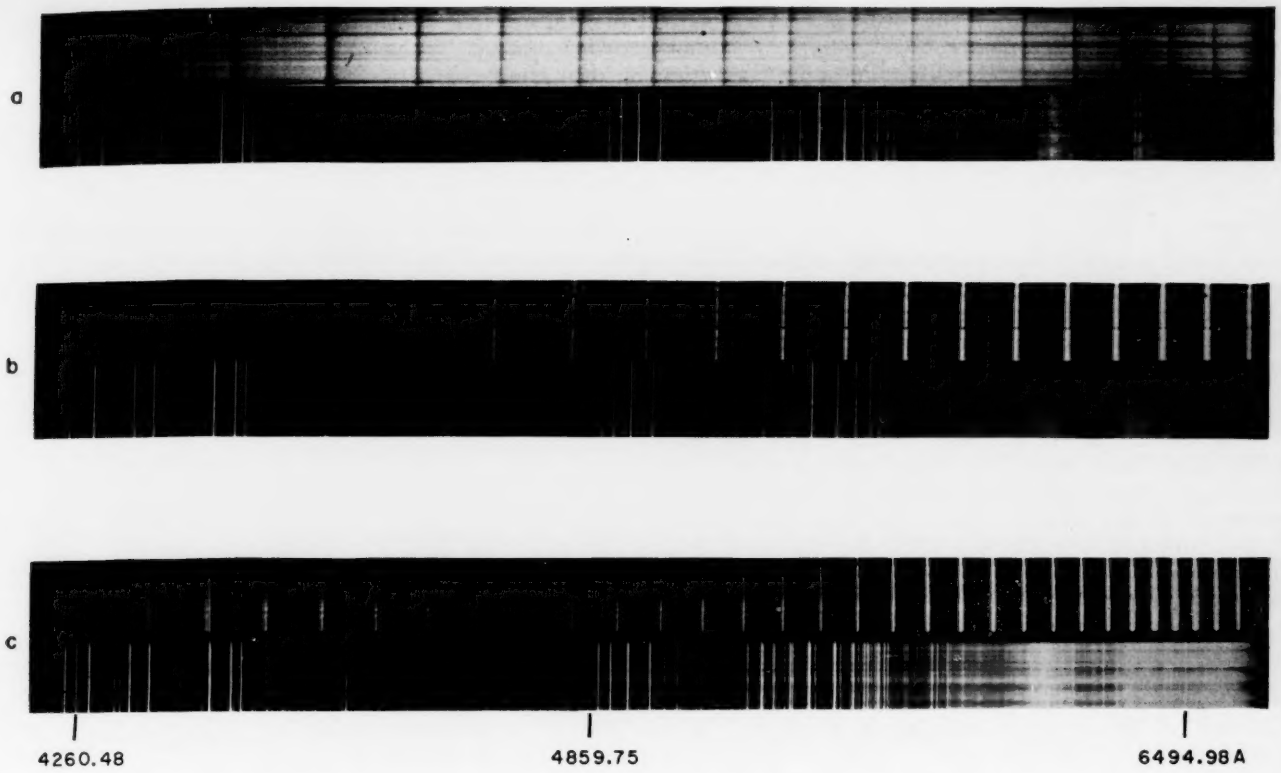

FIGURE 5. *Fringes of equal chromatic order with iron reference spectra (positive print).*

a. Aluminum films, reflection fringes, 10-μ spacer;
b. aluminum films, transmission fringes, 10-μ spacer;
c. 15 layer broadband films, transmission fringes, 17-μ spacer.

In c, the only obvious indication of the large dispersion of phase shift is the fact that the fringe spacing does not decrease monotonically with increasing wavelength. In the red the last few fringes are more widely spaced than those immediately preceding. Where several fringes are overexposed in the red the standard deviation in determination of wavelengths is about 0.4 A, whereas in other portions of the spectrum it is from 0.1 to 0.3 A.

tions for the centers of the ring pattern at known wavelengths λ_a, λ_b, λ_c, are:

$$(m_a+f_a)\lambda_a=2t+2\phi(\lambda_a), \tag{22}$$

$$(m_b+f_b)\lambda_b=2t+2\phi(\lambda_b), \tag{23}$$

$$(m_c+f_c)\lambda_c=2t+2\phi(\lambda_c). \tag{24}$$

Here again the quantity on the right side is a continuous function of λ, the curve being displaced upward from the curve $\tau_n(\lambda)$ by the amount $2(t-t')$. Therefore, in general the points $(m_a+f_a)\lambda_a$, $(m_b+f_b)\lambda_b$, and $(m_c+f_c)\lambda_c$ lie along a curve which is parallel to the τ_n curve.

5. Methods of Analysis

5.1. Method I

The first method for obtaining the order numbers n and m is used in cases where the phase shift dispersion is known approximately, as for example with metallic films with known optical constants for various wavelengths. For the *feco* an integer p is selected and the curve $\tau_p(\lambda)$ is determined by plotting $p\lambda_0$ versus λ_0, $(p+1)\lambda_1$ versus λ_1, etc. If it does not have the same shape as the known $2\phi(\lambda)$ curve, then other integers are tried until an integer, n, is found which makes $\tau_n(\lambda)$ essentially parallel to $2\phi(\lambda)$. This procedure is illustrated in figure 2.

Similarly for the Fabry-Perot data, integers m_a, m_b, m_c are found such that when $(m_a+f_a)\lambda_a$ is plotted against λ_a, $(m_b+f_b)\lambda_b$ against λ_b, etc., the points fall along a curve parallel to $\tau_n(\lambda)$. In order to measure an unknown wavelength, λ_x, in terms of a standard wavelength, λ_s, a modification of eq (8) is employed. Although the absolute values of $\phi(\lambda_x)$ and $\phi(\lambda_s)$ have not been determined, it can be seen from eq (21) that the difference, $2\phi(\lambda_x)-2\phi(\lambda_s)$, is given by

$$2\phi(\lambda_x)-2\phi(\lambda_s)=\tau_n(\lambda_x)-\tau_n(\lambda_s). \tag{25}$$

Therefore eq (8) becomes

$$\lambda_x=\frac{(m_s+f_s)\lambda_s+\tau_n(\lambda_x)-\tau_n(\lambda_s)}{m_x+f_x}. \tag{26}$$

The method has been described in terms of graphical procedures. A possible variation utilizes numerical calculations similar to those in the usual method of exact fractions. For wavelength λ_a the value of $\tau_n(\lambda_a)$ is found from the curve or by means of a numerical interpolation of the $\tau_n(\lambda)$ data. An

integer r_a is selected and the product $(r_a+f_a)\lambda_a$ is formed, also the difference $(r_a+f_a)\lambda_a-\tau_n(\lambda_a)$. This is done for all the integers, r_a, which lie within the range of possibility. Similarly different integers are tried for r_b and r_c until a set is found which satisfy the equation

$$(r_a+f_a)\lambda_a-\tau_n(\lambda_a)=(r_b+f_b)\lambda_b-\tau_n(\lambda_b)$$
$$=(r_c+f_c)\lambda_c-\tau_n(\lambda_c)$$

Once the correct integers have been found by this technique eq (26) can be used to compute unknown wavelengths.

5.2. Method II

The second, more general, method can be used when the phase shift dispersion is unknown. An *arbitrary* integer, q, is selected and the curve $\tau_q(\lambda)$ is determined as before. Then for the Fabry-Perot data, different integers are tried for r_a, r_b, and r_c, until a set is found for which the points $(r_a+f_a)\lambda_a$, $(r_b+f_b)\lambda_b$, and $(r_c+f_c)\lambda_c$ fall along a curve parallel to $\tau_q(\lambda)$. That is,

$$(r_a+f_a)\lambda_a-\tau_q(\lambda_a)=(r_b+f_b)\lambda_b-\tau_q(\lambda_b)$$
$$=(r_c+f_c)\lambda_c-\tau_q(\lambda_c) \qquad (27)$$

In appendix 9.1 it is shown that when the integers r_j are chosen in this manner then we have

$$(r_j+f_j)\lambda_j-\tau_q(\lambda_j)=2(t-t') \qquad (28)$$

regardless of the value of q. Here the subscript j represents the subscript a, b, c, s, or x.

The final step is to determine an unknown wavelength λ_x in terms of a standard wavelength, λ_s, and the measured fractions f_x and f_s. The integers r_s and r_x are determined in the same manner as r_a, r_b, and r_c. When these quantities are substituted in eq (28) two equations result which can be solved for λ_x:

$$\lambda_x=\frac{(r_s+f_s)\lambda_s+\tau_q(\lambda_x)-\tau_q(\lambda_s)}{r_x+f_x}. \qquad (29)$$

Just as in the standard method, the wavelength λ_x must be known in advance with sufficient accuracy that the proper integer, r_x, can be selected. The correct integer, r_x, is the one which makes the quantity $(r_x+f_x)\lambda_x$ fall closest to the curve $(r_j+f_j)\lambda_j$ versus λ_j.

6. Results

6.1. Evaporated Aluminum Films

Table 1 gives the wavelengths of *feco* obtained in transmission with a 10-μ spacer, the aluminum films having a transmittance of 5 to 8 percent. In principle the phase shift should be calculated taking into account the finite thickness of the aluminum films [32]. However, figure 2 shows that for the thicknesses used, the phase shift values calculated from the bulk constants yield a curve quite parallel to the experimental curve. Method I was used to determine the order number, n, as illustrated in figure 2.

For the 2-, 5-, and 20-mm spacers the integers, m, were found as described in 5.1 and illustrated in figure 6. With each spacer the points have the same vertical displacement from the curve τ_n, within experimental error.

TABLE 1. *Fabry-Perot and feco data obtained with aluminum films*

Ambient conditions for Fabry-Perot data, 20-mm, 5-mm spacers: 21.2°C, 754.6-mm Hg barometric pressure, 10-mm vapor pressure; 2-mm spacer: 22.0°C, 758.8-mm, 10-mm vapor pressure.

Wavelengths of *feco* λ_i	$n+i$	Optical path differences $(n+i)\lambda_i$	Wavelength of krypton line, λ_j (ambient)	Order, m, of interference plus fraction, f	Optical path difference, $(m+f)\lambda_j$
A		*A*	20-mm spacer		
6593.7	31	204,404	*A*		*A*
6379.8	32	204,153	6456.3448	62160.634	401,330,486
6180.7	33	203,962	6056.1779	66267.895	401,330,161
5993.7	34	203,787	5570.3369	72047.649	401,329,678
5817.1	35	203,599	4502.3929	89136.737	401,328,612
5650.9	36	203,433	4274.0066	93899.833	401,328,506
5493.8	37	203,272	5-mm spacer		
5345.5	38	203,129			
5205.1	39	202,998	6456.3448	15473.779	99,904,053
5071.6	40	202,862	6056.1779	16496.155	99,903,649
4944.7	41	202,734	5570.3369	17934.851	99,903,162
4824.2	42	202,616	4502.3929	22188.669	99,902,106
4709.5	43	202,510	4274.0066	23374.296	99,901,895
4600.1	44	202,404	2-mm spacer		
4495.5	45	202,295			
4395.4	46	202,191	6456.3399	6179.600	39,897,598
4300.3	47	202,112	6056.1733	6587.857	39,897,204
			5570.3326	7162.346	39,896,649
			4502.3894	8860.985	39,895,605
			4274.0033	9334.420	39,895,342

As an example, the wavelengths 5570.34 and 4502.39 are considered being known approximately to the nearest 0.02 A, this precision being necessary to establish the order numbers. The more precise values are to be determined by interferometric comparison with the standard line at 6056 A. From figure 6,

$$\tau_{31}(5570)-\tau_{31}(6056)=203{,}350-203{,}830=-480 \text{ A}.$$

Therefore from eq (26) we have

$$\lambda_x=\frac{66267.895\times6056.1779-480}{72047.649}$$
$$=5570.3369 \text{ A}.$$

Similarly for $\lambda_x=4502$ A

$$\lambda_x=\frac{66267.895\times6056.1779-1530}{89136.737}$$
$$=4502.3931 \text{ A}.$$

These values agree to experimental accuracy with the wavelengths for ambient conditions, as given in table 1.

In illustrating method II, rather than choose an arbitrary integer, we choose an integer, q, such that τ_q is as nearly constant as possible. As shown in figure 2, τ_{30} has only a very slight negative slope. The integers, r_j, which make the points $(r_j+f_j)\lambda_j$ lie

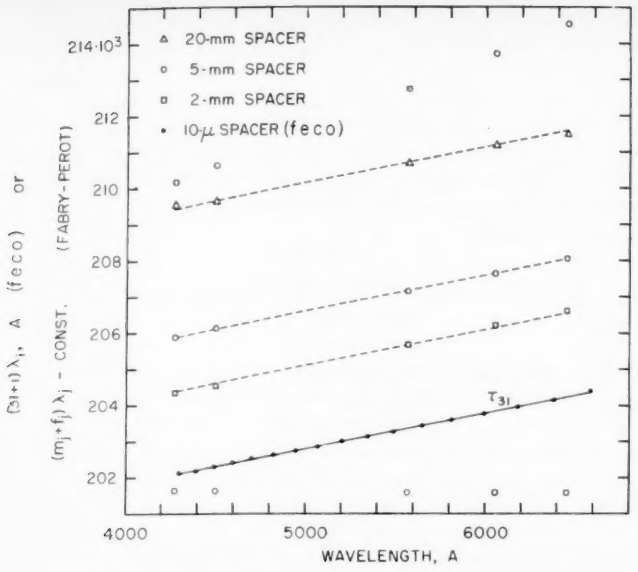

FIGURE 6. *Optical path differences: aluminum films.*

A constant was subtracted from the $(m_j+f_j)\lambda_j$ values to bring them on the same scale as the τ_{31} curve obtained from transmission *feco*. For the 20-, 5-, and 2-mm spacers the constants were 401119·10³, 99696·10³, and 39691·10³A respectively. For the 5-mm spacer (open circles) several different sets of integers, m_j, were tried together with the appropriate fractions, f_j. One set gives values of $(m_j+f_j)\lambda_j$ which lie along the dashed line, which is parallel to τ_{31}. The other sets give points which obviously do not lie along lines parallel to τ_{31}. For the 2- and 20-mm spacers the correct integers plus fractions are given in table 1, and the optical path differences are plotted above.

along a curve parallel to τ_{30} are one less than the corresponding integers m_j, in table 1. That is, for $\lambda=6456$, $r_j=62{,}159$.

Then for the unknown line, $\lambda_x \approx 4502.39$ A

$$\lambda_x=\frac{66266.89\times 56056.1779-197770+197{,}800}{89135.737}$$

$$=4502.3932 \text{ A}.$$

Thus with aluminum films if a certain integer, q, is chosen the $\tau_q(\lambda)$ curve is nearly constant and the phase shift correction is very small. Furthermore the quantities $(r_j+f_j)\lambda_j$ are nearly constant. In the standard method of exact fractions the integers are selected so that the quantities $(r_j+f_j)\lambda_j$ are equal. Therefore the method of exact fractions as normally used gives integers, r_j, which are each one less than the "true" order numbers, m_j.[4] This introduces no error into the determination of unknown wavelengths because only *differences* in order numbers for two different etalon spacings are used in the final calculation.

6.2. Fifteen-Layer Broadband Reflectors

Table 2 gives the wavelengths of *feco* obtained in transmission for a broadband multilayer [19] made from alternate layers of cerium dioxide and magnesium fluoride [33]. The measured reflectance was between 83 and 94 percent over the region 4500 to 7000 A. In figure 3 the theoretical phase shift curve was obtained from values published by Baumeister and Jenkins [20]. The experimental phase shift curve confirms the general shape of the theoretical curve. The displacement of about 400 A to longer wavelengths indicates that the individual layers are somewhat thicker than the theoretical values [19]. This is confirmed by the location of the reflectance maximums and minimums.

[4] The word "true" is in quotation marks because some authors use another convention for sign of the phase shift, which results in another order number. See section 2.

TABLE 2. *Fabry-Perot and feco data obtained with 15-layer broadband multilayers*

Ambient conditions for Fabry-Perot data: 19.5° C, 757.05 mm Hg barometric pressure, 6.5-mm vapor pressure.

Wavelengths of *feco* λ_i	$n+i$	Optical path difference $(n+i)\lambda_i$	Wavelength of krypton line, λ_j (ambient)	Order, m, of interference plus fraction, f	Optical path difference, $(m+f)\lambda_j$
A		*A*	20-mm spacer		
			A		*A*
6769.1	48	324,920	6456.3278	62168.014	401,377,077
6651.8	49	325,937	6056.1620	66276.498	401,381,209
6447.2	51	328,807	5570.3222	72057.199	401,381,815
6257.5	53	331,647	4502.3809	89148.651	401,381,184
6055.4	55	333,049	4273.9952	93912.374	401,381,036
5852.1	57	333,571			
5655.3	59	333,660			
5469.9	61	333,661	5-mm spacer		
5295.6	63	333,623			
5131.5	65	333,548	6456.3278	15470.386	99,881,883
4976.4	67	333,421	6056.1620	16493.291	99,886,042
4830.4	69	333,295	5570.3222	17931.927	99,886,611
4693.1	71	333,209	4502.3809	22185.150	99,885,996
4563.4	73	333,128	4273.9952	23370.598	99,885,824
4440.2	75	333,014			
4323.3	77	332,891	2-mm spacer		
4211.6	79	332,713			
			6456.3278	6183.25	39,921,087
			6056.1620	6592.49	39,925,189
			5570.3222	7167.60	39,925,841
			4502.3809	8867.57	39,925,178
			4273.9952	9341.38	39,925,013

For the 2-, 5-, and 20-mm spacers the integral orders of interference, m, were obtained as described in section 5.1. For each spacer, the total optical path differences $(m_j+f_j)\lambda_j$ plotted against λ_j fell along a curve parallel to the τ_{48} curve, as shown in figure 7.

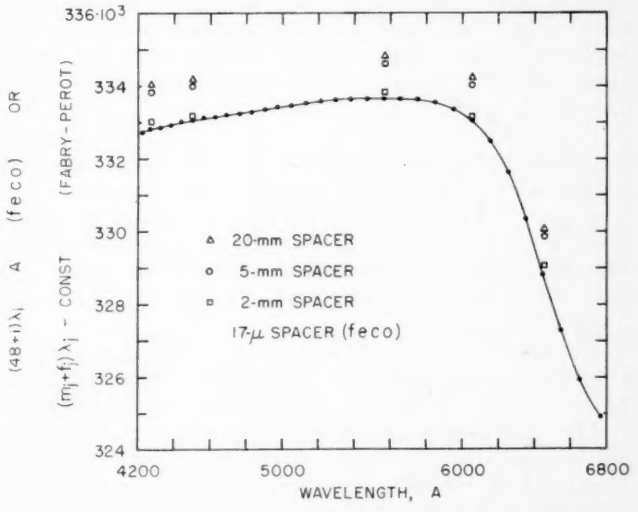

FIGURE 7. *Optical path differences: 15 layer broadband films.*

τ_{48} was obtained from *feco* in transmission. See table 2. For the 2-, 5-, and 20-mm spacers, the correct integers m_j were selected as described in section 5.1. Each set of points, $(m_j+f_j)\lambda_j$, lies along a curve parallel to the τ_{48} curve. The constants subtracted from $(m_j+f_j)\lambda_j$ values for the 20-, 5-, and 2-mm spacers were 401047·10³, 99552·10³ and 39592·10³A respectively.

Table 3 gives data for the calculation of wavelengths 5570 and 4502 A, taking as the standard the line at 6056 A. Both method I and the "standard" method (eq 6) have been used.

TABLE 3. *Wavelength calculations from Fabry-Perot and feco data obtained with multilayer reflectors*

a. Calculation using eq (26), 20-mm spacer and *feco*.

λ_s	(m_s+f_s)	$(m_s+f_s)\lambda_s$	$\tau_{48}(\lambda_s)$
A		*A*	*A*
6056.1620*	66276.498	401,381.209	333,030

λ_x†	$\tau_{48}(\lambda_x)$	(m_x+f_x)	λ_x	λ_x‡
A	*A*		*A*	*A*
5570.32	333,650	72057.199	*5570.3224	5570.3222
4502.38	333,070	89148.651	*4502.3816	4502.3809

b. Calculation using eq (6), 20-mm and 5-mm spacers.

λ_x†	$(m_s'+f_s')$	$(m_x'+f_x')$	λ_x
A			*A*
5570.32	16493.291	17931.927	*5570.3215
4502.38	16493.291	22185.150	*4502.3806

*The wavelengths of the standard line at 6056 A and of the unknown lines are for the ambient conditions given in table 2.
†Rough value.
‡From Bruce [31] (converted to ambient conditions).

6.3. Precision of Measurements

In the determination of wavelength of fringes the standard deviation for an individual reading was generally from 0.1 to 0.3 A. This resulted in a standard deviation for the values of τ of from 5 to 10 A, with a rare value as high as 30 A. With $\Delta\tau=10$ A as an example and $\lambda=5000$ A, the ratio $2\Delta\phi/\lambda$ discussed earlier in connection with eq (9) becomes $2\Delta\phi/\lambda=\Delta\tau/\lambda=0.002$. This is to be compared with the usual error in exact fraction determination, $\Delta f=0.01$.

The improvement in precision of wavelength measurement is not so dramatic, however, since this is limited by the errors in measuring the fractions f_s and f_x. For example, in the standard method, eq (6), we take data from the 20-mm and 5-mm spacers (table 2) on the known line and the unknown line, 5570 A. For $\Delta f_s=\Delta f_x=0.01$, eq (7) yields $\Delta\lambda_x=0.0022$ A.

To compute the error obtained in the method employing *feco*, we take $\Delta f_s=\Delta f_x=0.01$ and $2\Delta\phi(\lambda)/\lambda=\Delta\tau/\lambda=0.002$. Then eq (9) yields $\Delta\lambda_x=0.0012$ A.

The precision of both methods can, of course, be improved by repeated readings. For example, Stanley and Meggers [34] report that in the measurement of iron lines with 20- or 25-mm spacers, the average of 5 or 6 readings had a probable error of 1 part in 7 million.

The question arises as to the best etalon spacing to be used for *feco*. Since the wavelength is multiplied by the order number to obtain the τ curve, smaller spacings and the resulting low order numbers tend to give smaller errors. But smaller spacings give fringes widely spaced in the spectrum. If the phase shift has a nonlinear variation with wavelength, as with the broadband multilayer, it is desirable to have the experimental points fairly close together. In this case, the best spacing was found to be 10 to 20μ, whereas for aluminum the smallest possible spacing was desirable.

6.4. Differences Between Transmission and Reflection Data

By placing a semireflecting mirror between the collimator and interferometer in figure 4 it is possible to project the light reflected from the interferometer onto the spectograph slit. With a small separation between the interferometer plates the resulting spectrum consists of dark fringes crossing the bright continuum. See figure 5a.

If the reflecting surfaces are nonabsorbing, the principle of conservation of energy requires that the reflected spectrum be the exact complement of the transmitted spectrum. Under these circumstances the wavelengths of the fringes should be the same in the two spectra. Then the τ_n curve plotted from the reflection data should also give the phase shift dispersion.

If the reflecting films are partially absorbing, this conclusion does not necessarily hold. Holden [35] has shown that there can be asymmetry in the intensity distribution of fringes obtained in reflection.

Experiments were conducted to determine whether or not the τ_n curve obtained from reflection *feco* was the same as that obtained by transmission. Exposures were taken within a few minutes of each other, and the same areas of the reflecting films were used. As expected, the aluminum films showed a small but significant difference. As shown in figure 8 the slopes are different, the maximum discrepancy between 4200 and 6500 A amounting to about 40 A. The reflection fringes showed a definite asymmetry, which made determination of their wavelengths more difficult.

The two curves for the 15-layer multilayer showed a difference of about 150 A between 4800 and 6600 A. See figure 8. This result was unexpected because of the low absorption of dielectric multilayers. Transmittance and reflectance measurments on these multilayers indicated with the absorptance is no more than 2.5 percent at 4800 A and no more than 1 percent at 6000 A. However, no error is introduced if phase shift data obtained by transmission *feco* are used in connection with Fabry-Perot fringes obtained in transmission since both are governed by the interference eq (15). The reflection fringes are governed by a different interference condition [11, 35, 36].

6.5. Uniformity of Phase Shift Dispersion

With multilayer films the reflectance and phase shift on reflection are generally more sensitive

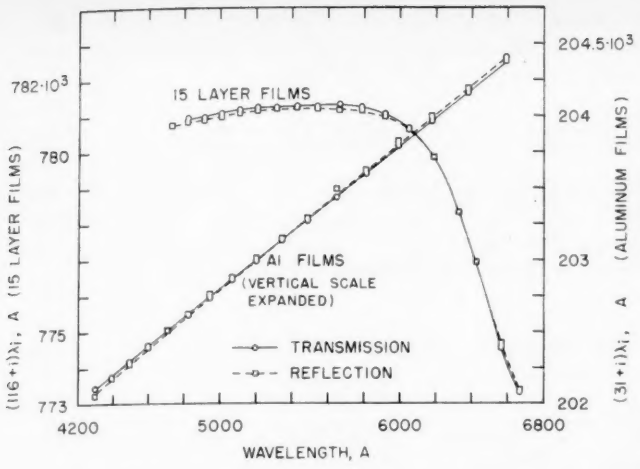

FIGURE 8. *Differences in data obtained by transmission and reflection.*

The experimental points represent $(n+i)\lambda_i$, where n is the order number of the fringe at λ_0, i is an integer, and λ_i is the wavelength of a fringe observed either by transmission or by reflection. In the case of the 15-layer films a relatively thick spacer (40μ) was used and fringes were closely spaced. Only about one-third of the fringes were measured and plotted. In the case of the aluminum films the vertical scale interval has been expanded to four times that of the multilayer in order to show more clearly the small but significant difference between the transmission and reflection data. Only the transmission *feco* should be used in connection with Fabry-Perot fringes obtained by transmission.

functions of the thickness of the individual layers than with metal reflectors. If the absolute value of the phase shift is not constant over the aperture, it has the same effect as nonflatness of the support plate. If the *dispersion* of phase shift is not constant, then the shape of the reflected wavefront will depend on the wavelength [37]. In particular, if two such mirrors are adjusted to be optically parallel when a green line is used, they may not be optically parallel in the red or blue.

The phase shift dispersion was measured at six points across the 15-layer films. Over a 40-mm distance there was a definite change in the shape of the curve, amounting to 300 A from the blue to the red end of the spectrum. For precision Fabry-Perot interferometry this variation is too large to be tolerated. For the experiments reported here a 10-mm-diam aperture was placed between the interferometer plates. The total variation in phase shift dispersion over this area was less than 100 A, which is the same order of magnitude as the departure from flatness of the support plates.

Freshly deposited aluminum films showed very little variation in phase shift dispersion over a 40-mm aperture, the maximum discrepancy being about 40 A over the region 4300 to 6600 A.

These results indicate that multilayers for interferometers in which several wavelengths are to be used should be checked for uniformity of phase shift dispersion. The use of *feco* provides a convenient and precise method.

7. Conclusions

It has been found that measurements of reflection phase shift dispersion by means of fringes of equal chromatic order are useful at three stages in wavelength comparisons by Fabry-Perot interferometry. First, for multilayer reflectors it must be established that the phase shift dispersion is sufficiently uniform over the aperture. This can be done by obtaining the *feco* at several points across the aperture.

Second, the phase shift data can be combined with the method of exact fractions to yield the integral order numbers. This is especially valuable in the case of multilayers where the dispersion of the phase shift is high and where calculated phase shifts may be in error due to poorly known layer thicknesses.

Third, the accuracy of measurements of unknown wavelengths can be improved somewhat. The basic reason is that for high reflection mirrors, wavelengths of *feco* can be measured to about ± 0.002 order, whereas the error in determining fractions in Fabry-Perot patterns is about ± 0.01 order. This difference is due primarily to the fact that *feco* are obtained from a very small area of the plate. Small departures from flatness of the substrate surface do not reduce the sharpness of the *feco*. On the other hand, the Fabry-Perot fringes result from interference over the entire aperture, and variations in the surface reduce the fringe sharpness. In return for the gain in precision afforded by the *feco* the necessary precaution is that the variation in phase shift dispersion across the aperture is sufficiently small.

The author benefited from many discussions with J. B. Saunders. Karl Nefflen kindly loaned much equipment. Calculations of wavelength were very much easier as a result of an IBM 704 program modified for this purpose by Stanley Prusch. The aluminum coatings were prepared by W. L. Griffith, Jr. Finally, the author is grateful to the National Academy of Sciences—National Research Council and to the National Bureau of Standards for the postdoctoral research associateship under which this work was performed.

8. References

[1] Ch. Fabry and H. Buisson, J. phys. **7,** 417 (1908).
[2] P. Eversheim, Ann. Physik **30,** 815 (1909).
[3] W. F. Meggers, Bull. BS. **12,** 198 (1915).
[4] J. Bauer, Ann. Physik **20,** 481 (1934).
[5] C. V. Jackson, Trans. Roy. Soc. (London) **A236,** 1 (1936).
[6] K. W. Meissner, J. Opt. Soc. Am. **31,** 405 (1941).
[7] H. Barrell and P. Teasdale-Buckell, Proc. Phys. Soc. (London) **B64,** 413 (1951).
[8] D. H. Rank and H. E. Bennett, J. Opt. Soc. Am. **45,** 69 (1955).
[9] L. G. Schulz, J. Opt. Soc. Am. **41,** 261, 1047 (1951).
[10] W. F. Koehler, J. Opt. Soc. Am. **43,** 738 (1953); **45,** 934 (1955).
[11] C. J. Koester, J. Opt. Soc. Am. **48,** 255 (1958).
[12] A. A. Michelson and R. Benoit, Trav. et Mem. Bur. Int. Pds. Mes. **11,** 1895.
[13] C. Candler, Modern interferometers, p. 117 (Hilger and Watts, Ltd., London, England, 1951).
[14] F. H. Rolt and H. Barrell, Proc. Roy. Soc. (London) **A122,** 122 (1929).
[15] C. H. Cartwright and A. F. Turner, Phys. Rev. **55,** 1128(A) (1939).
[16] C. Dufour, Ann. phys. **6,** 5 (1951).

[17] A. H. Jarrett, Nature **169,** 790 (1952).
[18] P. Giacomo, Rev. optique **35,** 317 (1956).
[19] P. W. Baumeister and J. M. Stone, J. Opt. Soc. Am. **46,** 228 (1956).
[20] P. W. Baumeister and F. A. Jenkins, J. Opt. Soc. Am. **47,** 57 (1957).
[21] W. H. J. Childs, J. Sci. Instr. **3,** 129 (1926).
[22] C. Candler, Modern interferometers, p. 118 (Hilger and Watts, Ltd., London, England, 1951).
[23] R. W. Pohl, Optik, p. 148 (Springer, Berlin, 1940).
[24] L. G. Schulz, J. Opt. Soc. Am. **44,** 357 (1954).
[25] L. G. Schulz and F. R. Tangherlini, J. Opt. Soc. Am. **44,** 362 (1954).
[26] A. Herpin, Compt. rend. **225,** 182 (1947).
[27] R. B. Muchmore, J. Opt. Soc. Am. **38,** 20 (1948).
[28] F. Abelés, Ann. phys. **5,** 596, 706 (1950).
[29] W. F. Koehler, J. Opt. Soc. Am. **45,** 934 (1955).
[30] S. Tolansky, Multiple-beam interferometry of surfaces and films, p. 96 (Oxford Univ. Press, N.Y., 1948).
[31] C. F. Bruce, Wavelength data and correction tables for length interferometry (tech. paper no. 8, Nat. Standards Lab., C.S.I.R.O., Australia, 1956).
[32] L. G. Schulz and E. J. Scheibner, J. Opt. Soc. Am. **40,** 761 (1950).
[33] G. Hass, J. B. Ramsey, and R. Thun, J. Opt. Soc. Am. **48,** 324 (1958).
[34] R. W. Stanley and W. F. Meggers, J. Research NBS **58,** 41 (1957).
[35] J. Holden, J. Opt. Soc. Am. **41,** 504 (1951).
[36] A. R. Cownie, J. Opt. Soc. Am. **47,** 132 (1957).
[37] P. Giacomo, J. phys. rad. **19,** 307 (1958).

9. Appendix

9.1. Derivation of Equation (28)

It is to be shown that for an arbitrary integer q and for integers, r_j, selected as described, the differences $(r_j+f_j)\ \lambda_j-\tau_q\ (\lambda_j)$ are equal to $2(t-t')$. To both sides of eq (19) we add the quantity $(q-n)\ \lambda_0$.

$$q\ \lambda_0=2t'+2\phi\ (\lambda_0)+(q-n)\ \lambda_0.$$

Adding $(q-n)\ \lambda_1$ to each side of eq (20) gives

$$(q+1)\ \lambda_1=2t'+2\phi\ (\lambda_1)+(q-n)\ \lambda_1.$$

Therefore the smooth curve connecting the points $q\lambda_0$, $(q+1)\ \lambda_1$, etc., is the continuous function

$$\tau_q(\lambda)\equiv 2t'+2\phi(\lambda)+(q-n)\lambda. \tag{30}$$

Now from eq (22) we obtain the relation

$$\begin{aligned}(r_a+f_a)\lambda_a&=(m_a+f_a)\lambda_a+(r_a-m_a)\lambda_a\\&=2t+2\phi(\lambda_a)+(r_a-m_a)\lambda_a\end{aligned} \tag{31}$$

The integers r_a, r_b, etc., are selected so as to satisfy eq (27). Substitution of eq (31) and the corresponding equation for λ_b into eq (27) yields

$$(r_a+f_a)\lambda_a-\tau_q(\lambda_a)=2t+2\phi(\lambda_a)+(r_a-m_a)\lambda_a$$

$$-[2t'+2\phi(\lambda_a)+(q-n)\lambda_a]=2t+2\phi(\lambda_b)+(r_b-m_b)\lambda_b$$

$$-[2t'+2\phi(\lambda_b)+(q-n)\lambda_b]$$

or $$(r_a-m_a-q+n)\lambda_a=(r_b-m_b-q+n)\lambda_b. \tag{32}$$

Since r, m, q, and n are integers, the only general way in which eq (32) can be satisfied is $r_a-m_a=r_b-m_b=q-n$, in which case

$$(r_j+f_j)\lambda_j-\tau_q(\lambda_j)=2(t-t') \tag{33}$$

where j stands for a, b, or c. Thus the difference between the etalon spacings can be determined, regardless of the phase shift dispersion and of the integer, q, which is arbitrarily selected.

9.2. Required Accuracy of Theoretical Phase Shift Curve

The phase shift curve must be known from theoretical calculations with a certain accuracy if the "true" order numbers are to be determined, as in section 5.1. We wish to show that the slope of the curve 2ϕ versus λ must be known to better than ± 0.5.

With *feco* the criterion for selection of the true order number, n, for the fringe at λ_0 is that the plot of $n\lambda_0$ versus λ_0, $(n+1)\lambda_1$ versus λ_1, etc., gives a curve $\tau_n(\lambda)$ which is parallel to $2\phi(\lambda)$, i.e., $\tau_n(\lambda)=2t'+2\phi(\lambda)$. The curve which results for an incorrect integer, q, is given by eq (30). Now the smallest possible error is one unit, i.e., $q=n+1$. Then by eq (30),

$$\tau_{n+1}(\lambda)=2t'+2\phi(\lambda)+\lambda.$$

It is evident that at all values of λ the slope of the $\tau_{n+1}(\lambda)$ curve is greater by one than the slope of the $\tau_n(\lambda)$ curve. Thus the possible τ_q curves are a family of curves which at a given value of λ differ in slope by one. In order to make the correct selection of n, therefore, the slope of the $2\phi(\lambda)$ curve should be known to better than ± 0.5.

Similarly for Fabry-Perot data, the criterion for selection of the order numbers $m_j(j=a,b,\text{or } c)$ is that when the values of $(m_j+f_j)\lambda_j$ are plotted against λ_j the points fall along a curve, A, parallel to $2\phi(\lambda)$. If the integers, m_j, are each increased by one, the resulting points $(m_j+1+f_j)\lambda_j$ versus λ_j fall along a curve having a slope greater by one than curve A. Therefore in order to make the correct selection of m_j, the slope of the $2\phi(\lambda)$ curve should be known to better than ± 0.5.

This is not a severe restriction, amounting to a maximum permissible uncertainty in $\epsilon=2\pi\phi/\lambda$ of about $\pm 35°$ over the wavelength interval between 5000 and 6000 A. Therefore in most cases of metallic reflectors and multilayers the theoretical phase shift will be known accurately enough to calculate the true order numbers. When it is not known with sufficient accuracy, method II can be used.

Washington, D.C. (Paper 64A3-43)

JOURNAL OF RESEARCH of the National Bureau of Standards—A. Physics and Chemistry
Vol. 64A, No. 3, May–June 1960

[1] Infrared Absorption Spectrum of Methane From 2470 to 3200 cm^{-1}

Earle K. Plyler, Eugene D. Tidwell, and Lamdin R. Blaine

(January 11, 1960)

The absorption spectrum of methane has been measured from 2470 to 3200 cm^{-1} with a high-resolution infrared spectrometer. Pressures from 0.01 to 4.5 cm of the gas were used in order to observe both intense and weak lines. A total of 2,460 lines were measured in the entire region. The ν_3 band at 3018 cm^{-1} was measured at very slow scanning rates and the lines of the P and R branches were resolved into several components. The observed spectrum is shown in five figures.

1. Introduction

A number of researches have been made on the infrared spectrum of methane since the first interpretation of the observed spectrum was made by Dennison in 1925 [1].[2] It is now well established that the tetrahedral model is in accord with all the measurements of the infrared and the Raman spectrum. There are four fundamental vibrations which occur at about 2914, 1534, 3018, and 1306 cm^{-1} which are designated as ν_1, ν_2, ν_3, and ν_4, respectively. For a rigid molecule of this symmetry only the ν_3 and ν_4 vibrations are active in the infrared, but on account of interactions ν_2 becomes active in the infrared spectrum. This band has been measured by Burgess, Bell, and Nielsen [2]. More recently it has been shown by Allen and Plyler [3] that the ν_3 vibration at 3018 cm^{-1} which is triply degenerate has a weak component with a $Q(F^+)$ branch at 3022 cm^{-1}. The $Q(F^-)$ branch is also probably active, but it has not been observed and may be strongly overlapped by the strong $Q(F^\circ)$ branch.

When the ν_3 band of methane is measured with low resolution the lines of the P and R branches are observed as single. With better resolution lines having large J's begin to split up into several components. This splitting was found by Nielsen [4] to be rather large in ν_4, and Childs and Jahn [5] explained the splitting as produced by the Coriolis interaction between ν_2 and ν_4. The rotational structure of ν_3 also shows splittings in the P and R branches, but the separation between the components is much less than in ν_4. With a resolution of 0.05 cm^{-1} the lines of the P branch with $J \geq 2$ and the lines of the R branch with $J \geq 3$ have all been split into components (see ref. 3), the lines from P 9 to P 15 each showing four components. The present investigation was undertaken to ascertain if, with higher resolution, the rotational lines of the P and R branches of ν_3 could be split into a greater number of components and to search for other bands which may appear in the region 2470 to 3200 cm^{-1}.

2. Experimental Method

There was available in the Radiometry Section of the Bureau an infrared spectrometer which has a resolution between 0.02 and 0.03 cm^{-1}. The instrument is equipped with a 10,000 line/inch grating which has a ruled surface of 4¾ x 8 in. The grating is double-passed and the energy is detected by a cooled PbS cell. A full description of the instrument is given in a previous paper [6]. The spectra were measured by using the fringes of a Fabry-Perot interferometer to interpolate between standard lines. As this method of measurement has been previously described [7] the details will not be repeated.

The methane gas was obtained from the Matheson Company and the purity was given as 99 percent. No further purification of the gas was made. In the measurement of the spectra the gas pressure for different spectral regions was varied from 0.1 mm to 4.5 cm. The absorption cell had a path of 6 m which made it possible to use very low pressures in the regions of strong absorption. The spectrum was observed at various scanning speeds. In the regions where it was desired to bring out as much structure as possible, the spectrum was scanned at the rate of one wavenumber in 10 min, but in scanning the entire region from 2470 to 3200 cm^{-1} one wavenumber was recorded per minute. Even at this faster rate 12 hr were necessary and 32 ft of recorder paper were required for scanning the entire region. For the measuring charts a slower speed was used and 60 hr were required to cover the region included in figures 1, 2, and 3.

3. Experimental Results

Photographs of the recorder traces of the observed spectrum are shown in figures 1, 2, and 3. Figure 1

[1] This work was supported by the Geophysics Research Directorate, Air Force.
[2] Figures in brackets indicate the literature references at the end of this paper.

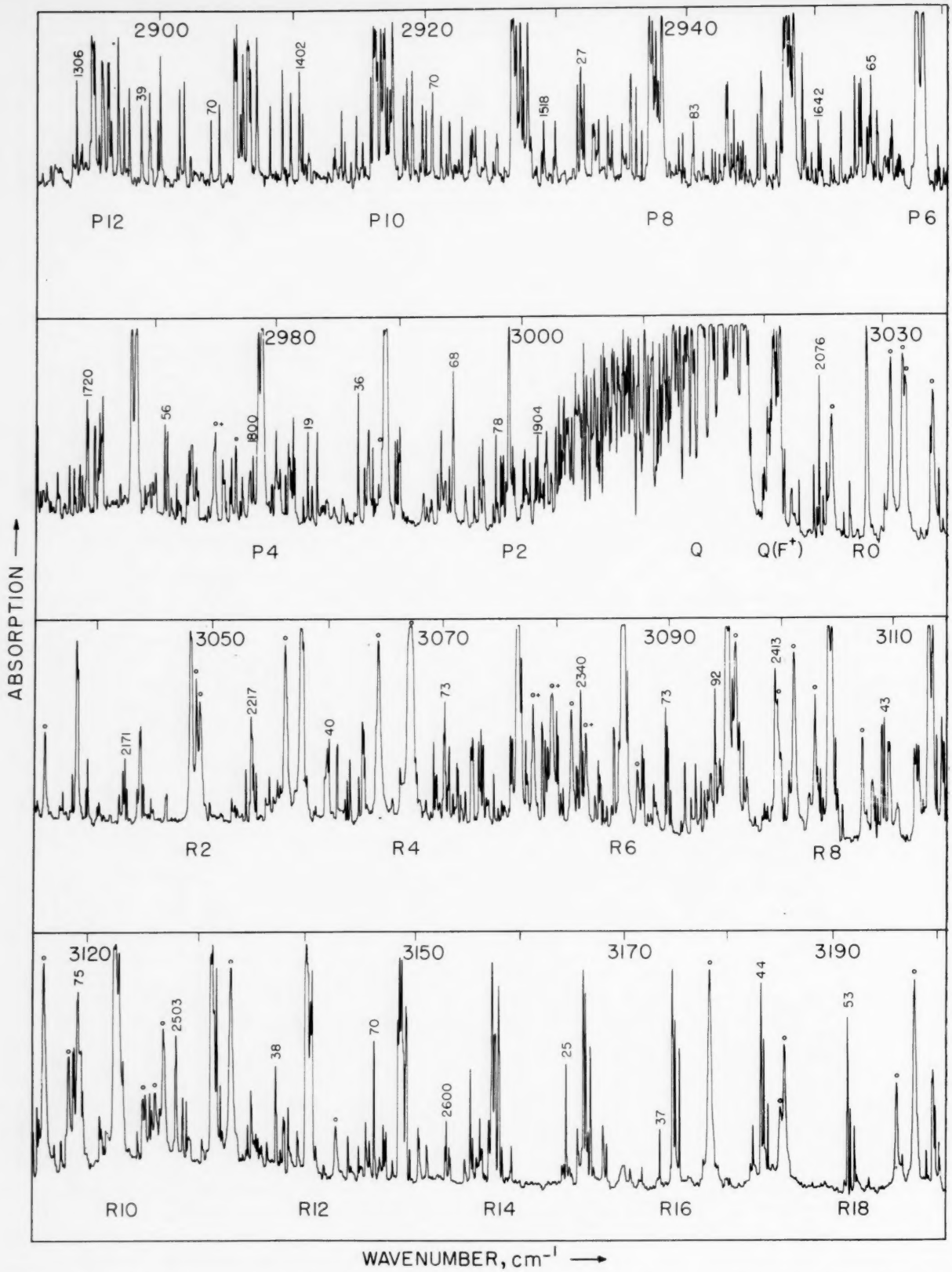

FIGURE 1. *The infrared absorption of methane from 2890 to 3200 cm^{-1} as observed with a 10,000 lines/in grating used double pass.*

The gas pressure was 2 cm in a 6-m cell. The numbers on the lines correspond with those given in table 1.

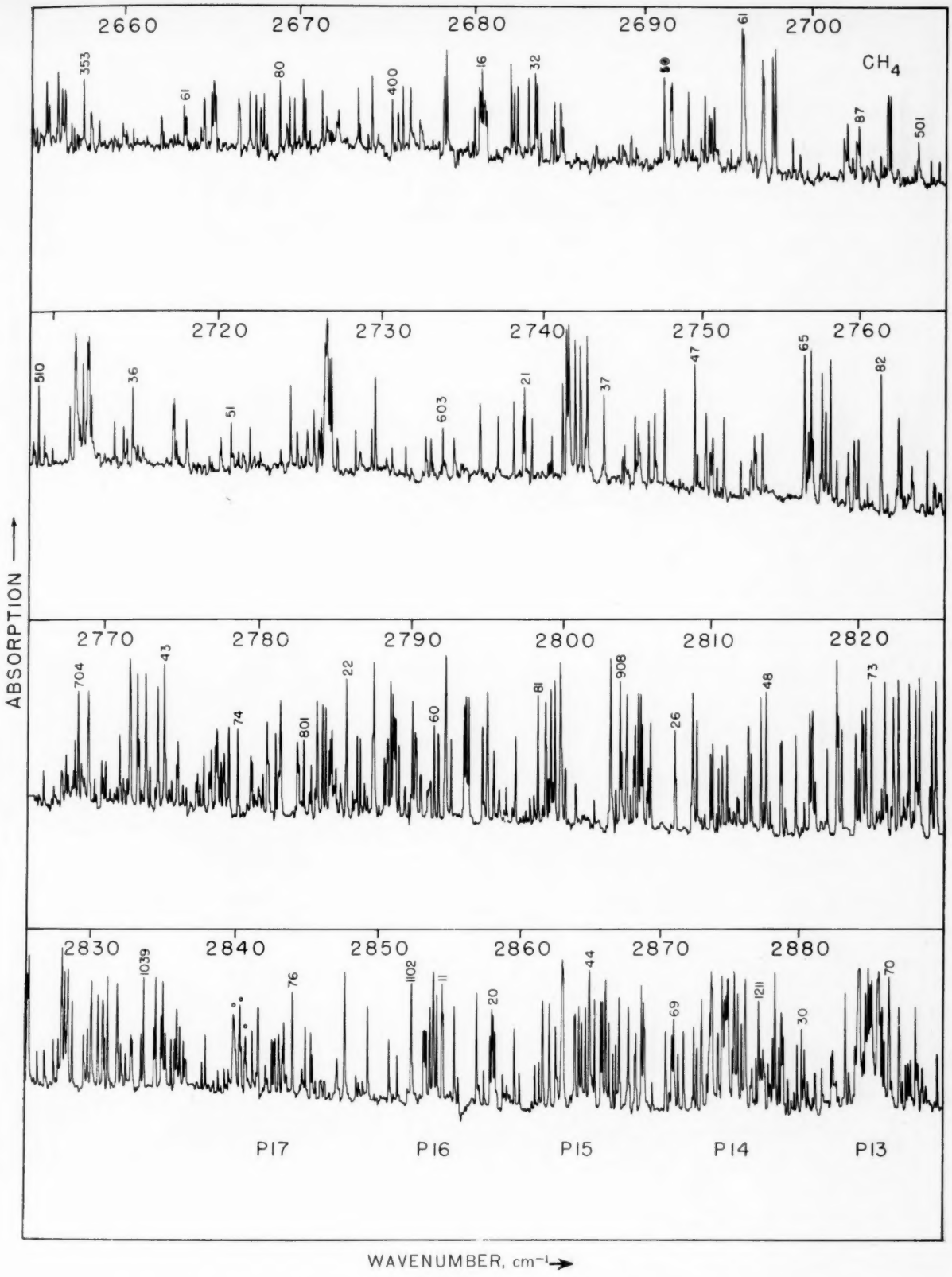

FIGURE 2. *The observed spectrum of methane from 2655 to 2890 cm⁻¹.*

The conditions of measurement were the same as for figure 1.

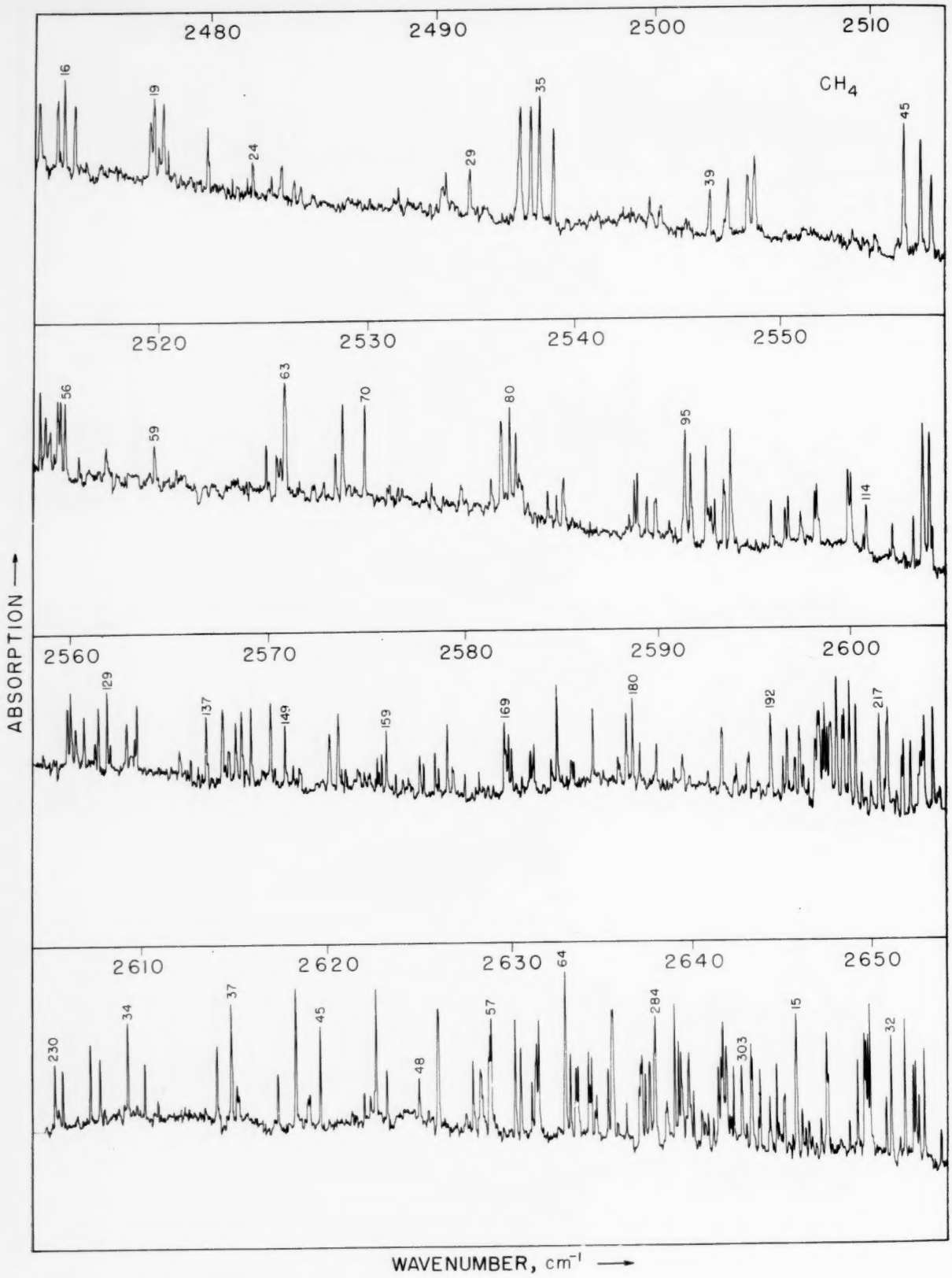

FIGURE 3.- *The observed spectrum of methane from 2470 to 2655 cm^{-1}.*

The pressure of the gas was 4.5 cm. The other conditions of measurement were the same as for the spectra in figures 1 and 2.

covers the region from 2890 to 3200 cm^{-1} and includes the intense component of ν_3 from R 18 to P 12. The pressure of the gas in the cell was 2 cm for the spectrum in figures 1 and 2 and 4.5 cm for the results shown in figure 3. These pressures were selected in order to make it possible to observe the lines between the P and R branches of the main band.

About 2,650 lines were measured in the region from 2470 to 3200 cm^{-1} and serial numbers were placed on the figures which correspond with the line numbers given in table 1. This makes it possible to ascertain the wavenumber of any line in the observed spectrum.

The amount of gas was too large and the scanning speed was too rapid to properly measure the components of the lines in the P, Q, and R branches of the most intense component of ν_3. In figure 4 is shown the spectrum of the Q branch and the P branch of this component as observed with 0.1 mm of pressure of methane.

The $Q(F^{\circ})$ branch has very intense lines and the spectrum can be better represented by using less gas and scanning at a slower speed. The Q branch of this band, shown at the bottom strip of figure 5, was observed with a pressure between 0.1 and 0.01 mm and the scanning speed is one-third of that used in figure 4.

TABLE 1. *Vibration-rotation wavenumbers of methane from 2,450 to 3,200 cm^{-1}*

Line No.	cm^{-1}	Line No.	cm^{-1}	Line No.	cm^{-1}	Line No.	cm^{-1}	Line No.	cm^{-1}	Line No.	cm^{-1}
1	2450.87	60	2525.17	120	2557.55	181	2589.01	242	2618.90	300	2642.13
2	2451.10	61	2525.68	121	2559.83	182	2589.87	243	2618.94	301	2642.24
3	2452.32	62	2525.85	122	2560.00	184	2591.21	244	2619.03	302	2642.55
4	2452.87	63	2526.05	123	2560.20	185	2591.56	245	2619.59	303	2642.70
5	2459.59	64	2526.10	124	2560.57	186	2593.26	245a	2622.50	304	2642.98
6	2459.80	65	2527.38	125	2560.64	187	2593.91	246	2622.61	305	2643.22
7	2463.38	66	2527.46	126	2561.11	188	2593.99	247	2623.19	306	2643.29
8	2464.70	67	2527.94	127	2561.19	189	2594.60	248	2624.93	307	2643.64
9	2464.93	68	2528.46	128	2561.35	190	2594.65	249	2625.95	308	2643.72
10	2465.74	69	2528.81	129	2561.82	191	2595.18	250	2625.98	309	2643.82
11	2466.58	70	2529.88	130	2561.96	192	2595.79	251	2627.86	310	2644.18
12	2467.16	71	2530.96	131	2562.78	193	2596.43	252	2627.96	311	2644.24
13	2471.03	72	2531.08	132	2562.98	194	2596.66	253	2628.26	312	2644.65
14	2472.50	73	2531.46	133	2563.19	195	2597.09	254	2628.32	313	2645.04
15	2473.31	74	2533.09	134	2563.31	196	2597.28	255	2628.70	314	2645.09
16	2473.61	75	2534.53	135	2565.44	197	2597.34	256	2628.76	315	2645.73
17	2474.05	76	2535.99	136	2566.04	198	2597.52	257	2628.86	316	2646.04
18	2477.35	77	2536.45	137	2566.82	199	2598.13	258	2630.17	317	2646.24
19	2477.51	78	2536.49	138	2567.65	200	2598.27	259	2630.48	318	2646.40
20	2477.72	79	2536.68	139	2567.81	201	2598.36	260	2631.08	319	2646.58
21	2477.91	80	2536.88	140	2567.95	202	2598.53	261	2631.27	320	2646.84
22	2478.12	81	2537.01	141	2568.02	203	2598.65	262	2631.34	321	2647.08
23	2479.86	82	2537.17	142	2568.30	204	2598.76	263	2631.47	322	2647.31
24	2481.86	83	2537.33	143	2568.61	205	2598.88	264	2632.93	323	2647.42
25	2483.16	84	2537.39	144	2568.72	206	2598.92	265	2633.21	324	2647.50
26	2483.70	85	2538.72	145	2569.10	207	2598.97	266	2633.44	325	2648.66
27	2490.32	86	2539.17	146	2569.64	208	2599.27	267	2633.52	326	2649.14
28	2490.50	87	2539.48	147	2570.10	209	2599.52	268	2633.62	327	2649.52
29	2491.62	88	2542.94	148	2570.31	210	2599.57	269	2634.21	328	2649.61
30	2493.09	89	2543.08	149	2570.83	211	2599.64	270	2634.30	329	2649.71
31	2493.70	90	2543.55	150	2573.06	212	2599.79	271	2634.39	330	2649.83
32	2493.82	91	2543.92	151	2573.46	213	2599.93	272	2634.58	331	2650.74
33	2493.90	92	2544.00	152	2573.53	214	2600.27	273	2634.66	332	2651.02
34	2494.38	93	2545.28	153	2573.73	215	2600.58	274	2635.29	333	2651.50
35	2494.77	94	2545.35	154	2573.92	216	2601.06	275	2635.50	334	2651.81
36	2495.40	95	2545.39	155	2575.12	217	2601.49	276	2635.56	335	2652.29
37	2499.81	96	2545.68	156	2575.50	218	2601.86	277	2636.31	336	2652.42
38	2500.30	97	2546.42	157	2575.60	219	2601.92	278	2636.99	337	2652.59
39	2502.58	98	2546.54	158	2575.73	221	2602.66	279	2637.07	338	2652.92
40	2503.40	99	2546.66	159	2575.98	222	2602.76	280	2637.14	339	2653.85
41	2504.30	100	2546.84	160	2576.46	223	2603.02	281	2637.33	340	2654.58
42	2504.38	101	2547.12	161	2576.82	224	2603.13	282	2637.58	341	2654.72
43	2504.58	102	2547.27	162	2577.11	225	2603.57	283	2637.85	342	2654.98
44	2504.63	103	2547.36	163	2577.70	226	2603.66	284	2637.90	343	2655.54
45	2511.55	104	2547.62	164	2577.89	227	2603.77	285	2638.45	344	2655.68
46	2512.33	105	2549.59	166	2578.48	228	2603.86	286	2638.52	345	2655.85
47	2512.84	106	2550.26	167	2578.67	229	2604.32	287	2638.97	346	2655.96
47a	2512.92	107	2550.42	168	2579.09	230	2605.34	288	2639.18	347	2656.14
48	2514.50	108	2551.03	169	2582.01	230a	2605.52	289	2639.30	348	2656.21
49	2514.67	109	2551.74	170	2582.08	231	2605.75	290	2639.37	349	2656.36
50	2514.75	110	2551.84	171	2582.22	232	2607.25	290a	2639.60	350	2656.44
51	2514.90	111	2553.38	172	2582.39	233	2607.75	291	2639.71	351	2656.62
52	2514.96	112	2553.50	173	2583.35	234	2609.25	292	2639.76	352	2656.65
53	2515.14	113	2553.58	174	2583.52	235	2610.16	293	2639.83	353	2657.71
54	2515.31	114	2554.28	175	2584.42	236	2614.16	294	2640.00	354	2658.11
55	2515.45	115	2555.54	176	2584.73	237	2614.77	295	2641.41	355	2658.58
56	2515.66	116	2555.64	177	2586.59	238	2615.06	296	2641.54	356	2659.90
57	2516.28	117	2556.60	178	2588.30	239	2615.18	297	2641.66	357	2662.06
58	2517.58	118	2557.08	179	2588.40	240	2617.29	298	2641.85	358	2662.10
59	2519.84	119	2557.42	180	2588.64	241	2618.27	299	2642.03	359	2663.01

TABLE 1. *Vibration-rotation wavenumbers of methane from 2,450 to 3,200 cm⁻¹*—Continued

Line No.	cm⁻¹	Line No.	cm⁻¹	Line No.	cm⁻¹	Line No.	cm⁻¹	Line No.	cm⁻¹	Line No.	cm⁻¹
360	2663.28	450	2691.20	530	2712.94	619	2738.14	702	2767.96	784	2780.26
361	2663.38	451	2691.39	531	2713.05	620	2738.68	703	2768.06	785	2780.53
362	2663.48	452	2691.59	532	2713.66	621	2738.79	704	2768.27	786	2780.60
364	2664.51	353	2691.66	533	2714.22	622	2739.26	705	2768.45	787	2780.64
366	2664.77	453a	2692.31	534	2714.35	623	2740.24	705a	2768.52	788	2780.73
367	2664.96	454	2692.64	535	2714.43	624	2740.36	706	2768.59	789	2780.90
368	2665.07	455	2693.40	536	2714.76	625	2740.48	707	2768.64	790	2781.08
369	2665.16	456	2693.62	537	2715.06	626	2741.19	708	2768.91	791	2781.21
370	2665.27	457	2693.88	538	2716.84	627	2741.44	709	2768.94	792	2781.26
371	2666.28	458	2693.99	539	2717.07	628	2741.58	710	2769.05	793	2781.40
372	2666.47	459	2694.17	540	2717.21	629	2741.96	711	2769.21	794	2781.48
373	2666.53	460	2694.37	541	2717.29	630	2742.28	712	2769.32	795	2781.93
374	2667.13	461	2695.82	542	2717.42	631	2742.35	713	2769.43	796	2782.37
375	2667.46	462	2695.85	543	2717.95	632	2742.55	714	2769.52	797	2782.51
376	2667.74	463	2695.89	544	2718.05	633	2742.60	715	2769.67	798	2782.61
377	2667.94	464	2695.95	545	2718.13	634	2742.73	716	2769.73	799	2782.71
378	2668.10	465	2696.01	546	2718.20	636	2743.68	717	2769.78	800	2782.77
379	2668.24	466	2696.24	547	2719.46	637	2743.78	718	2769.88	801	2782.93
380	2668.85	467	2696.55	548	2719.62	638	2744.94	719	2770.04	802	2783.22
383	2669.25	468	2696.64	549	2720.10	639	2745.08	720	2770.20	803	2783.28
384	2669.41	469	2696.95	550	2720.15	640	2745.72	721	2770.32	804	2783.34
385	2669.70	470	2697.00	551	2720.78	641	2745.84	722	2770.45	805	2783.42
386	2669.92	471	2697.06	552	2720.90	642	2745.93	723	2770.62	806	2783.68
387	2670.20	472	2697.12	553	2721.13	643	2746.04	724	2770.76	807	2783.78
388	2670.32	473	2697.49	554	2721.23	644	2746.57	725	2770.82	808	2783.83
390	2670.54	474	2697.66	555	2721.38	645	2746.95	726	2770.94	809	2784.08
391	2671.28	475	2697.81	556	2721.49	646	2747.61	727	2771.05	810	2784.15
392	2671.53	376	2698.83	557	2721.78	647	2749.49	728	2771.18	811	2784.36
394	2672.12	477	2699.19	558	2721.90	648	2749.66	729	2771.27	812	2784.58
395	2672.22	478	2699.26	559	2721.94	649	2750.16	730	2771.43	813	2784.67
398	2673.35	478a	2700.37	560	2722.10	650	2750.20	731	2771.60	814	2784.76
399	2674.15	479	2701.51	561	2722.20	651	2750.45	732	2771.67	815	2784.90
400	2675.28	480	2701.61	562	2722.42	652	2750.62	733	2772.09	816	2785.01
401	2675.64	481	2701.90	563	2723.79	653	2750.88	734	2772.21	817	2785.10
402	2675.91	482	2702.03	564	2723.90	654	2751.31	735	2772.56	818	2785.20
403	2676.27	483	2702.10	565	2724.26	655	2752.40	736	2772.63	819	2785.26
404	2676.34	484	2702.40	566	2724.35	656	2752.60	737	2772.73	820	2785.32
405	2676.92	385	2702.66	567	2724.40	657	2752.99	738	2772.92	821	2785.68
406	2677.01	486	2702.72	568	2724.79	658	2753.07	739	2773.26	822	2785.72
407	2677.64	487	2702.81	569	2725.04	659	2753.24	740	2773.43	823	2786.10
408	2678.30	488	2703.31	570	2725.29	660	2753.33	741	2773.71	824	2786.26
409	2678.34	489	2703.59	571	2725.40	663	2753.75	742	2773.77	825	2786.42
410	2678.48	490	2704.11	572	2725.48	664	2756.37	743	2773.84	826	2786.63
411	2678.70	491	2704.32	573	2725.81	665	2756.46	744	2773.96	827	2786.82
412	2679.20	492	2704.56	574	2726.12	666	2756.61	745	2774.14	828	2786.88
413	2680.00	493	2704.61	575	2726.27	667	2756.71	746	2774.32	829	2787.07
414	2680.37	494	2704.73	576	2726.43	668	2756.88	747	2774.65	830	2787.21
415	2680.46	495	2704.82	577	2726.50	669	2756.98	748	2774.73	831	2787.28
416	2680.55	496	2705.13	578	2726.63	670	2757.14	749	2774.94	832	2787.44
417	2680.64	499	2706.17	580	2726.68	671	2757.46	750	2775.05	833	2787.51
418	2680.68	500	2706.34	581	2726.79	672	2757.58	751	2775.30	834	2787.84
419	2680.80	501	2706.40	582	2726.91	673	2757.82	752	2775.52	835	2788.19
420	2681.37	502	2706.50	583	2727.25	674	2758.13	753	2775.93	836	2788.32
421	2681.56	503	2706.76	584	2728.37	675	2758.54	754	2776.02	837	2788.39
422	2682.23	504	2707.15	585	2728.63	676	2759.10	755	2776.18	838	2788.43
423	2682.35	505	2707.28	586	2728.69	677	2759.18	756	2776.38	839	2788.60
424	2682.42	506	2707.64	587	2729.34	678	2759.27	757	2776.44	840	2788.72
425	2682.61	507	2708.52	588	2729.56	679	2759.63	758	2776.78	841	2788.76
426	2682.72	508	2708.73	589	2730.10	680	2759.70	759	2776.92	842	2788.84
427	2682.86	509	2708.82	590	2730.29	681	2759.92	760	2777.10	843	2788.94
429	2683.25	510	2709.05	591	2730.61	682	2761.35	761	2777.18	844	2789.15
430	2683.45	511	2709.41	592	2730.70	683	2762.34	762	2777.28	845	2789.55
431	2683.52	512	2709.51	593	2713.46	684	2762.47	763	2777.31	846	2789.66
432	2683.64	513	2709.91	594	2731.80	685	2762.65	764	2777.39	847	2789.77
433	2683.75	514	2710.08	597	2732.68	686	2763.33	765	2777.51	848	2789.93
434	2683.95	515	2710.96	598	2733.00	687	2763.40	766	2777.55	849	2790.06
435	2684.58	516	2711.27	599	2733.13	688	2764.30	767	2777.69	850	2790.23
436	2684.64	517	2711.32	601	2733.56	689	2764.74	768	2777.74	851	2790.30
437	2684.74	518	2711.41	602	2733.68	690	2764.83	769	2777.84	852	2790.42
438	2685.12	519	2711.46	603	2733.74	691	2765.06	770	2777.95	853	2790.56
439	2685.25	520	2711.49	604	2733.83	692	2765.20	771	2778.04	854	2790.60
441	2687.18	521	2711.58	605	2733.88	693	2765.72	774	2778.64	856	2791.03
442	2688.52	522	2711.71	606	2733.94	694	2766.02	776	2779.48	857	2791.10
443	2688.72	523	2711.76	607	2734.44	695	2766.68	777	2779.57	858	2791.17
444	2689.17	524	2711.95	610	2734.90	696	2767.18	778	2779.72	859	2791.24
445	2689.25	525	2712.05	611	2735.00	697	2767.23	779	2779.76	860	2791.47
446	2689.33	526	2712.11	613	2735.44	698	2767.48	780	2779.87	861	2791.75
447	2689.53	527	2712.14	614	2736.04	699	2767.62	781	2779.98	862	2792.14
448	2689.60	528	2712.27	617	2737.04	700	2767.70	782	2780.07	863	2792.22
449	2690.96	529	2712.36	618	2737.16	701	2767.86	783	2780.20	864	2792.24

TABLE 1. *Vibration-rotation wavenumbers of methane from 2,450 to 3,200 cm⁻¹*—Continued

Line No.	cm⁻¹	Line No.	cm⁻¹	Line No.	cm⁻¹	Line No.	cm⁻¹	Line No.	cm⁻¹	Line No.	cm⁻¹
865	2792.58	948	2813.72	1049	2836.48	1208	2876.66	1351	2901.05	1497	2925.62
865a	2793.33	949	2813.99	1049b	2836.67	1210	2876.95	1352	2901.30	1511	2928.14
866	2793.44	951	2814.70	1049d	2837.75	1211	2877.15	1353	2901.50	1512	2928.22
867	2793.55	952	2814.79	1049e	2837.97	1212	2877.29	1354	2901.85	1513	2928.42
868	2793.58	953	2815.00	1049h	2839.29	1213	2877.36	1355	2902.23	1514	2928.50
869	2793.68	954	2815.74	1051	2839.91	1214	2877.47	1356	2902.28	1515	2928.59
870	2793.74	955	2816.32	1052	2839.96	1215	2877.53	1357	2902.34	1516	2928.98
871	2794.64	957	2816.70	1053	2840.00	1216	2877.62	1358	2902.53	1517	2929.01
872	2794.76	958	2816.84	1054	2840.10	1217	2877.84	1368	2903.60	1518	2929.14
872a	2794.94	959	2816.90	1055	2840.33	1218	2877.97	1370	2903.83	1520	2929.53
873	2794.97	960	2817.06	1056	2840.36	1219	2878.02	1373	2904.48	1522	2929.74
875	2795.41	962	2817.88	1057	2840.46	1220	2878.16	1374	2905.07	1523	2929.89
876	2795.69	963	2818.55	1059	2840.71	1221	2878.33	1391	2907.56	1524	2930.01
877	2795.75	964	2818.63	1060	2840.75	1222	2878.58	1392	2907.92	1525	2931.41
878	2795.93	965	2818.86	1063	2841.21	1223	2878.62	1393	2908.29	1526	2931.72
879	2796.06	966	2819.82	1064	2841.61	1224	2878.81	1394	2908.52	1527	2931.96
880	2796.20	967	2820.03	1066	2842.14	1225	2878.84	1395	2908.72	1528	2932.08
880b	2796.62	968	2820.20	1068	2842.59	1226	2878.93	1396	2908.88	1529	2932.22
880c	2796.83	969	2820.26	1069	2842.72	1227	2879.26	1397	2909.23	1530	2932.87
880e	2797.10	970	2820.33	1070	2842.80	1228	2879.38	1399	2909.54	1531	2932.96
880f	2797.32	971	2820.51	1071	2843.06	1229	2879.93	1401	2909.85	1532	2932.99
880g	2797.52	973	2820.90	1072	2843.30	1230	2880.27	1402	2910.52	1533	2933.04
880h	2797.77	977	2821.59	1073	2843.33	1231	2880.39	1403	2910.62	1534	2933.13
880i	2797.84	978	2821.81	1074	2843.41	1232	2880.49	1404	2910.78	1535	2933.18
880j	2798.06	979	2821.94	1076	2844.01	1233	2880.70	1405	2910.95	1537	2933.33
881	2798.31	983	2822.37	1077	2844.49	1234	2880.86	1406	2911.15	1539	2933.59
882	2798.49	984	2822.47	1078	2844.56	1235	2881.07	1407	2911.24	1540	2933.70
883	2798.62	985	2822.72	1079	2844.67	1236	2881.22	1410	2911.59	1541	2934.01
884	2798.81	987	2823.05	1081	2844.91	1237	2881.26	1420	2912.70	1542	2934.08
885	2798.87	990	2823.34	1082	2845.30	1238	2881.73	1423	2913.08	1543	2934.17
886	2799.03	991	2823.46	1083	2845.40	1241	2882.39	1424	2913.15	1544	2934.20
887	2799.18	993	2823.89	1093	2847.14	1242	2882.47	1425	2913.27	1545	2934.33
888	2799.32	994	2824.00	1094	2847.68	1243	2882.52	1426	2913.32	1546	2934.38
889	2799.42	995	2824.14	1095	2848.48	1244	2882.69	1427	2913.58	1548	2934.94
892	2799.81	996	2824.86	1096	2849.29	1245	2882.78	1428	2913.76	1549	2935.13
893	2799.87	997	2824.99	1097	2850.79	1247	2882.97	1429	2913.81	1550	2935.25
894	2799.94	998	2825.19	1098	2851.38	1249	2883.42	1431	2914.02	1551	2935.37
896	2800.15	999	2825.28	1114	2855.61	1250	2883.68	1432	2914.47	1552	2935.44
898	2800.34	1001	2825.48	1115	2856.94	1251	2884.13	1433	2914.89	1554	2935.76
899	2800.84	1002	2825.60	1116	2857.10	1252	2884.28	1434	2915.24	1555	2935.81
900	2801.30	1003	2825.66	1117	2857.44	1271	2886.74	1435	2915.30	1556	2936.20
902	2802.10	1004	2825.74	1119	2857.90	1272	2887.30	1436	2915.39	1557	2936.63
904	2803.10	1005	2825.78	1120	2858.00	1273	2887.37	1437	2915.56	1572	2938.77
905	2803.21	1006	2826.35	1121	2858.11	1274	2887.57	1452	2917.68	1573	2938.82
907	2803.55	1007	2826.86	1122	2858.24	1275	2887.80	1453	2917.83	1574	2938.93
908	2803.84	1008	2827.49	1124	2858.78	1276	2887.95	1455	2918.03	1576	2939.27
909	2803.94	1009	2827.83	1126	2859.60	1277	2888.01	1456	2918.46	1578	2939.49
911	2804.19	1010	2828.06	1127	2859.96	1278	2888.18	1457	2918.71	1579	2939.61
912	2804.25	1010a	2828.11	1128	2861.09	1279	2888.31	1459	2919.09	1580	2939.80
913	2804.30	1011	2828.25	1129	2861.37	1280	2888.52	1460	2919.19	1581	2939.98
914	2804.46	1012	2828.40	1130	2861.61	1281	2888.66	1463	2919.70	1582	2940.50
915	2804.55	1013	2828.48	1131	2861.65	1281a	2888.70	1464	2919.88	1583	2940.64
917	2804.76	1014	2828.77	1148	2865.90	1283	2888.92	1465	2919.97	1584	2940.98
918	2804.86	1015	2829.56	1149	2866.11	1284	2889.03	1466	2920.16	1585	2941.38
919	2805.07	1018	2829.86	1151	2866.35	1291	2890.12	1467	2920.27	1587	2941.79
920	2805.23	1020	2830.07	1152	2866.65	1293	2890.63	1469	2920.58	1588	2942.08
921	2805.35	1021	2830.13	1153	2866.84	1296	2891.32	1470	2920.65	1589	2942.33
923	2805.66	1022	2830.58	1155	2867.09	1300	2891.90	1471	2921.30	1590	2942.65
924	2805.75	1023	2830.89	1156	2867.74	1304	2892.57	1472	2921.70	1591	2942.76
925	2805.90	1024	2830.94	1158	2868.21	1305	2893.51	1473	2921.91	1593	2943.03
926	2807.54	1025	2831.05	1159	2868.27	1306	2893.82	1474	2921.95	1594	2943.12
927	2807.61	1026	2831.25	1160	2868.69	1308	2894.07	1475	2922.10	1595	2943.19
928	2808.62	1027	2831.90	1161	2868.82	1309	2894.14	1476	2922.29	1596	2943.21
929	2808.73	1028	2831.95	1162	2868.90	1310	2894.22	1477	2922.44	1597	2943.30
930	2808.79	1029	2832.00	1164	2869.44	1312	2894.36	1478	2922.63	1599	2943.59
931	2809.02	1030	2832.16	1165	2870.35	1313	2894.42	1479	2922.88	1600	2943.66
933	2809.93	1032	2832.49	1166	2870.40	1314	2894.53	1480	2923.37	1601	2943.78
934	2810.07	1034	2832.86	1168	2870.87	1335	2897.35	1481	2923.42	1602	2943.99
935	2810.34	1035	2832.96	1169	2870.99	1336	2897.57	1482	2923.53	1603	2944.09
936	2810.48	1037	2833.56	1171	2871.30	1338	2897.75	1483	2923.65	1604	2944.12
937	2810.71	1039	2833.73	1173	2871.68	1339	2898.65	1484	2923.71	1605	2944.29
938	2811.05	1040	2834.45	1174	2872.32	1340	2899.23	1485	2923.77	1606	2944.46
939	2811.20	1041	2834.57	1175	2872.44	1341	2899.28	1486	2923.83	1607	2944.50
940	2811.75	1042	2834.94	1176	2872.67	1342	2899.36	1487	2923.91	1608	2944.69
942	2811.24	1043	2835.04	1178	2872.96	1343	2899.48	1488	2924.00	1609	2944.75
943	2812.48	1044	2835.23	1179	2873.01	1345	2899.88	1490	2924.62	1610	2945.01
944	2812.54	1045	2835.63	1180	2873.39	1346	2900.08	1491	2924.77	1611	2945.20
945	2812.69	1046	2835.90	1181	2873.53	1347	2900.28	1493	2925.27	1612	2945.40
946	2813.35	1047	2836.01	1206	2876.53	1348	2900.43	1495	2925.49	1613	2945.51
947	2813.55	1048	2836.22	1207	2876.62	1350	2900.67	1496	2925.56	1614	2945.62

TABLE 1. *Vibration-rotation wavenumbers of methane from 2,450 to 3,200 cm⁻¹*—Continued

Line No.	cm⁻¹	Line No.	cm⁻¹	Line No.	cm⁻¹	Line No.	cm⁻¹	Line No.	cm⁻¹	Line No.	cm⁻¹
1615	2945.92	1703	2962.51	1790	2976.56	1887	2999.12	2139	3034.24	2250	3063.20
1616	2945.95	1704	2962.64	1791	2976.66	1888	2999.20	2140	3034.32	2251	3064.19
1617	2946.05	1705	2962.70	1792	2976.79	1889	2999.32	2141	3034.48	2252	3064.40
1518	2946.25	1706	2962.87	1794	2977.16	1890	2999.46	2142	3034.68	2253	3064.50
1619	2946.48	1707	2963.00	1795	2977.34	1891	2999.68	2143	3034.78	2254	3065.58
1620	2946.65	1708	2963.10	1797	2977.87	1892	2999.81	2144	3034.81	2255	3066.28
1621	2947.09	1709	2963.15	1800	2978.21	1893	3000.00	2145	3035.14	2256a	3067.00
1633	2948.56	1710	2963.42	1801	2979.38	1895	3000.17	2146	3035.61	2257	3067.64
1634	3948.73	1711	2963.48	1802	2979.51	1896	3000.31	2147	3035.77	2258	3067.76
1635	2949.10	1712	2963.63	1803	2979.74	1897	3000.44	2152	3037.26	2259	3068.04
1636	2949.24	1713	2963.86	1804	2979.77	2021	3019.00	2153	3037.33	2260	3068.15
1637	2949.32	1714	2964.95	1805	2979.95	2022	3019.10	2155	3037.57	2261	3068.31
1638	2949.53	1715	2964.26	1806	2980.03	2023	3019.18	2157	3037.93	2262	3068.52
1639	2949.81	1716	2964.31	1807	2980.07	2024	3019.31	2158	3038.13	2262a	3068.59
1640	2949.89	1717	2965.51	1808	2980.19	2025	3019.47	2162	3038.69	2263	3068.98
1641	2950.13	1718	2964.60	1809	2980.39	2026	3019.58	2165	3039.27	2264	3069.16
1642	2950.33	1719	2964.78	1810	2980.59	2027	3019.62	2166	3039.42	2265	3069.24
1643	2950.52	1720	2964.86	1811	2980.73	2028	3019.67	2167	3042.06	2266	3069.42
1644	2950.65	1721	2964.94	1812	2980.84	2029	3019.81	2170	3042.41	2267	3069.54
1645	2950.85	1722	2965.09	1813	2981.08	2030	3019.88	2171	3042.57	2268	3069.63
1646	2951.30	1723	2965.28	1814	2981.17	2031	3020.02	2172	3042.73	2269	3069.72
1647	2951.38	1724	2965.45	1815	2981.31	2032	3020.15	2173	3043.59	2270	3069.79
1648	2951.56	1725	2965.51	1816	2981.46	2033	3020.22	2174	3043.74	2271	3070.01
1649	2952.04	1726	2965.59	1817	2981.59	2034	3020.38	2175	3043.79	2272	3070.13
1650	2952.11	1727	2965.74	1818	2982.26	2035	3020.46	2176	3043.90	2273	3070.22
1651	2952.40	1727a	2965.83	1819	2982.64	2036	3020.55	2177	3043.97	2274	3070.32
1652	2952.46	1728	2965.86	1820	2982.98	2037	3020.67	2178	3044.11	2275	3070.48
1653	2952.65	1729	2965.96	1821	2983.38	2038	3020.78	2179	3044.17	2276	3070.58
1654	2952.77	1730	2966.00	1822	2983.45	2039	3020.85	2180	3044.56	2277	3070.61
1655	2952.87	1731	2966.10	1823	2983.61	2040	3020.93	2181	3044.78	2278	3070.93
1656	2953.08	1732	2966.46	1824	2983.69	2041	3021.06	2182	3044.95	2279	3071.10
1657	2953.18	1733	2966.56	1825	2983.81	2042	3021.17	2183	3045.98	2281	3071.31
1658	2953.40	1734	2966.62	1827	2984.08	2043	3021.30	2184	3046.04	2282	3071.41
1659	2953.53	1735	2966.78	1828	2984.16	2044	3021.38	2185	3046.10	2283	3071.62
1660	2953.67	1736	2966.86	1831	2985.36	2045	3021.46	2186	3047.91	2284	3071.72
1661	2953.71	1737	2967.03	1832	2985.42	2046	3021.49	2190	3048.58	2285	3072.00
1663	2954.15	1738	2967.10	1836	2986.70	2047	3021.63	2191	3048.65	2286	3072.06
1664	2954.34	1739	2967.23	1837	2987.22	2048	3021.78	2192	3048.77	2287	3072.53
1665	2954.44	1740	2967.50	1838	2987.43	2049	3021.82	2193	3048.94	2288	3072.57
1666	2954.54	1741	2967.70	1839	2987.53	2051	3022.31	2194	3049.01	2289	3072.66
1667	2954.60	1742	2967.85	1840	2987.70	2052	3022.37	2196	3049.80	2290	3072.71
1668	2954.70	1744	2969.10	1841	2987.88	2053	3022.43	2198	3050.17	2291	3073.10
1669	2954.76	1745	2969.28	1842	2988.03	2056	3022.69	2199	3050.29	2292	3073.21
1670	2954.91	1746	2969.46	1843	2988.13	2057	3022.82	2204	3051.71	2293	3073.30
1671	2955.00	1747	2969.64	1844	2988.18	2058	3022.93	2206	3051.92	2294	3073.42
1672	2955.17	1748	2969.70	1845	2988.34	2059	3023.03	2209	3052.19	2295	3073.58
1673	2955.42	1749	2969.78	1846	2989.69	2060	3023.12	2211	3052.64	2296	3073.63
1674	2955.47	1750	2969.89	1847	2989.88	2073	3024.28	2213	3052.93	2298	3073.85
1675	2955.54	1751	2970.07	1848	2989.98	2074	3024.42	2216	3053.28	2299	3073.99
1676	2955.69	1752	2970.12	1849	2990.08	2075	3024.56	2217	3053.39	2300	3074.06
1677	2955.76	1753	2970.24	1850	2990.22	2076	3024.72	2218	3053.46	2301	3074.55
1678	2955.93	1754	2970.32	1851	2990.36	2077	3025.07	2219	3053.49	2302	3074.90
1679	2955.98	1755	2970.38	1852	2990.70	2080	3025.35	2220	3053.60	2303	3075.07
1680	2956.08	1756	2971.06	1853	2991.92	2081	3025.46	2221	3053.83	2304	3075.22
1680a	2956.13	1757	2971.27	1854	2991.99	2082	3025.57	2223	3054.64	2305	3075.41
1680b	2956.30	1758	2971.34	1855	2992.27	2083	3025.68	2225	3054.97	2306	3075.99
1680c	2956.39	1759	2971.59	1856	2992.53	2084	3025.73	2226	3055.06	2307	3076.13
1680d	2956.52	1761	2972.02	1857	2992.67	2085	3025.77	2227	3055.33	2308	3076.17
1680e	2956.63	1762	2972.15	1859	2993.19	2086	3025.82	2228	3055.65	2309	3076.36
1689f	2956.74	1763	2972.36	1860	2993.47	2087	3025.87	2229	3055.89	2313	3077.16
1681	2959.50	1767	2972.83	1861	2993.53	2088	3025.96	2231	3056.34	2314	3077.36
1682	2959.60	1768	2973.01	1862	2993.63	2089	3026.07	2231a	3056.53	2315	3077.44
1683	2959.73	1769	2973.18	1863	2993.73	2092	3026.35	2232	3057.90	2316	3077.53
1684	2959.85	1770	2973.23	1864	2993.84	2097	3026.79	2233	3058.18	2318	3077.87
1686	2960.20	1771	2973.56	1866	2994.14	2098	3026.94	2234	3058.80	2319	3077.95
1687	2960.38	1772	2973.62	1867	2994.29	2102	3027.30	2235	3058.95	2320	3078.02
1688	2960.66	1773	2973.77	1868	2994.46	2107	3027.88	2236	3059.47	2321	3078.12
1689	2960.77	1774	2974.57	1871	2995.46	2111	3028.82	2237	3059.73	2322	3078.77
1690	2960.86	1775	2974.83	1873	2996.16	2114	3029.17	2238	3059.89	2323	3078.82
1691	2960.94	1777	2975.01	1874	2996.60	2122	3030.21	2239	3059.94	2324	3079.04
1692	2961.14	1778	2975.09	1875	2996.88	2125	3030.68	2240	3060.10	2325	3079.13
1693	2961.32	1779	2975.13	1876	2996.99	2126	3030.73	2241	3060.79	2326	3079.27
1694	2961.43	1781	1975.68	1877	2997.71	2127	3030.85	2242	3060.84	2327	3079.44
1695	2961.65	1782	2975.74	1878	2997.96	2131	3031.71	2243	3061.42	2328	3079.58
1697	2961.85	1783	2975.78	1879	2998.10	2132	3031.77	2244	3061.49	2329	3079.66
1698	2961.99	1784	2975.86	1880	2998.27	2133	3031.91	2245	3061.69	2329a	3079.72
1699	2962.13	1785	2975.93	1881	2998.36	2134	3032.04	2246	3061.91	2330	3080.05
1700	2962.19	1786	2976.03	1882	2998.45	2135	3032.14	2247	3062.68	2331	3080.18
1701	2962.31	1788	2976.33	1883	2998.58	2137	3033.98	2248	3063.00	2332	3080.42
1702	2962.43	1789	2976.45	1884	2998.78	2138	3034.06	2249	3063.10	2333	3080.62

TABLE 1. *Vibration-rotation wavenumbers of methane from 2,450 to 3,200 cm⁻¹*—Continued

Line No.	cm⁻¹	Line No.	cm⁻¹	Line No.	cm⁻¹	Line No.	cm⁻¹	Line No.	cm⁻¹	Line No.	cm⁻¹
2334	3081.10	2380	3091.29	2425	3103.40	2473	3118.64	2533	3135.93	2605	3155.42
2336	3081.35	2381	3091.46	2426	3103.59	2474	3118.94	2534	3136.41	2606	3155.63
2338	3081.82	2382	3092.00	2427	3103.77	2475	3119.01	2535	3136.61	2607	3155.99
2339	3081.92	2383	3092.40	2428	3104.90	2476	3119.16	2536	3136.88	2608	3156.16
2340	3082.17	2384	3092.70	2429	3105.08	2477	3119.41	2538	3137.26	2609	3156.32
2341	3082.22	2385	3092.84	2430	3105.52	2478	3119.51	2539	3137.34	2610	3156.47
2342	3082.35	2386	3092.89	2432	3107.33	2479	3120 95	2540	3137.70	2611	3156.54
2343	3082.52	2387	3093.21	2433	3107.65	2480	3121.10	2541	3137.82	2612	3156:72
2344	3082.62	2388	3093.29	2434	3107.74	2481	3121.18	2542	3137.97	2613	3156.88
2345	3082.71	2389	3093.47	2435	3107.90	2482	3121.33	2543	3138.08	2614	3157.15
2346	3082.82	2390	3093.68	2436	3108.17	2484	3123.11	2544	3138.44	2615	3157.40
2347	3083.41	2391	3093.76	2437	3108.24	2485	3123.66	2545	3138.52	2620	3158.14
2348	3083.50	2392	3094.14	2438	3108.34	2486	3124.42	2546	3138.72	2621	3158.38
2349	3083.74	2393	3094.24	2439	3108.52	2487	3124.66	2547	3138.89	2622	3159.26
2350	3083.87	2394	3094.38	2440	3108.72	2488	3124.88	2549	3139.26	2623	3164.04
2351	3083.96	2395	3094.46	2441	3109.10	2489	3124.94	2550	3139.36	2624	3164.20
2353	3084.15	2396	3094.53	2442	3109.14	2490	3125.12	2557	3140.98	2625	3164.41
2354	3084.35	2397	3094.64	2443	3109.33	2493	3125.56	2558	3141.71	2628	3164.96
2355	3084.48	2399	3095.79	2444	3109.67	2494	3125.68	2559	3142.66	2629	3165.48
2355a	3084.81	2400	3095.95	2445	3109.79	2495	3125.72	2560	3142.77	2630	3165.61
2355b	3084.87	2401	3096.29	2446	3109.90	2496	3126.01	2561	3142.88	2635	3167.90
2355c	3084.92	2402	3096.66	2447	3110.33	2497	3126.44	2562	3143.98	2636	3168.25
2355d	3084.99	2403	3096.92	2448	3110.48	2498	3126.81	2563	3144.23	2637	3173.34
2356	3085.11	2404	3097.04	2449	3110.65	2499	3126.89	2564	3144.97	2638	3174.55
2357	3085.15	2405	3098.30	2451	3111.32	2501	3127.75	2567	3145.62	2642	3181.97
2358	3085.57	2406	3098.36	2452	3111.74	2502	3127.91	2568	3145.70	2643	3182.20
2360	3087.19	2407	3098.52	2453	3111.91	2503	3127.97	2569	3145.95	2650	3184.83
2361	3087.27	2408	3098.66	2454	3112.03	2504	3128.53	2570	3146.41	2651	3185.24
2362	3087.34	2409	3098.80	2455	3112.13	2505	3128.59	2571	3146.78	2652	3191.29
2363	3087.44	2410	3098.88	2456	3112.20	2506	3128.92	2572	3146.89	2653	3191.36
2364	3087.55	2410a	3099.14	2457	3112.39	2507	3129.05	2575	3147.25	2654	3191.70
2365	3087.66	2411	3099.28	2458	3112.77	2508	3129.18	2576	3147.40	2655	3192.00
2365a	3087.71	2412	3099.34	2459	3114.50	2513	3130.34	2577	3147.53	2656	3196.09
2366	3087.82	2413	3099.50	2461	3114.50	2519	3132.09	2581	3148.14	2657	3197.84
2367	3088.14	2414	3099.69	2462	3114.71	2520	3132.25	2594	3149.77	2658	3199.57
2368	3088.40	2415	3099.81	2463	3114.86	2523	3133.06	2595	3150.54	2659	3199.67
2369	3088.68	2416	3099.98	2464	3114.93	2524	3134.52	2596	3150.63	2660	3199.69
2369a	3088.77	2417	3100.05	2465	3115.27	2525	3134.64	2597	3150.76	2661	3200.26
2370	3088.86	2418	3100.35	2466	3115.42	2526	3134.95	2598	3151.34		
2371	3088.90	2419	3100.65	2467	3115.88	2527	3135.04	2599	3153.05		
2372	3089.04	2420	3100.72	2468	3117.42	2528	3135.09	2600	3153.19		
2373	3089.75	2421	3101.17	2469	3117.90	2529	3135.28	2601	3153.44		
2374	3089.90	2422	3102.51	2470	3118.12	2530	3135.42	2602	3153.56		
2375	3090.01	2423	3103.06	2471	3118.27	2531	3135.58	2603	3154.78		
2376	3090.19	2424	3103.30	2472	3118.55	2532	3135.78	2604	3154.88		

The two upper strips of figure 5 represent the $R(F^-)$ branch of the ν_3 band as observed with 0.2-mm pressure. The regions between the successive R lines were not recorded as at this low pressure very few lines were observed. Some lines of the atmospheric water band, $2\nu_2$, overlap this region and they are marked by small circles. The atmospheric water vapor lines are much broader than the methane lines on account of pressure broadening and they can be identified easily.

In table 2 the wavenumbers of the lines of the P, Q, and R branches are listed. This table applies to the experimental results shown in figures 4 and 5. The lines in the P and R branches are grouped under the J values so they can be related to the observed spectrum.

4. Discussion of Results

The spectrum of methane recorded in figures 1, 2, and 3 shows many lines which may be associated with several bands. The most prominent band is the allowed component of ν_3 which has $P(F^+)$,$Q(F^\circ)$, and $R(F^-)$ branches. The P, Q, and R branches of this band have been split into several components for each J as is shown by the experimental results in figures 4 and 5. Other normally forbidden transitions with components comprising the $P(F^\circ)$, $P(F^-)$, $Q(F^-)$, $R(F^\circ)$, and $R(F^+)$ branches occur in the same region as the strong component of ν_3, but with much less intensity. The $Q(F^+)$ branch is the prominent feature near 3021.18 cm^{-1}. Other lines in this region may arise from isotopic molecules and from hot bands. Boyd and Thompson [8] showed the presence of a hot band in this region by measuring the absorption spectrum at elevated temperatures. There appears to be some experimental evidence for a weak Q branch at 3070 cm^{-1}. The Raman spectra shows an intense line in this region and it has been classified as $2\nu_2$. If the forbidden components of this band become active by interactions, there would be a total of two Q branches. A double type Q branch is observed in the region from 2820 to 2835 cm^{-1} which is one component of $\nu_2+\nu_4$. If all transitions are active there is a possibility for six components of this band. The ν_1 band, which arises from the totally symmetric vibration at 2914.4 cm^{-1}, is the most intense in the Raman spectrum, but there is no evidence of a Q branch in this region of the observed spectrum. That is, at a pressure of 2 cm for a cell length of 6 m this band is not observed.

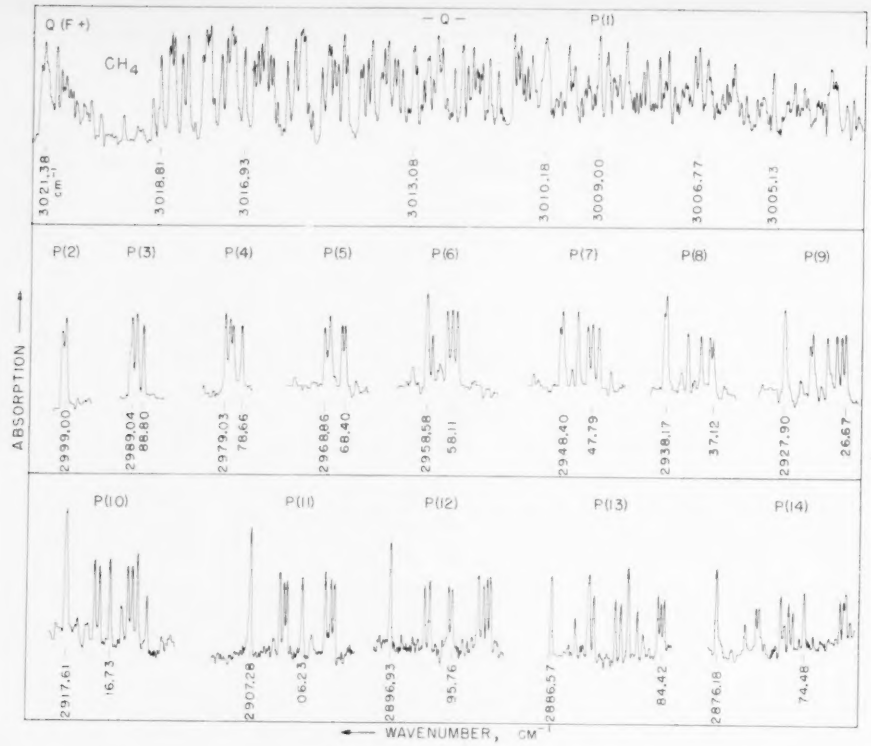

FIGURE 4. *The* $Q(F^+)$ *and* $Q(F^\circ)$ *branches and the* $P(F^+)$ *branch of* ν_3 *of methane as measured with slow scanning speeds and a pressure 0.1 mm in a 6-m cell.*

The regions between consecutive J's were omitted.

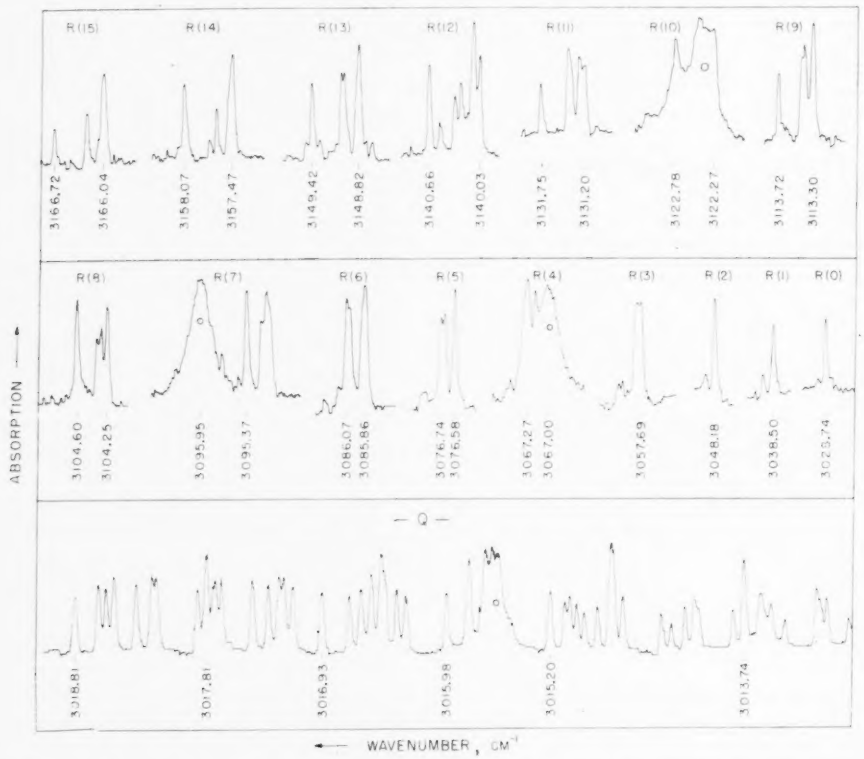

FIGURE 5. *The* $R(F^-)$ *branch of methane as measured with a pressure 0.2 mm and the* $Q(F^\circ)$ *branch as measured with a pressure* <0.1 *mm.*

TABLE 2. *Vibration-rotation wavenumbers for the ν_3 fundamental band of methane at 3018.9 cm^{-1} at low pressures*

P	cm^{-1}	Line No.	*R*	cm^{-1}	Line No.	*Q*	cm^{-1}	Line No.
			0	3028.744	2110		3018.815	2020
							3018.649	2019n
1	3009.000	1975	1	3038.498	2160		3018.602	2019m
							3018.533	2019l
							3018.349	2019k
2	2999.057	1886	2	3048.180	2188		3018.230	2019j
	2999.000	1885					3018.210	2019i
							3017.874	2019h
3	2989.045	1845d	3	3057.692	2231b$_1$		3017.820	2019g
	2988.945	1845c		3057.739	2231b$_2$		3017.748	2019f
	2978.800	1845b					3017.708	2019e
							3017.453	2019d
4	2979.033	1800d	4	3067.167	2256a		3017.325	2019c
	2978.937	1800c		3067.266	2256b		3017.245	2019b
	2978.872	1800b					3017.167	2019a
	2988.656	1800a					3016.930	2019
							3016.730	2018f
5	2968.861	1743d	5	3076.576	2310		3016.640	2018e
	2968.748	1743c		3076.696	2310a		3016.573	2018d
	2968.456	1743b		3076.738	2311		3016.480	2018c
	2968.404	1743a					3016.384	2018b
							3016.304	2018a
6	2958.636	1680p	6	3085.862	2358a		3015.978	2018
	2958.508	1680o		3086.046	2358b$_1$		3015.790	2017b
	2958.430	1680n		3086.070	2358b$_2$		3015.660	2017a
	2958.210	1680m					3015.549	2017
	2958.109	1680l					3015.208	2016f
	2958.009	1680k						
7	2948.465	1632	7	3095.110	2397a			
	2948.405	1631		3095.174	2397b			
	2948.230	1629		3095.368	2397c			
	2948.120	1628		3095.680	2398			
	2948.081	1627						
	2947.888	1625						
	2947.792	1624						
	2947.660	1623						
	2947.415	1622						
8	2938.222	1569	8	3104.248	2427a			
	2938.168	1568		3104.309	2427b			
	2937.928	1566		3104.374	2427c			
	2937.900	1565		3104.598	2427d			
	2937.736	1564						
	2937.620	1563						
	2937.456	1562						
	2937.260	1560						
	2937.208	1559						
9	2927.932	1510	9	3113.300	2458a			
	2927.903	1509		3113.403	2458b			
	2927.378	1506		3113.423	2458b$_1$			
	2927.342	1505		3113.720	2458c$_2$			
	2927.025	1503						
	2926.837	1501						
	2926.750	1500						
	2926.670	1499						
10	2917.610	1451	10	3122.272	2482a			
	2917.032	1447		3122.382	2482b			
	2916.938	1446		3122.435	2482c			
	2916.730	1445		3122.775	2483			
	2916.480	1444						
	2916.373	1443						
	2916.293	1442						
	2916.173	1441						
	2915.983	1440						
11	2907.285	1390	11	3131.197	2515			
	2906.688	1385		3131.259	2515a			
	2906.592	1384		3131.382	2516			
	2906.560	1383		3131.749	2518			
	2906.232	1381						
	2906.062	1380						
	2905.770	1377						
	2905.647	1376						
	2905.507	1375						
12	2896.932	1333	12	3140.028	2551			
	2896.253	1330		3140.107	2552			
	2896.157	1329		3140.235	2553			
	2895.765	1325		3140.320	2554			
	2895.705	1324		3140.515	2555			
	2895.187	1320		3140.660	2556			
	2895.078	1319						
	2895.000	1318						
	2894.960	1317						

TABLE 2. *Vibration-rotation wavenumbers for the ν_3 fundamental band of methane at 3018.9 cm^{-1} at low pressures*—Continued

P	cm^{-1}	Line No.	*R*	cm^{-1}	Line No.	*Q*	cm^{-1}	Line No.
13	2886.570	1270	13	3148.815	2587			
	2886.070	1268		3149.010	2588a			
	2885.813	1266		3149.050	2588b			
	2885.718	1265		3149.095	2589			
	2885.310	1262		3149.345	2591			
	2885.190	1261		3149.423	2592			
	2885.050	1260		3149.480	2593			
	2884.867	1258						
	2884.720	1257						
	2884.620	1256						
	2884.463	1255						
	2884.413	1254						
	2884.348	1253						
14	2876.182	1205	14	3157.470	2616			
	2875.622	1202		3157.660	2617			
	2875.402	1200		3157.730	2618			
	2875.368	1199		3158.070	2619			
	2874.937	1195						
	2874.873	1194						
	2874.783	1193						
	2874.693	1192						
	2874.558	1190						
	2874.477	1189						
	2873.790	1185						
	2873.723	1184						
	2873.695	1183						
	2873.603	1182						
15	2865.770	1147	15	3166.040	2631			
	2865.340	1146		3166.270	2632			
	2864.952	1144		3166.490	2633			
	2864.683	1143		3166.720	2634			
	2864.403	1142						
	2864.213	1141						
	2863.960	1140						
	2863.890	1139						
	2863.110	1138						
	2863.040	1137						
	2863.005	1136						
	2862.930	1135						
16	2854.577	1112	16	3174.80	2639			
	2854.507	1111		3175.22	2640			
	2854.137	1110		3178.08	2641			
	2853.912	1109						
	2853.863	1108						
	2853.663	1107						
	2853.420	1106						
	2853.310	1105						
	2853.217	1104						
	2852.377	1102						
	2852.310	1101						
			17	3183.01	2644			
				3183.14	2645			
				3183.23	2646			
				3183.37	2647			
				3183.46	2648			
				3183.66	2649			

In figure 3 there is a concentration of lines near 2600 cm^{-1} which is a Q branch of $2\nu_4$. Since ν_4 is triply degenerate $2\nu_4$ could, with Coriolis interactions, consist of six separate subbands and may account for the large number of lines observed in the region from 2470 to 2650 cm^{-1}.

Many features of the spectrum have been explained on the basis of the theoretical work of Jahn [9]. His calculations of the Coriolis interactions carried to a second order approximation have explained the splitting of the lines of the P, Q, and R branches into components. However his results are not adequate to give a quantitative agreement with the experimental results given in this paper. In order to properly account for the observed spectrum still higher order corrections must be included. A theoretical treatment of the spectrum of CH_4, which has recently been carried out by Professor Karl Hecht of the University of Michigan, should make possible a better detailed analysis than is known at present. He has obtained excellent agreement with the experimental results for the ν_3 band for values of $J \lesssim 8$, and a good agreement for values of $J > 8$. His results will appear in a separate publication.

5. References

[1] D. M. Dennison, Astrophys. J. **62,** 84 (1925).
[2] J. S. Burgess, E. E. Bell, and H. H. Nielsen, J. Opt. Soc. Am. **43,** 1058 (1953).
[3] H. C. Allen, Jr., and Earle K. Plyler, J. Chem. Phys. **26,** 972 (1957).
[4] A. H. Nielsen and H. H. Nielsen, Phys. Rev. **48,** 864 (1935).
[5] W. H. T. Childs and H. A. Jahn, Proc. Roy. Soc. [A] **169,** 451 (1939).
[6] Earle K. Plyler and L. R. Blaine, J. Research NBS **62,** (1959) RP2922
[7] Earle K. Plyler, L. R. Blaine, and Eugene D. Tidwell, J. Research NBS **55,** 279 (1955) RP2630.
[8] D.R.J. Boyd and H.W. Thompson, Proc. Roy. Soc. [A] **213,** 42 (1952).
[9] H. A. Jahn, Proc. Roy. Soc. [A] **171,** 450 (1939).

WASHINGTON, D.C. (Paper 64A3–44)

JOURNAL OF RESEARCH of the National Bureau of Standards—A. Physics and Chemistry
Vol. 64A, No. 3, May–June 1960

Elastic Constants of Synthetic Single Crystal Corundum at Room Temperature

J. B. Wachtman, Jr., W. E. Tefft, D. G. Lam, Jr., and R. P. Stinchfield

(January 21, 1960)

The six elastic constants (and six elastic compliances) of corundum were determined in the kilocycle per second frequency range by an accurate resonance method. The results were checked in the megacycle per second range with a less accurate, pulse velocity method. The elastic moduli for polycrystalline alumina calculated from the single crystal compliances determined by the resonance method are in good agreement with experimental values obtained on high density polycrystalline alumina. The variation of Young's modulus and of the shear modulus with orientation was calculated from the compliances and the results are shown graphically. The results of the present work do not agree well with previous work on single crystal sapphire. The specification of orientation and the theory used to calculate the elastic constants are given in detail to support the contention that the results of the present work are correct.

1. Introduction

The purpose of the present paper is to present a set of values for the elastic constants of single crystal corundum [1] at room temperature and to argue that these values are correct despite the fact that they disagree with values reported in three other investigations. Fifty-six independent measurements on 29 different specimens yielded consistent results for the six elastic constants which this material should have.[2]

The complete set of six elastic compliances and six elastic constants were first reported by Sundara Rao [1] [3] for synthetic sapphire. A similar determination was made by Bhimasenachar [2] using natural sapphire; very good agreement with Sundara Rao was found except for c_{33}. More recently, Mayer and Hiedemann [3] have redetermined the elastic constants and compliances for synthetic sapphire with results which are rather different from the previous investigators' values. Mayer and Hiedemann suggest possible causes of incorrect resonance frequency measurements in the experimental method used by the Indian workers.

The present work began with measurements of Young's modulus which were intended as the basis of a study of the changes in elastic moduli and internal friction as a function of temperature. These Young's modulus values permit calculation of four compliance constants which were found to be inconsistent with either of the previously reported sets of compliance constants. All of the previous work was done at frequencies in the megacycle per second range, but the present determination of Young's modulus values was made in the low kilocycle per second range. A possible frequency dependence thus required consideration. The present authors undertook a broadened program with the objectives of determining a complete set of elastic constants in the kilocycle per second range and checking the results in the megacycle per second range. The results of the broadened investigation are reported in this paper.

In all the work discussed so far the classical theory of elasticity was used. This classical theory has been considered correct for more than 50 years and is still accepted by most scientists. Briefly, it assumes a linear relationship (Hooke's law) between 6 independent components of stress and 6 independent components of strain. The theory leads to 21 independent elastic constants for the most general nonisotropic medium such as a crystal with no symmetry, and to 6 independent constants for a crystal with the symmetry of sapphire. This theory was challenged in 1951 by Laval who asserted that there are 9 independent components of stress and 9 independent components of strain which would lead to 45 independent elastic constants for a crystal with no symmetry. This idea was developed by Laval and Le Corre, and independently by Raman and his collaborators. A good list of references is given by Joel and Wooster [4]. For the case of crystals with the symmetry of sapphire, Raman [5] asserts that there are 10 independent constants instead of 6 as in the classical theory. If this generalized theory were correct, discrepancies in reported values of elastic constants might result from analysis of data in terms of a 6 constant theory when a 10-constant theory should have been used. However, results of the present work show that the classical,

[1] Corundum is pure aluminum oxide, Al_2O_3, in the stable, α phase. The term sapphire is used synonymously in this paper.
[2] A generalized theory, due to Laval and Raman, requires 10 constants and is discussed later.
[3] Figures in brackets indicate the literature references at the end of this paper.

6-constant theory represents the elastic behavior of sapphire in the kilocycle frequency range quite well. All equations in this paper are based on the classical theory. Because the present results do disagree with previous work, this paper presents the theory and experimental procedure in some detail.

2. Specification of Crystal Orientation

The values of the elastic constants (or compliances) of a nonisotropic material depend upon the choice of coordinate system. The use of a rectangular coordinate system is conventional. For each crystalline material, the orientation of this rectangular coordinate system is usually chosen to take maximum advantage of its point group symmetry, and the use of this system is implied when elastic constants are discussed. In this section the coordinate system appropriate for sapphire (called the $x_1x_2x_3$ system) is described in terms of the point group symmetry and the back reflection Laue pattern. Elastic property measurements on a crystal must be related to this coordinate system in order to interpret the results of the measurements in terms of elastic constants. The line in a specimen along which Young's modulus, the shear modulus, or the velocity of sound was measured, will be referred to as the specimen axis (SA). It is convenient to distinguish between the opposite ends of this line and the reference end will be taken as positive (+SA).

The point group of sapphire is $3m$ [6]. Figure 1 is a stereographic projection showing the symmetry elements, the rectangular system $x_1x_2x_3$ to which the elastic constants are referred, and the hexagonal coordinate system $xyuz$ which is used for Miller-Bravais indices. This notation for both systems is used by Nye [7] and will be used throughout this paper to refer to these coordinate systems.

Figure 2 shows a stereographic projection of prominent poles in a back reflection Laue pattern of sapphire. Figure 2a shows the letter symbols of

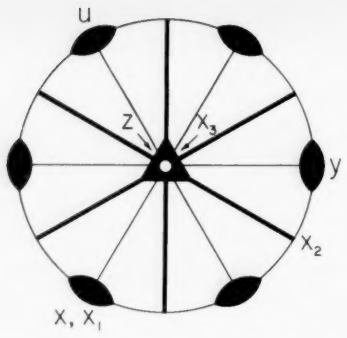

FIGURE 1. *Stereogram of point group* $\bar{3}$ m.

The heavy lines indicate mirror planes, the open triangle indicates the $\bar{3}$ axis, and the diad symbols indicate 2-fold axes. $x_1x_2x_3$ is the right-handed coordinate system used for elastic constant specification. $x\ y\ u\ z$ is the Miller-Bravais coordinate system.

morphological crystallography [8] which can be assigned by measuring the angles between poles. This process is without ambiguity and is described in section 6. Figure 2b shows the Miller-Bravais indices for the conventional choice of coordinate system. Figure 2a is based on angular values obtained from Winchell [8]. The recent X-ray pattern by Swanson and Fuyat [9] gives $c/a=1.365$ for the morphological unit cell. The distinction between the morphological and the structural cells is discussed by Kronberg [10].

The $x_1x_2x_3$ system is not uniquely defined by figure 1 alone. Any 1 of 6 directions might be chosen for $+x_1$; i.e., $+x_1$ might be chosen in either direction along any of the three 2-fold axes. However, opposite ends of a 2-fold axis can be distinguished even though point group $3m$ has a center of symmetry. The opposite ends are designated $+a$ and $-a$ in figure 2a. The distinction between $+a$ and $-a$ is illustrated in figure 3. The three $+a$ directions can be identified by examining the neighboring points on the stereographic projection. The choice of which is to be called $+a$ and which $-a$ is, of

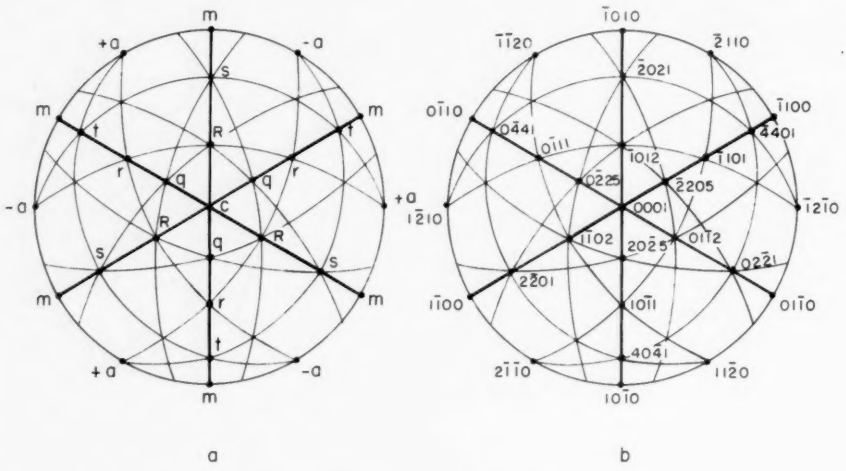

a b

FIGURE 2. *Stereograms of poles of prominent planes in sapphire.*

Figure 2a shows the letter symbols which can be assigned by measuring the angles between poles. Figure 2b gives the Miller-Bravais indices which require a choice of coordinate system.

course, a convention. This choice is important because the sign of the elastic compliance s_{14} depends upon it.[4] No convention for this choice for a nonpiezoelectric crystal is given by Nye [7] or by the *Standards on Piezoelectric Crystals* [11]. The convention used here has been chosen to agree with that implied by figure 151 from Phillips [12], by figure 2 from Kronberg [10], and by figure 5 and table 1 from Winchell [8]. The angles specifying the orientation of the specimen axis are shown in figure 4. Theta, the colatitude, or zenith angle, is the angle between $+x_3$ and SA. Phi is the angle in the x_1x_2 plane from $+x_1$ to the projected specimen axis (PSA). The angle θ is exactly the same as the angle ρ used by Winchell [8]. However, his angle ϕ is measured from $-a$ instead of from $+a$ and is measured clockwise (looking in the $-x_3$ direction). Winchell's definition of ϕ is not used here because we wish to adhere to the usual spherical polar angles in a right-handed system.

[4] This can be seen by examining a coordinate system $y_1y_2y_3$ with $y_1=-x_1$. If $y_3=x_3$, then one must have $y_2=-x_2$ to maintain right-handedness. Examination of the transformation of s_{14} shows that it is equal in magnitude but opposite in sign when expressed in the $y_1y_2y_3$ system.

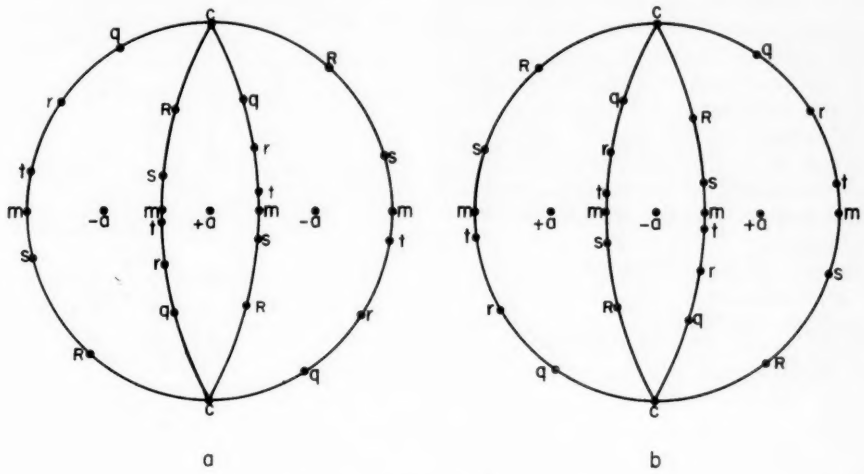

FIGURE 3. *Distinction between* +a *and* −a.

The stereogram in figure 3a is centered on $+a$ and shows that the sequence of poles $m\ t\ r\ q\ c\ R\ s$ in the nearer mirror planes has counterclockwise sense. Figure 3b, centered on $-a$, shows that the corresponding sequence has clockwise sense.

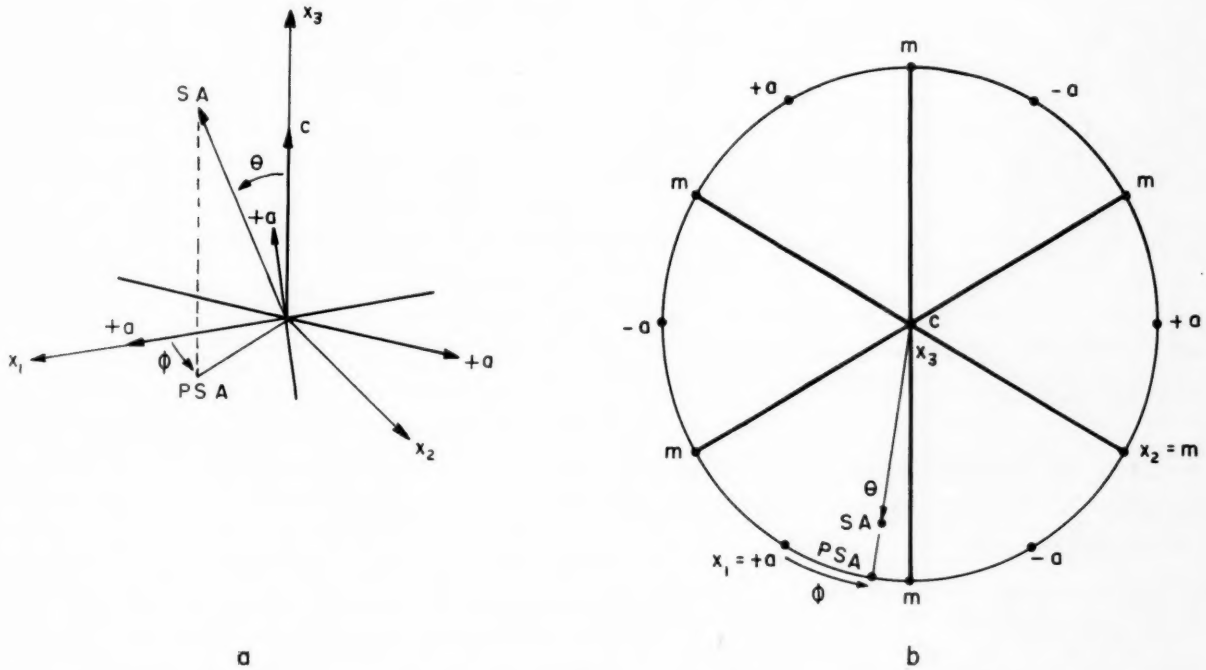

FIGURE 4. *The angles used in specifying the direction of the specimen axis, SA, and its projection, PSA, in the* x_1x_2 *plane.*

4a shows a perspective of the important orientation angles. 4b shows a stereographic representation of the orientation angles.

In discussing the range of θ and ϕ it is convenient to introduce the concept of the asymmetric triangle, which is the largest spherical triangle on a stereogram not containing any symmetry related directions. Any direction outside this triangle has a symmetry related direction within it.

The range $0° \leq \theta \leq 90°$ and $-30° \leq \phi \leq 30°$ is sufficient to specify the orientation. That is, on a stereographic projection the range $0° \leq \theta \leq 90°$ and $-30° \leq \phi \leq 30°$ defines an asymmetric spherical triangle. However, this range of ϕ is not sufficient to distinguish between equivalent points with mirror-image environment. For example, the environment of $(11\bar{2}0)$ is the mirror image of the environment of $(2\bar{1}\bar{1}0)$. To distinguish such directions a range of $0° \leq \theta \leq 90°$ and $-30° \leq \phi \leq 90°$ is useful, and Kebler and Rudness [13] have recommended the use of this range in specifying the orientation. The range of $-30° \leq \phi \leq +30°$ is adequate for specifying any physical property, such as elastic properties, which depend only on the direction of measurement and not upon the left-handed or right-handed distribution of neighboring points.

In carrying out the actual measurement of ϕ either of two equivalent methods may be used. In the first method ϕ is measured from PSA to x_1 and the fact that $\phi = 30° + \delta$ is equivalent to $\phi = 30° - \delta$ is used to reduce any values larger than 30° to the range $-30° \leq \phi \leq 30°$. In the second method ϕ is measured from PSA to the nearest a-type direction without regard to whether it is $+a$ or $-a$. The rule shown in figure 5 is then used to determine the sign of ϕ.

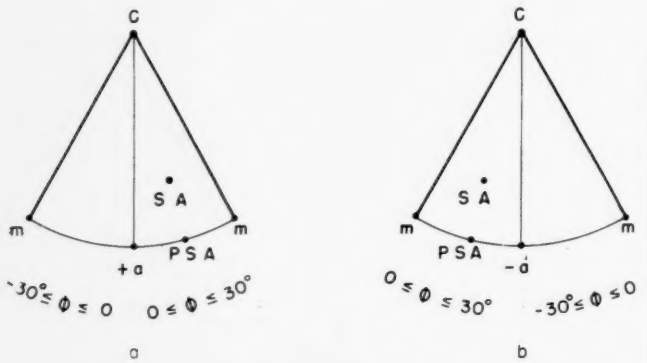

FIGURE 5. *Stereograms illustrating the sign convention for ϕ.*

Note that the position of SA must be considered. The sign of ϕ cannot be determined from the position of PSA alone.

3. Relation of Young's Modulus and Shear Modulus to Elastic Compliances and to Orientation

The stresses σ_i, and the strains, ϵ_i, will be written in Nye's matrix notation [7]. Hooke's law can be written in terms of the elastic constants, c_{ij}, as

$$\sigma_i = \sum_j c_{ij} \epsilon_j \qquad (1)$$

or in terms of the elastic compliances, s_{ij}, as

$$\epsilon_i = \sum_j s_{ij} \sigma_j \qquad (2)$$

where the matrix of the s_{ij} is the inverse of the matrix of the c_{ij}. For any material, $c_{ij} = c_{ji}$ (and $s_{ij} = s_{ji}$) which reduces the number of independent constants (or compliances) to 21. For sapphire, the symmetry of point group $\bar{3}m$ further reduces the number of independent elastic constants (or compliances) to six and the resulting matrices are shown in table 1.

TABLE 1. *Elasticity matrices*

General elastic constant matrix

c_{11}	c_{12}	c_{13}	c_{14}	c_{15}	c_{16}
c_{12}	c_{22}	c_{23}	c_{24}	c_{25}	c_{26}
c_{13}	c_{23}	c_{33}	c_{34}	c_{35}	c_{36}
c_{14}	c_{24}	c_{34}	c_{44}	c_{45}	c_{46}
c_{15}	c_{25}	c_{35}	c_{45}	c_{55}	c_{56}
c_{16}	c_{26}	c_{36}	c_{46}	c_{56}	c_{66}

Elastic constant matrix for sapphire referred to the coordinate system $x_1x_2x_3$

c_{11}	c_{12}	c_{13}	c_{14}	0	0
c_{12}	c_{11}	c_{13}	$-c_{14}$	0	0
c_{13}	c_{13}	c_{33}	0	0	0
c_{14}	$-c_{14}$	0	c_{44}	0	0
0	0	0	0	c_{44}	c_{14}
0	0	0	0	c_{14}	$\frac{1}{2}(c_{11}-c_{12})$

Elastic compliance matrix for sapphire referred to the coordinate system $x_1x_2x_3$

s_{11}	s_{12}	s_{13}	s_{14}	0	0
s_{12}	s_{11}	s_{13}	$-s_{14}$	0	0
s_{13}	s_{13}	s_{33}	0	0	0
s_{14}	$-s_{14}$	0	s_{44}	0	0
0	0	0	0	s_{44}	$2s_{14}$
0	0	0	0	$2s_{14}$	$2(s_{11}-s_{12})$

In relating the elastic compliances to Young's modulus, it is necessary to distinguish between the "free" Young's modulus, E_f, and the "pure" Young's modulus, E_p, when analyzing flexural or torsional tests. The free Young's modulus is the value obtained when the specimen is completely free to deform elastically under the applied tensile stress. The pure Young's modulus is the value obtained when the specimen is tested in flexure and is prevented from twisting. In an isotropic medium the free and pure moduli are identical. Calculation of Young's modulus from flexural vibrations of long, thin rods of nonisotropic material corresponds to measurement of E_f. A similar distinction must be made with the shear modulus, G. For rods of nonisotropic material of the dimensions used in this work, the modulus determined from torsional vibrations is very accurately the pure shear modulus, G_p. The proof that E_f and G_p are the measured quantities involves the substitution in equations given by Hearmon [14] and by Brown [15]. We shall omit the proof here and give the results connecting the quantities determined experimentally, E_f and G_p, with the elastic compliances. Consider a rectangular coordinate system $x_1'x_2'x_3'$ with the x_3' axis along SA. For stress application along the x_3' axis [14, 15]:

$$s'_{33}=\frac{1}{E_f}, \tag{3}$$

$$\frac{s'_{44}+s'_{55}}{2}=\frac{1}{G_f}, \tag{4}$$

$$G_f=G_p(1-\epsilon'), \tag{5}$$

where

$$\epsilon'=\frac{s'^2_{34}+s'^2_{35}}{s'_{33}(s'_{44}+s'_{55})}. \tag{6}$$

Equations (4), (5), and (6) can be combined to give

$$\frac{1}{G_f}=\frac{1}{G_p}+\frac{s'^2_{34}+s'^2_{35}}{2s'_{33}}, \tag{7}$$

which is a more useful relation between G_p and G_f than eq (5).

The primed quantities in eqs (3), (4), and (7) must be related to the orientation and to the elastic compliances measured in the $x_1x_2x_3$ system. It can be shown [14] that the values of s'_{33}, $s'_{44}+s'_{55}$, and $s'^2_{34}+s'^2_{35}$ depend only upon the direction of x'_3 and not upon the direction of x'_1 and x'_2. Accordingly x'_1 and x'_2 were chosen to simplify the transformation equations as much as possible subject to the condition that $x'_1x'_2x'_3$ form a right-handed rectangular set. This was accomplished by choosing x'_2 to lie in the x_1x_2 plane, then choosing x'_1 orthogonal to x'_2 and x'_3. The relation of $x'_1x'_2x'_3$ to $x_1x_2x_3$ is shown in figure 6.

Equation 25 on page 70 and equation 10 on page 61 of Cady [16] give the general transformation for s'_{33} and $s'_{44}+s'_{55}$ respectively. An error in sign was found in 12 of the last 18 terms of the equation for $s'_{44}+s'_{55}$. When this error is corrected, the resulting expressions are:

$$s'_{33}=\frac{1}{E_f(\theta,\phi)}=s_{11}\sin^4\theta+s_{33}\cos^4\theta$$

$$+(2s_{13}+s_{44})\sin^2\theta\cos^2\theta$$

$$+2s_{14}\sin^3\theta\cos\theta\sin3\phi, \tag{8}$$

and

$$\frac{s'_{44}+s'_{55}}{2}=\frac{1}{G_f(\theta,\phi)}=(s_{11}-s_{12})\sin^2\theta+s_{44}\left(\frac{1+\cos^2\theta}{2}\right)$$

$$+2(s_{11}+s_{33}-2s_{13}-s_{44})\sin^2\theta\cos^2\theta$$

$$-4s_{14}\sin^3\theta\cos\theta\sin3\phi, \tag{9}$$

which agree with eqs 48 and 49, page 76 of Cady [16] for trigonal symmetry.

The transformations for s'_{34} and s'_{35} were obtained by using the general transformation law for fourth rank tensors, then reducing this to the trigonal symmetry of sapphire and making use of the particular choice of $x'_1x'_2$ described above. The resulting expressions are

$$s'_{34}=3s_{14}\sin^2\theta\cos\theta\cos3\phi, \tag{10}$$

and

$$s'_{35}=2(2s_{13}+s_{44}-s_{11}-s_{33})\sin\theta\cos^3\theta$$

$$+2\left(s_{11}-s_{13}-\frac{s_{44}}{2}\right)\sin\theta\cos\theta$$

$$+s_{14}\sin\theta\sin3\theta\sin3\phi. \tag{11}$$

A set of elastic compliances can be determined from these equations in the following manner: It is necessary to determine the values of E_f and G_p on at least four rods of known orientation. Equation (8) is written for each rod and the resulting system of simultaneous linear equations is solved for s_{11}, s_{33}, $2s_{13}+s_{44}$, and s_{14}. These values are substituted into eqs (8), (10), and (11) and the results are used in eq (7) to calculate G_f for each rod. These values of G_f, θ, and ϕ are substituted into eq (9) for each rod. The resulting system of simultaneous linear equations is solved for $s_{11}-s_{12}$, s_{44}, $s_{11}+s_{33}-2s_{13}-s_{44}$, and s_{14}.

4. Relation of Elastic Moduli to Resonance Frequencies

The values of E_f and G_p needed for the calculation of the elastic compliances were obtained by resonance frequency measurements on thin, circular rods. Young's modulus was calculated from the longitudinal resonance frequency and independently from the flexural resonance frequency. The shear modulus was calculated from the torsional resonance frequency. For both of the Young's modulus calculations, the equation relating the resonance frequency to the appropriate modulus is approximate, but the approximations are very good.

For longitudinal vibrations, Young's modulus of an isotropic medium can be calculated from Rayleigh's equation [17] which can be written

$$E=4\rho l^2f^2\left(1+\frac{\pi^2\sigma^2r^2}{4l^2}\right)^2, \tag{12}$$

where ρ is the density in grams per cubic centimeter, l is the length in centimeters, f is the longitudinal resonance frequency in cycles per second, σ is Poisson's ratio, r is the radius in centimeters, and E is Young's modulus in dynes per square centimeter; 1 dyne/cm^2=10^{-9} kilobars=1.020×10^{-6} kg/cm^2=1.450×10^{-5} lb/in.^{2}. The term in parenthesis is the Rayleigh correction term for the finite thickness of the rod and neglects higher powers of r/l. Bancroft [18] has made an accurate calculation of the velocity of longitudinal waves as a function of r/λ, where λ is the wavelength which is equal to $2l$ for resonance in the fundamental mode. The smallest value for which Bancroft gives a numerical result corresponds to $r/l=0.05$. Assuming Poisson's ratio is 0.25, the Rayleigh correction for this value is 1.00077 and

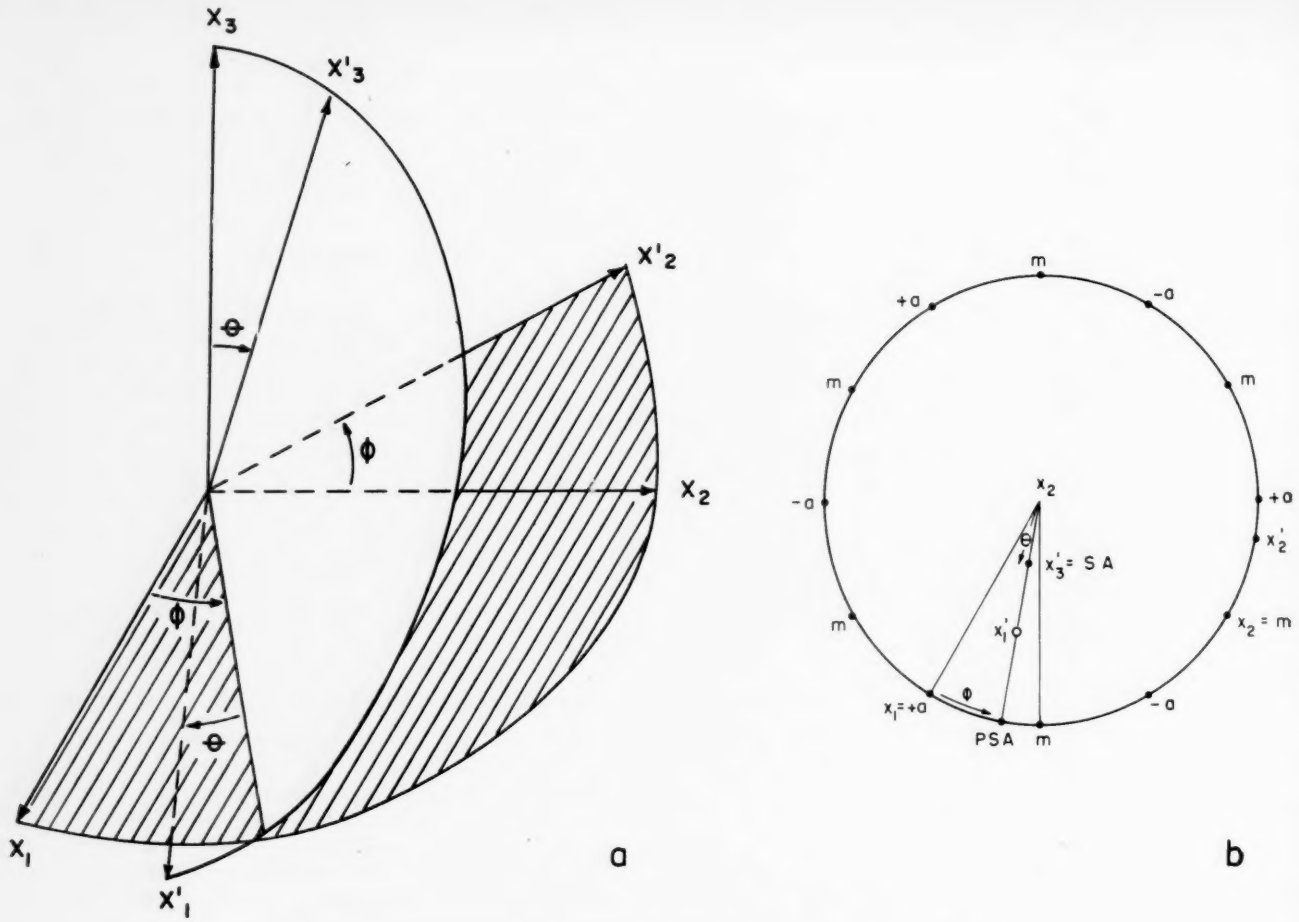

	X'_1	X'_2	X'_3
X_1	$\cos\theta \cos\phi$	$-\sin\phi$	$\sin\theta \cos\phi$
X_2	$\cos\theta \sin\phi$	$\cos\phi$	$\sin\theta \sin\phi$
X_3	$-\sin\theta$	0	$\cos\theta$

c

FIGURE 6. *The rotated coordinate system* $X_1X_2X_3$ *and the direction cosine scheme.*

Figure 6a is a perspective drawing of the relation between $x'_1x'_2x'_3$ and $x_1x_2x_3$. Figure 6b shows the relation stereographically. Figure 6c gives the values of the direction cosines.

Bancroft's results give 1.00078. Evidently the Rayleigh correction is very good for small values of r/l. The largest value of r/l used in the present work was 0.0125 so that eq (12) is thought to be very accurate. For the range of r/l used in this work, the entire correction factor can be taken to be 1.0000. This equation was derived on the assumption of elastic isotropy, but the actual specimens were anisotropic. Equation (12) gives E_f for crystalline rods of the dimensions used. The value of Poisson's ratio varies somewhat for single crystals but for polycrystalline alumina is about 0.25, and since this only enters in the correction term, it seems that eq (12) can be used with this value of Poisson's ratio.

For flexural vibrations of an isotropic medium the best existing theory seems to be that based on an approximate differential equation derived by Timoshenko [19] and studied by Goens [20] and by Pickett [21]. Pickett's results are given in the form of a correction factor, T, which multiplies the result for an infinitely thin rod. His results can be expressed as

$$E=0.31547\frac{\rho l^4 f^2}{r^2}T, \tag{13}$$

where E is in dynes per square centimeter, and the symbols have the same meaning as in eq (12) except f which here is the flexural resonance frequency. In his original paper, Pickett [21] gives equations for calculating T for Poisson's ratio values of zero, 1/6, and 1/3. A subsequent ASTM Standard [22] gives an interpolation formula without giving the derivation or stating the range of validity. It seems best to use Pickett's original formula and interpolate using a quadratic approximation. The question is not significant for rods of the size used in this investigation, the thinnest rods having $r=0.050$ in. $(r/l=0.0083)$ and $T=1.0015$, the thickest rods having $r=0.075$ in. $(r/l=0.0125)$ and $T=1.0033$.

The equation relating the shear modulus to the resonance frequency of an isotropic cylinder can be derived by considering the propagation of torsional waves and requiring that the wavelength have a value such that standing waves are formed. The result is

$$G=4\rho l^2 f^2, \tag{14}$$

where G is the shear modulus in dynes per square centimeter, f is the torsional resonance frequency, ρ is the density in grams per square centimeter, and l is the length. The significance of this equation for crystalline cylinders has been considered by Brown [15] and by Hearmon [14]. The details are complicated, but the result is, as previously stated, that for thin rods eq (14) gives G_p and eq (13) gives E_f.

5. Relation of Elastic Constants to the Velocity of Ultrasonic Waves

The theory required for the determination of the elastic constants of sapphire from resonance frequency measurement was given in sections 3 and 4. The present section presents the theory required for elastic constant determinations from wave velocity measurements. The velocity of sound as a function of specimen size has been studied by Tu, Brennan, and Sauer [23]. They found that in cylindrical rods the velocity of longitudinal waves depended upon r/λ where r is the radius of the rod and λ is the wavelength of the sound wave. For values of r/λ larger than 2.5, the longitudinal waves traveled at the speed of plane waves in an infinite medium.

Similar results should hold for waves propagated in a rectangular block. The longest wavelength used in the present work was about 0.11-cm and the smallest block was 1.25-cm thick. These values give a thickness to wavelength ratio of 11.4. It seems that the theory for plane waves in an infinite medium can therefore be used.

This theory is summarized by Kolsky [24] and by Markham [25]. The results are contained in a cubic equation in the variable $x=\rho v^2$ where ρ is the density and v is the velocity. This equation can conveniently be written in determinant form

$$\begin{vmatrix} A-x & H & G \\ H & B-x & F \\ G & F & C-x \end{vmatrix}=0. \tag{15}$$

where

$$A=c_{11}l^2+c_{66}m^2+c_{55}n^2+2c_{16}lm+2c_{56}mn+2c_{15}nl, \tag{16}$$

$$B=c_{66}l^2+c_{22}m^2+c_{44}n^2+2c_{26}lm+2c_{24}mn+2c_{46}nl, \tag{17}$$

$$C=c_{55}l^2+c_{44}m^2+c_{33}n^2+2c_{45}lm+2c_{34}mn+2c_{35}nl, \tag{18}$$

$$F=c_{56}l^2+c_{24}m^2+c_{34}n^2+(c_{25}+c_{46})lm+(c_{23}+c_{44})mn+(c_{36}+c_{45})nl, \tag{19}$$

$$G=c_{15}l^2+c_{46}m^2+c_{35}n^2+(c_{14}+c_{56})lm+(c_{36}+c_{45})mn+(c_{13}+c_{55})nl, \tag{20}$$

and

$$H=c_{16}l^2+c_{26}m^2+c_{45}n^2+(c_{12}+c_{66})lm+(c_{25}+c_{46})mn+(c_{14}+c_{56})nl. \tag{21}$$

In these equations the c_{ij} are the elastic constants and l, m, n are the direction cosines of the normal to the wave front. The distinction between velocity surface and wave surface for elastic waves has been discussed by Musgrave [26] and Markham [25]. It is sufficient to state that the measured velocities in the direction defined by lmn are those given by eq (15). It is important to notice that both the elastic constants and the direction cosines are referred to the same coordinate system. For sapphire, if the coordinate system is chosen to be the $x_1x_2x_3$ system previously described, the matrix of elastic constants given in table 1 may be substituted to simplify eqs (16) through (21). This simplification has been done by Bhimasenachar [27] for calcite which has the same point group and consequently the same elastic constant matrix as sapphire. The resulting equations can be expressed directly in terms of the orientation by substituting $l=\sin\theta\cos\phi, m=\sin\theta\sin\phi$, and $n=\cos\theta$. These substitutions give

$$A=c_{11}\sin^2\theta\cos^2\phi+\frac{1}{2}(c_{11}-c_{12})\sin^2\theta\sin^2\phi+c_{44}\cos^2\theta+2c_{14}\sin\theta\cos\theta\sin\phi, \tag{22}$$

$$B=\frac{1}{2}(c_{11}-c_{12})\sin^2\theta\cos^2\phi+c_{11}\sin^2\theta\sin^2\phi+c_{44}\cos^2\theta-2c_{14}\sin\theta\cos\theta\sin\phi, \tag{23}$$

$$C=c_{44}\sin^2\theta+c_{33}\cos^2\theta, \tag{24}$$

$$F=c_{14}\sin^2\theta(1-2\sin^2\phi)+(c_{13}+c_{44})\sin\theta\cos\theta\sin\phi, \tag{25}$$

$$G=2c_{14}\sin^2\theta\sin\phi\cos\phi+(c_{13}+c_{44})\sin\theta\cos\theta\cos\phi, \tag{26}$$

and

$$H=\frac{1}{2}(c_{11}+c_{12})\sin^2\theta\sin\phi\cos\phi+2c_{14}\sin\theta\cos\theta\cos\phi. \tag{27}$$

To solve for the velocity of sound in a given direction, the direction cosines must be substituted into the expressions for $A \ldots H$ which must then be substituted into (15) and the resulting cubic equation solved. For some directions this calculation is easy. For example, waves propagated along the $\bar{3}$ axis will have $l=0$, $m=0$, $n=1$.

Equation (15) reduces to

$$\begin{vmatrix} c_{44}-x & 0 & 0 \\ 0 & c_{44}-x & 0 \\ 0 & 0 & c_{33}-x \end{vmatrix} = 0 \tag{28}$$

which gives three roots

$$\rho v^2 = c_{33},\ c_{44},\ c_{44}. \tag{29}$$

These roots correspond to the propagation of a longitudinal wave with velocity $\sqrt{c_{33}/\rho}$ and two transverse waves with velocity $\sqrt{c_{44}/\rho}$. For other directions eq (15) does not reduce to such a simple form and the waves are quasi-longitudinal and quasi-transverse rather than truly longitudinal and transverse.

A simplified method of treating directions for which eq (15) is difficult to solve has been used by each of the previous workers on the elastic constants of sapphire. The method has been most fully described by Mayer and Hiedemann [3]. They assert that for any direction the velocity of the quasi-longitudinal and quasi-transverse waves are given respectively by

$$\rho v_L^2 = c'_{33} \tag{30}$$

and

$$\rho v_S^2 = c'_{44} \tag{31}$$

where c'_{33} and c'_{44} are the value of c_{33} and c_{44} when the coordinate system is transformed into one with the x'_3 axis in the direction of propagation. Expressions for c'_{33} and c'_{44} are given by Mayer and Hiedemann [3]. The present writers do not question the transformation equations for c'_{33} and c'_{44} but do assert that eqs (30) and (31) are not true in general. That is, ρv_L^2 or ρv_S^2 will in general be a more complicated function of the elastic constants and direction of propagation which may reduce to eqs (30) and (31) for certain directions of propagation.

An example of a direction for which the simplified method gives a different answer than the general eq (15) is the x_1 direction (parallel to a 2-fold axis) in sapphire. Using eqs (30) and (31) Mayer and Hiedemann obtain for ρv^2 the three values

$$\rho v_L^2 = c_{11}, \tag{32}$$

$$\rho v_S^2 = c_{44}, \tag{33}$$

and

$$\rho v_S^2 = c_{66} = \tfrac{1}{2}(c_{11}-c_{12}) \tag{34}$$

Actually substituting into eq (15) gives

$$\rho v_L^2 = c_{11}, \tag{35}$$

$$\rho v_S^2 = \tfrac{1}{2}(c_{66}+c_{44}) \pm \tfrac{1}{2}(c_{66}-c_{44}) \times \sqrt{1+\frac{4c_{14}^2}{(c_{66}-c_{44})^2}}. \tag{36}$$

The results agree for the longitudinal wave but do not agree for the transverse wave unless c_{14} is zero. In practice it might happen that $4c_{14}^2/(c_{66}-c_{44})^2$ is small compared with one. If this were so, eqs (30) and (31) would give a good approximation for this particular direction but might not for a different direction. It seems that the results calculated from (30) and (31) would have to be checked against the results obtained from the fundamental eq (15), for each direction of propagation. This fact, of course, would mean that no time would be saved by the use of the simplified method. In the present work, only the exact eq (15) was used.

It is perhaps worth noting why the simplified method should not be expected to be correct. If the $x_1x_2x_3$ coordinate system is transformed into the $x'_1x'_2x'_3$ system, every term in eq (15) can be transformed to give a correct result. Equation (28), however, is a special case of (15) resulting from a special choice of coordinate system and direction of propagation. If the nonzero terms are transformed by a rotation of the coordinate system, eqs (30) and (31) will result, but these equations cannot be expected to hold in general for directions of propagation other than the direction assumed in deriving eq (28).

The error in the simplified method can perhaps be more easily seen from a physical argument. The transformed constants c'_{33}, c'_{44}, and c'_{55}, would be appropriate for calculation of the velocities of waves traveling in the x'_3 direction and with particle motion along the x'_3, x'_2, and x'_1 axes, respectively. However, as Cady [16] has shown, these are not necessarily the directions of motion of the particles, and the deviation in some cases can be quite large.

A method of solving eq (15) for the elastic constants which utilizes tensor transformations has been developed by Neighbours [28]. In his method all terms are taken into account, and in place of eqs (30) and (31) a set of equations is obtained each of which contains an infinite series which presumably converges rapidly. Equations (30) and (31) are equivalent to the zeroth approximation in this perturbation method of Neighbours. He shows how rapidly the approximations converge in some cases but does not discuss the trigonal system.

In his paper on calcite, Bhimasenachar [27] uses equations equivalent to (30) and (31) but explicitly states that small coupling terms have been neglected. In his subsequent paper on sapphire, Bhimasenachar [2] uses the simplified method without mentioning that it is approximate. Both Sundara Rao [1] and Mayer and Hiedemann [3] also use the simplified method but present it as if it were exact.

6. Specimens and Experimental Procedure

The single crystal sapphire specimens were of two types: rods and blocks. The dimensions, mass, surface condition, and orientation of the 29 rod specimens are described in table 2. Two rectangular block specimens were ground to our order by the Linde Company. The first block, SB1, was supposed to be 1 x ½ x ½ in. with the long axis parallel to the x_3 axis and one face perpendicular to the x_1 axis. The second block, SB2, was specified as 1 x ¾ x ¾ in. with the long axis in the x_2x_3 plane making an angle of 135° with x_3 and with one face perpendicular to x_1. The actual orientations are shown in figure 7. It will be seen that for SB1 the θ values are correct, but ϕ is 6° instead of zero. For SB2 the ϕ values are correct, but θ is 47.5 instead of 45.0°.

TABLE 2. *Dimensions and orientation of specimens*

Specimen	Mass [a]	Nominal diameter	Actual length	Surface condition	θ	ϕ
	g	*in.*	*cm*			
SR 1	2.9876	0.100	14.700	f.p.	13.6°	+13.0°
SR 2	3.1008	.100	15.244	f.p.	10.7	+17.0
SR 3	3.0737	.100	15.224	f.p.	65.4	−2.8
SR 4	3.0767	.100	15.232	f.p.	29.4	−24.0
SR 5	2.1516	.100	10.664	f.p.	45.6	+2.0
SR 6	3.0647	.100	15.188	f.p.	41.2	+2.0
SR 7	3.0872	.100	15.218	f.p.	67.8	−8.0
SR 8	3.0902	.100	15.258	f.p.	12.5	+20.0
SR 9	3.0636	.100	15.240	f.p.	89.0	−0.5
SR 10	1.9297	.100	9.591	f.p.	88.6	+2.1
SR 11	6.9436	.150	15.240	f.p.	59.5	−2.0
SR 12	6.9374	.150	15.282	e.g.	36.2	+23.0
SR 13	6.9610	.150	15.280	e.g.	11.9	+27.0
SR 14	6.9192	.150	15.268	e.g.	3.0	−30.0
SR 15	6.9099	.150	15.288	e.g.	18.8	+11.0
SR 16	6.9151	.150	15.212	e.g.	45.0	−29.0
SR 17	6.9334	.150	15.244	e.g.	40.7	−28.3
SR 18	6.9219	.150	15.268	e.g.	59.6	−28.0
SR 19	6.9231	.150	15.280	e.g.	64.0	−1.0
SR 20	4.7551	.125	15.260	e.g.	43.5	−1.0
SR 21	4.7527	.125	15.228	e.g.	48.8	−0.5
SR 22	3.1152	.100	15.292	f.p.	89.0	+3.0
SR 23	3.1115	.100	15.282	f.p.	89.5	−3.5
SR 24	3.1024	.100	15.246	f.p.	89.5	−2.8
SR 25	3.1127	.100	15.300	f.p.	89.0	−3.6
SR 26	3.1154	.100	15.296	f.p.	90.0	−3.7
SR 27	3.1155	.100	15.300	f.p.	88.8	−2.5
SR 28	3.1121	.100	15.296	f.p.	89.5	−3.0
SR 29	3.1173	.100	15.316	f.p.	89.0	−3.0

[a] Corrected for air buoyancy.

NOTE: e.g. means centerless-ground. f.p. means flame polished after centerless grinding. The nominal diameters were not used in calculations. Instead, the average radius was computed from the actual length, mass, and density, $\rho = 3.9860 \pm 0.0010$ g/cm³.

A Laue camera of conventional design was used to determine the orientation; 35KVp X-radiation (copper target) was used with exposure times of about 6 to 10 hr. The samples were supported with the specimen axis perpendicular to the X-ray beam and parallel to the edge of a small shield on the film holder. The shadow cast by this shield on the film established the reference line on the film. A specimen to film distance of 3 cm was used, and the stereographic projection was made according to the procedure described by Barrett [29] using the Greninger chart given in his figure 22 on page 170, and a 21-in. Wulff net. The resulting projection was then indexed with the letter symbols shown in figure 2a. This indexing was done by a trial and error method of making a tentative assignment and comparing angles with the values for sapphire given by Winchell [8]. This process was continued until the proper fit was obtained.

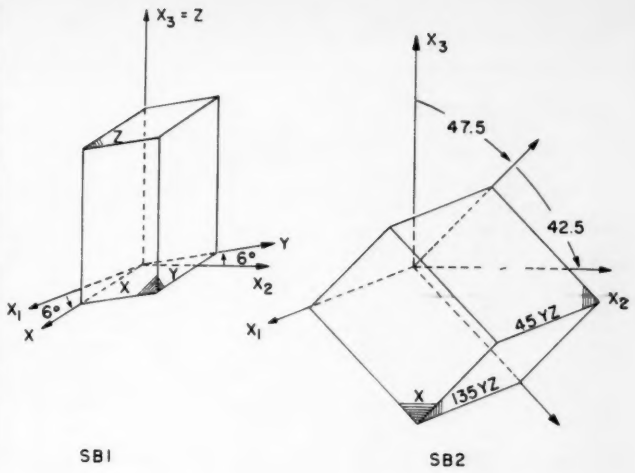

FIGURE 7. *The orientation of the two rectangular block specimens.*

The second method of measuring ϕ, described in section 2, was used. The actual construction obtained from a back reflection Laue pattern always resembled the projection shown in figure 8, that is, the opposite ends of the specimen axis were at opposite points of the stereographic equator. The value of θ can be read directly from this projection, as shown, but the specimen axis must be projected on the x_1x_2 plane to measure ϕ. Projection of +SA would require rotation of the whole pattern because PSA would lie on the hemisphere not shown in figure 8. This projection can be done but requires more graphical construction with attendant possibility of error. It is more convenient to project −SA and choose x_1 as the $\pm a$ direction nearest −PSA. The sign convention for determining ϕ is shown in figure 5. Orientations were determined twice on 12 specimens with the resulting standard deviations $\Delta\theta = 0.6°$ and $\Delta\phi = 1.6°$.

The longitudinal resonance frequency of each rod shaped specimen was measured by hanging the specimen vertically from a crystal pickup. A single, fine cotton thread was tied around the specimen somewhat off center so that the specimen hung approximately vertically. The other end of the thread was tied to the needle of a high output Rochelle salt pickup. Vibration was excited by placing a high frequency speaker just under the specimen and driving through air. The electronic components used to drive the speaker, to amplify the pickup signal, and to measure the frequency have been described [30]. With this system it was possible to detect resonances in the range 30 to 50 kc. The response was weak but very sharp, and careful hunting was sometimes necessary.

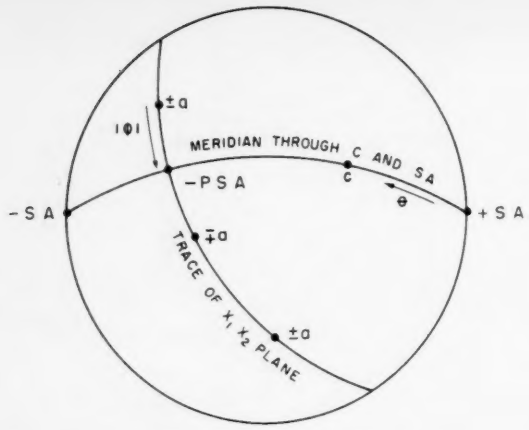

FIGURE 8. *Stereogram illustrating the actual measurement of ϕ and θ.*

The flexural resonance frequency was measured with the specimen suspended horizontally on two threads near the nodes. One thread was driven by a magnetic cutting head. The other thread was connected to a crystal pickup. Each specimen would vibrate in two flexural modes at right angles to each other. By turning the specimen in the string it was possible to excite either mode at will and to determine the direction of vibration for each. The two resonance frequencies usually differed by a few cycles, presumably because of small variations in the diameter of the specimen. The average of the two resonance frequencies was used in eq (13). An average value of r^2, for each rod calculated from the density, the mass, and the length, was used. This approach was used because the density could be determined accurately by hydrostatic weighing, but the average radius was more difficult to measure accurately.

The torsional resonance frequency was determined with the same speaker and pickup used in the longitudinal resonance frequency measurements. The tweeter was modified by covering its output opening with a sheet of paper. The thread used to drive the specimen was fastened to the center of this sheet. The thread was wrapped around the specimen several times to provide an off-center driving force and the pickup thread was wrapped around the specimen in the opposite direction. Careful hunting was again necessary to find the weak but sharp resonance. It was necessary to distinguish between the fundamental of torsion and the overtones of flexure. This distinction was accomplished by moving the driving and pickup strings until the nodes were located. The counter used for frequency measurements had an accuracy of ± 0.1 cps.

The velocity of sound measurements on the two block specimens were made by sending an ultrasonic pulse into the specimen and measuring the transit time. A quartz crystal 0.5 in. in diameter and cut to resonate at 10 Mc was used as transmitter and pickup. An X-cut crystal was used to generate longitudinal waves, and an AC-cut crystal was used for transverse waves. These crystal cuts are described by Buchanan [31]. The crystals were mounted on the specimen with salol (phenyl salicylate). The specimen was coated with a very thin layer of evaporated aluminum before the crystals were mounted in order to provide a ground.

The crystals were excited and the echoes were amplified with a commercial ultrasonic generator and receiver. This unit had a pulsed oscillator of variable frequency with a fixed pulse repetition rate of 100/sec. The amplified output of the oscillator was connected to an electrode on a quartz crystal. The same electrode served as an input connector for the receiver. The output of the receiver was connected to one input of an oscilloscope with a dual trace preamplifier. A crystal controlled 1–Mc oscillator was connected to the other input of the dual trace preamplifier. The oscilloscope thus displayed the standard 1–Mc signal on one trace followed by the echo pattern on the next trace. These two traces were simultaneously visible, and the 1–Mc pattern was used as a time scale for the transit time measurement. The general technique of pulse velocity measurement is reviewed by Huntington [32].

The sweep expansion feature of the oscilloscope could be read to 0.01 μsec. The actual measurements were much less accurate, however, because the pulses were rounded and did not have a sharply defined leading edge. Consequently the maximum of the pulse envelope was used as a reference point. Repeated measurements suggested that the resulting transit time might have an error of several percent. For this reason no transit time correction, such as that discussed by Overton and Gaffney [33], was made. The measured velocities given in this report should be examined with this in mind. They are provided as a rough check on the accurate values determined by the resonance methods to show that the values of the elastic constants, within the accuracy of pulse velocity measurements, show no frequency dependence.

7. Results

The resonance frequencies are summarized in table 3. These values were used to calculate E_f and G_p using the equations of section 4. The method described in section 3 was then used to calculate the elastic compliances, s_{ij}. Tables 3 through 7 show various stages in these calculations and indicate the precision. The reciprocals of the E_f values used in solving eq (8) are given in table 4, and the resulting values of the compliance combinations are given in the first half of table 6. The difference column in table 4 shows how well the observations on all 29 rods were fitted by the four parameters of eq (8). The shear modulus calculations are summarized in table 5, and the resulting compliance combinations are given in the second half of table 6. The difference column of table 5 shows how accurately eq (9) fitted the data.

TABLE 3. *Resonance frequencies of sapphire rods*

Specimen	Flexural [a]		Longitudinal	Torsional
	f_1	f_2		
SR 1	1100.1	1100.7	35673	20850
SR 2	1032.5	1033.7	34739	19940
SR 3	971.5	972.6	32747	21033
SR 4	990.0	990.9	33397	20547
SR 5	1908.9	1907.3	45060	
SR 6	945.1	943.6	31746	21600
SR 7	998.3	997.5	33538	20616
SR 8	1021.9	1023.7	34464	20037
SR 9	993.8	1010.3	33868	20505
SR 10	2518.0	2539.3	53817	
SR 11	1431.9	1432.7	32200	21210
SR 12	1378.7	1380.1	31145	21763
SR 13	1536.0	1537.0	34607	19943
SR 14	1557.1		35175	19704
SR 15	1487.6	1488.4	33703	20346
SR 16	1483.0	1484.1	33336	20596
SR 17	1472.5	1473.5	33160	20587
SR 18	1508.0	1507.7	34068	20152
SR 19	1433.7	1434.1	32420	20992
SR 20	1166.7	1169.2	31778	21331
SR 21	1172.7	1174.9	31819	21436
SR 22	1015.4	989.0	33727	20251
SR 23	1015.9	992.2	33786	20247
SR 24	1022.6	999.1	33871	20332
SR 25	1015.0	989.9	33768	20236
SR 26	1013.5	989.2	33735	20230
SR 27	1007.7	996.0	33757	20219
SR 28	1013.1	986.3	33715	20233
SR 29	1010.6	995.6	33790	20240

[a] The two flexural frequencies correspond to vibrations at right angles. The average value was used for calculations. All values are in cycles per second.

TABLE 4. *Reciprocal Young's modulus of sapphire*

All values are in units of 10^{-13} cm²/dyne. The standard deviation for $1/E$, computed using the tabulated differences is $\pm 0.0052 \times 10^{-13}$ cm²/dyne.

Specimen	$1/E_f$ Flexural	$1/E_f$ Longitudinal	$1/E_f$ Calculated [a]	Difference [b]
SR 1	2.2764	2.2805	2.2759	0.0046
SR 2	2.2392	2.2366	2.2369	−.0003
SR 3	2.5242	2.5233	2.5193	.0040
SR 4	2.4262	2.4237	2.4277	−.0040
SR 5	2.7124	2.7167	2.7119	.0048
SR 6	2.6968	2.6976	2.6876	.0100
SR 7	2.4088	2.4079	2.4147	−.0068
SR 8	2.2684	2.2681	2.2621	.0060
SR 9	2.3530	2.3540	2.3529	.0011
SR 10	2.3543	2.3540	2.3564	−.0024
SR 11	2.6020	2.6048	2.5967	.0081
SR 12	2.7684	2.7685	2.7708	−.0023
SR 13	2.2505	2.2461	2.2545	−.0084
SR 14	2.1795	2.1744	2.1744	.0000
SR 15	2.3679	2.3624	2.3632	−.0008
SR 16	2.4414	2.4390	2.4404	−.0014
SR 17	2.4570	2.4546	2.4567	−.0021
SR 18	2.3214	2.3180	2.3125	.0055
SR 19	2.5564	2.5556	2.5645	−.0089
SR 20	2.6689	2.6674	2.6670	.0004
SR 21	2.6709	2.6717	2.6826	−.0109
SR 22	2.3537	2.3579	2.3560	.0019
SR 23	2.3488	2.3527	2.3515	.0012
SR 24	2.3424	2.3521	2.3518	.0003
SR 25	2.3440	2.3497	2.3502	−.0005
SR 26	2.3535	2.3554	2.3529	.0025
SR 27	2.3482	2.3512	2.3509	.0003
SR 28	2.3436	2.3477	2.3517	−.0040
SR 29	2.3486	2.3521	2.3507	.0014

[a] Calculated from eq (7) using the data of table 6.
[b] Difference = longitudinal value minus calculated value.

TABLE 5. *Reciprocal shear modulus of sapphire*

All values are in units of 10^{-13} cm²/dyne. The standard deviation for $1/G_f$ calculated from the difference column is $\pm .0178 \times 10^{-13}$ cm²/dyne.

Specimen	$\frac{(s'_{34})^2+(s'_{35})^2}{2\,s'_{33}}$	$1/G_f$ Torsional	$1/G_f$ Calculated	Difference
SR 1	0.0421	6.7186	6.7296	−0.0110
SR 2	.0291	6.8175	6.8066	.0109
SR 3	.0716	6.1888	6.2242	−.0354
SR 4	.0124	6.4156	6.4294	−.0138
SR 5 [a]				
SR 6	.0521	5.8792	5.9099	−.0307
SR 7	.0564	6.4282	6.4295	−.0013
SR 8	.0390	6.7491	6.7569	−.0078
SR 9	.0002	6.5208	6.5396	−.0188
SR 10 [a]				
SR 11	.0734	6.0765	6.0763	.0002
SR 12	.0664	5.7365	5.7468	−.0103
SR 13	.0371	6.8003	6.7718	.0285
SR 14	.0020	6.9320	6.9302	.0018
SR 15	.0643	6.5469	6.5571	−.0102
SR 16	.0049	6.3939	6.3990	−.0051
SR 17	.0010	6.3692	6.3690	.0002
SR 18	.0189	6.6439	6.6407	.0032
SR 19	.0748	6.1704	6.1355	.0349
SR 20	.0506	5.9698	5.9498	.0200
SR 21	.0564	5.9428	5.9153	.0275
SR 22	.0024	6.5421	6.5334	.0087
SR 23	.0014	6.5528	6.5425	.0103
SR 24	.0008	6.5282	6.5419	−.0137
SR 25	.0010	6.5439	6.5451	−.0012
SR 26	.0019	6.5520	6.5396	.0124
SR 27	.0004	6.5544	6.5435	.0109
SR 28	.0009	6.5445	6.5421	.0024
SR 29	.0007	6.5319	6.5440	−.0121

[a] Too short for use.

TABLE 6. *Best estimates of some compliances*

Compliance	Value	Standard deviation
Calculated from Young's modulus values [a]		
s_{11}	2.3529×10^{-13} cm²/dyne	0.0016×10^{-13} cm²/dyne
s_{33}	2.1694	.0024
$s_{44}+2s_{13}$	6.2183	.0088
s_{14}	0.4901	.0057
Calculated from shear modulus values [b]		
$s_{11}-s_{12}$	3.0696×10^{-13} cm²/dyne	0.0067×10^{-13} cm²/dyne
s_{44}	6.9400	.0084
$s_{11}+s_{33}-(2s_{13}+s_{44})$	−1.6539	.0197
s_{14}	0.4868	.0101

[a] Calculated by fitting eq (7) to Young's modulus values calculated from longitudinal resonance frequencies.
[b] Calculated by fitting eq (8) to shear modulus values.

The final result for the elastic compliances and constants is given in table 7. The six compliances were calculated from the eight values in table 6 by weighting each value according to its standard deviation. The constants were calculated from the compliances using the standard matrix inversion equations given, for example, by Nye [7].

The c_{ij} values of table 7 were used in eq (15) to calculate the velocity of sound for comparison with the measured velocities for all directions of propagation normal to the faces of SB1 and SB2. In some cases this necessitated the solution of a cubic

equation by successive approximations. The results are given in table 8 along with the measured values. In this table the faces have been described by the labels shown in figure 9, e.g., the 45YZ face. The actual orientation was used in the calculations, however; that is, the 45YZ face normal actually had $\theta = 47.50°$ instead of 45°.

The s_{ij} values were used to calculate E_f and G_f as a function of orientation. The results are shown in figures 9 and 10 and in contour form in figures 11 and 12.

8. Discussion

The values of the elastic constants and compliances for sapphire which have been reported by other investigators are given in table 7. Mayer and Hiedemann have suggested that the method of

TABLE 7. *Elastic compliances and constants of sapphire*

All s_{ij} values in units of 10^{-13}cm²/dyne. All c_{ij} values in units of 10^{12}dyne/cm².

	Sundara Rao	Bhimasenachar	Mayer & Hiedemann	Present work
s_{11}	2.84	2.32	2.18	2.353±0.002
s_{33}	2.21	1.93	2.02	2.170± .002
s_{44}	5.47	5.77	5.04	6.940± .008
s_{12}	−0.95	−1.05	−0.50	−0.716± .007
s_{13}	−.47	−0.38	−.16	−.364± .006
s_{14}	−1.52	−1.71	−.49	.489± .005
c_{11}	4.66	4.65	4.96	4.968±0.018
c_{33}	5.06	5.63	5.02	4.981± .014
c_{44}	2.35	2.33	2.06	1.474± .002
c_{12}	1.27	1.24	1.09	1.636± .018
c_{13}	1.17	1.17	0.48	1.109± .022
c_{14}	0.94	1.01	.38	−0.235± .003

TABLE 8. *Velocity of sound in sapphire*

All velocities in 10^3cm/sec.

Direction [a]	Mode [b]	Calculated velocity	Measured velocity	Percent difference
Specimen SB1				
X	*L*	1117	1092	−2.2
	T pol *Y*	667	669	+0.3
	T pol *Z*	585	579	−1.0
Y	*L*	1118	1116	−0.2
	T pol *X*	651	645	−0.9
	T pol *Z*	600	609	+1.5
Z	*L*	1118	1100	−1.7
	T	608	594	−2.3
Specimen SB2				
X	*L*	1116	1088	−2.5
	T pol *Y*	676	662	−2.1
	T pol *Z*	575	564	−1.9
45°***YZ***	*L*	1095	1146	+4.7
	T pol *X*	581	609	+4.0
	T other pol	691	710	+2.7
135°***YZ***	*L*	1041	1040	−0.1
	T pol *X*	671	659	−1.8
	T other pol	690	687	−0.4

[a] The present directions are the actual face normals shown in figure 8.
[b] "*L*" means longitudinal, "*T* pol *Y*" means transverse with the direction of vibration along *Y*, and "*T* other pol" means transverse with the direction of vibration perpendicular to the other two modes.

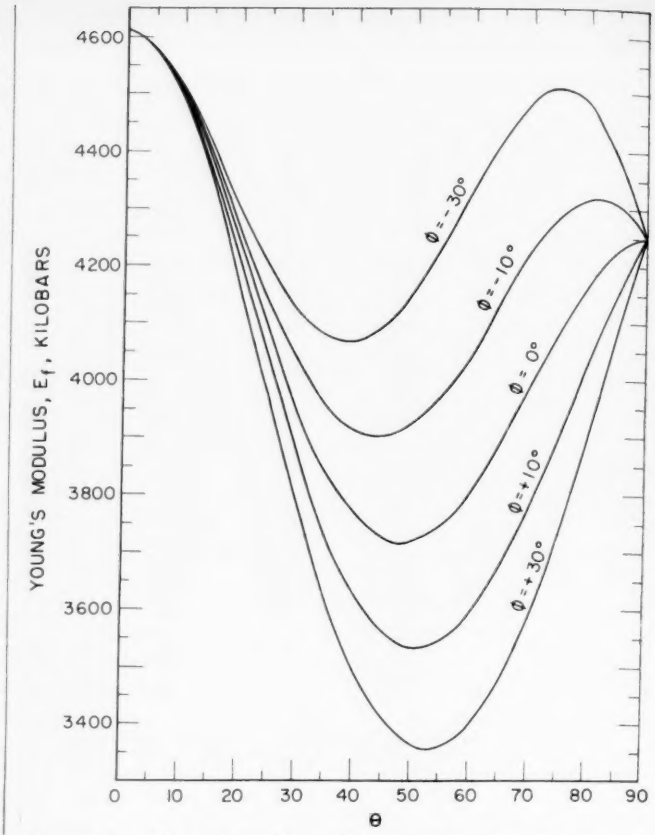

FIGURE 9. *Young's modulus, E_f, as a function of orientation for single crystal sapphire.*

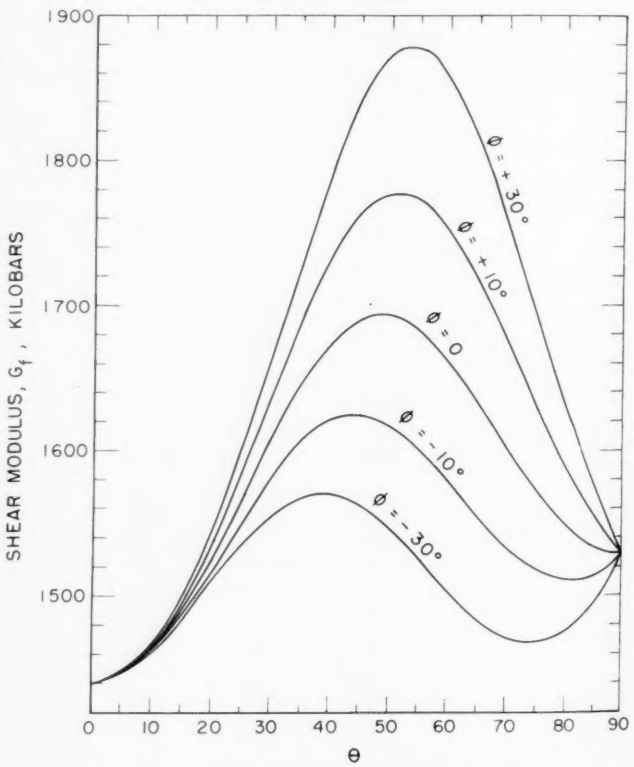

FIGURE 10. *The shear modulus, G_f, as a function of orientation for single crystal sapphire.*

exciting vibrations used by the Indian workers may give spurious resonances. For this reason we compare primarily with the set of values given by Mayer and Hiedemann.

The method used by Mayer and Hiedemann gave the c_{ij} values directly; an error in a single one of the c_{ij} might lead to errors in several of the s_{ij} values. Accordingly we compare c values rather than s values. c_{11} and c_{33} are in good agreement, but the other values are not. The difference in sign of c_{14} is striking. As was pointed out earlier, the sign of c_{14} (and s_{14}) depends on which end of the 2-fold axis is taken as $+x_1$. The conventions given by Nye [7] and by the *Standards on Piezoelectric Crystals* [11] leave this unspecified. This point is not mentioned by any of the previous workers on sapphire, and we have not been able to find any information in their papers on which choice was made. If Mayer and Hiedemann used the opposite end of a 2-fold axis as $+x_1$, the difference in sign of c_{14} would be accounted for and the values of c_{14} would be in fair agreement. The most troublesome disagreement is that between the value of c_{44} obtained in the present work, 1.47×10^{12} dyne/cm^2, and the value of 2.06×10^{12} dyne/cm^2 obtained by Mayer and Hiedemann. The 1.47 value cannot be very much in error because the value of the velocity of the transverse wave in the x_3 direction depends only on this constant, and the measured value is -2.3 percent from the calculated value as shown in table 8. The fact that eqs (30) and (31), used by Mayer and Hiedemann, are not strictly correct was pointed out in section 5. However, it does not seem that this fact has any connection with the disagreement in the values of c_{44} because these equations are not needed for a wave propagated in the x_3 direction.[4]

A comparison can be made to support the validity of the present data. Lang [34] has reported values of elastic moduli determined dynamically on hot pressed polycrystalline alpha alumina of density 3.983 g/cm^3. This density is so close to the value of 3.986 g/cm^3 obtained on single crystals that the

[4] In a private communication dated March 28, 1960, R. H. Truell (Brown University) gives as tentative results from his joint investigation with P. H. Levy (Brookhaven National Laboratory) using a pulse velocity technique, $C_{33}=5.013\times 10^{12}$ dynes/cm^2 and $C_{44}=1.478\times 10^{12}$ eynes/cm^2. These values are seen to be in good agreement with the results presented here.

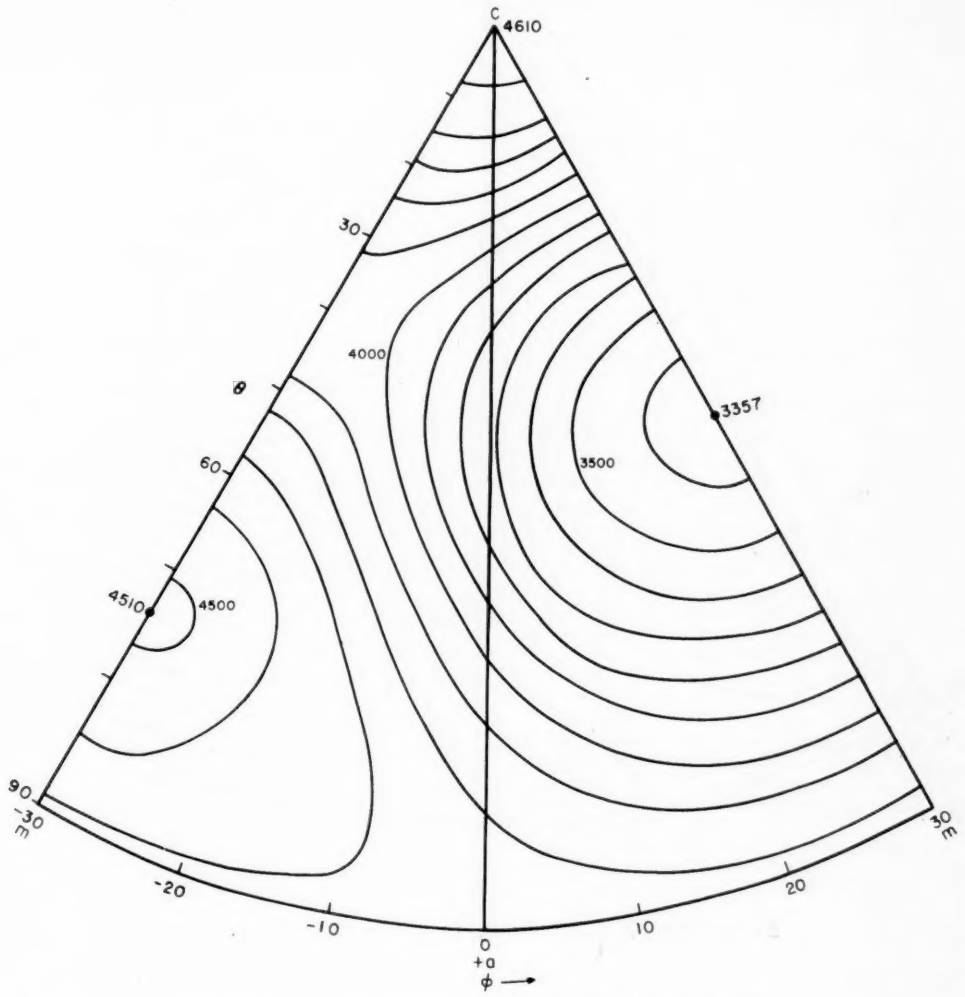

FIGURE 11. *Young's modulus, E_f, intervals of 100 kilobars.*

values of the elastic moduli of his specimens must be only slightly less than the values for zero porosity. He gives $E=4012$ kilobars and $G=1591$ kilobars as his best values. An exact theoretical relationship between single crystal elastic constants and polycrystalline moduli has not been developed, but two good approximations are discussed by Huntington [32]. One method, due to Voigt, should give values slightly too high, and the other method, due to Reuss, should give values slightly too low. Using the elastic constant and compliance data of table 7 and the equations given in Huntington's article, one obtains the results shown in table 9. The values of E and G calculated from the elastic constants obtained in this investigation are in rather good agreement with Lang's values.

All elastic constants, compliances, and moduli so far discussed have been for adiabatic conditions; i.e., measured under conditions when appreciable heat flow could not occur during one cycle of vibration. Isothermal values are measured in static tests. Hearmon [14] gives an equation from which the difference between isothermal and adiabatic values can be calculated. This difference ranges from 0.2 percent for s_{11} to 1 percent for s_{13}.

TABLE 9. *Comparison of calculated and measured elastic moduli for polycrystalline alumina*

All values in kilobars.

		Young's modulus	Shear modulus
Measured (Lang)		4012	1591
Present data	Reuss theory	3973	1606
	Voigt theory	4084	1660
Mayer & Hiedemann	Reuss theory	4554	1996
	Voigt theory	4682	2070

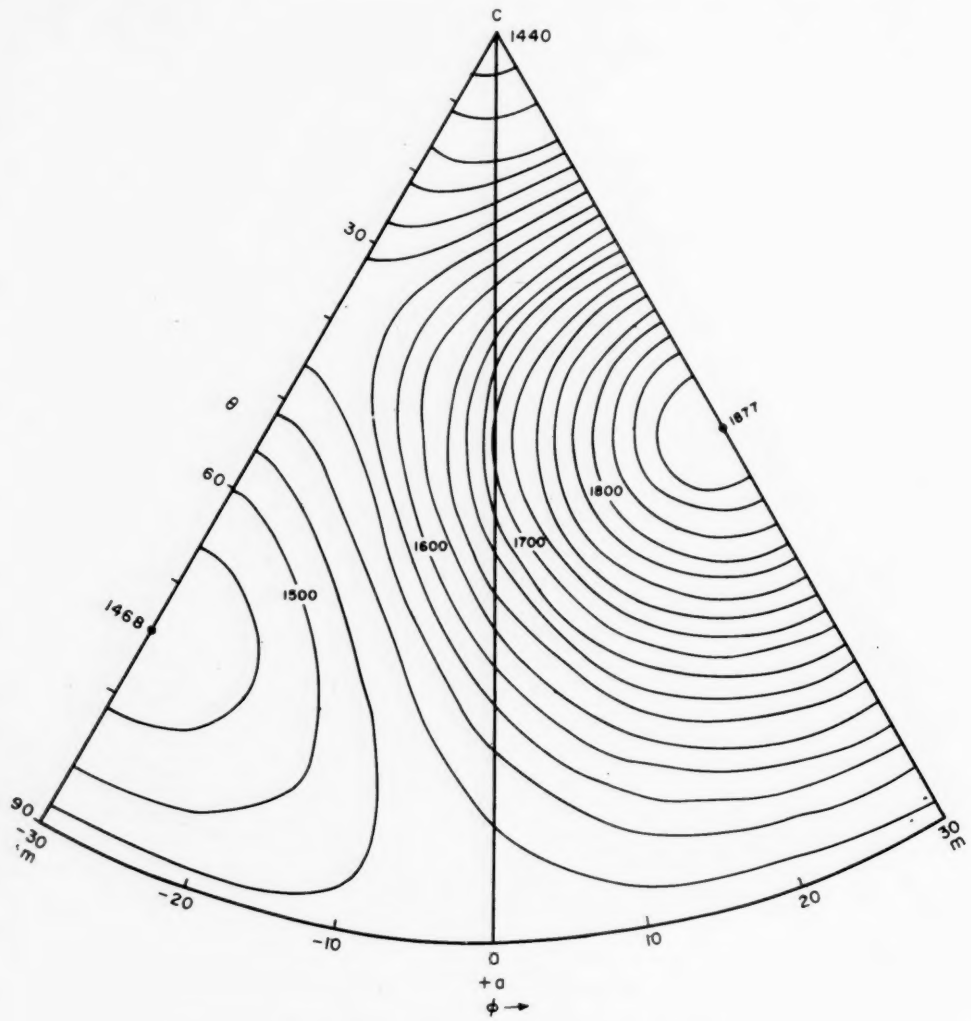

FIGURE 12. *Shear modulus,* G_t, *intervals of 20 kilobars.*

The compressibilities can be calculated from the compliances using equations given by Nye [7]. The adiabatic compressibilities calculated in this way are given in table 10. These should differ from the isothermal compressibilities by about 1 percent. Values of the isothermal compressibilities measured in static tests by Bridgman [35] and by Madelung and Fuchs [36] are given in table 10. Bridgman's linear compressibility parallel to the x_3 axis is based on the initial slope of his curve and is inconsistent with all the other data. It is listed in the first row of measured values in table 10 even though it does not appear to be consistent with his reported value of volume compressibility. If the slope of the subsequent section of Bridgman's curve is used, the values labeled "Bridgman, interpreted" are obtained. The present work is in somewhat better agreement with the experimental values of volume compressibility than the results of Mayer and Hiedemann. Visual inspection of Bridgman's curves suggests that the difference between the value of 3.6×10^{-13} cm²/dyne, calculated from his data, and 3.988×10^{-13} cm²/dyne may be largely due to experimental error in his data.

TABLE 10. *Comparison of compressibilities calculated from elastic compliances with values measured directly*

All values in 10^{-13} cm² dyne.

	Linear compressibility		Volume compressibility
	Parallel to x_3	Perpendicular to x_3	
	Calculated from compliances		
Present data, 25° C	1.442	1.273	3.988
Mayer and Hiedemann, 27° C	1.70	1.52	4.74
	Measured		
Bridgman, 30° C, as reported	0.40	1.13	3.23
Bridgman, 30° C, interpreted	1.35	1.13	3.6
Madelung and Fuchs, 0° C			3.8

Finally, the difference columns in table 4 and table 5 show how well the classical, 6-constant theory fits the accurate results obtained in the kilocycle per second range. The standard deviation calculated from either set of differences is 0.3 percent of the average value of $1/E$ or $1/G$, respectively. The worst disagreement for either $1/E$ or $1/G$ is only 0.6 percent. It is evident that the classical theory of elasticity gives a very accurate representation of the elastic behavior in the kilocycle per second range.

9. Summary

(1) The complete set of elastic constants and compliances for sapphire calculated from resonance measurements in the kilocycle per second frequency range is given.

(2) Less accurate pulse velocity measurements in megacycle per second range indicate little, if any, frequency dependence of the elastic constants.

(3) The values of c_{11} and c_{33} agree well with the results of the most accurate previous measurements, but the remaining constants and all of the compliances are in serious disagreement.

(4) Values of Young's modulus and the shear modulus for polycrystalline alumina calculated from the compliances are in good agreement with experimental values.

(5) Curves for estimating Young's modulus and the shear modulus for single crystal sapphire of any orientation are given.

The authors thank the Wright Air Development Center for supporting this work and the Linde Company for supplying specimens. They are gratefull to R. W. Kebler and R. G. Rudness for a copy of their memorandum on the orientation of sapphire. The authors thank H. S. Peiser and D. K. Smith for discussion of the orientation process and of the equations relating moduli and compliances.

10. References

[1] R. V. G. Sundara Rao, Elastic constants of alumina, Proc. Indian Acad. Sci. [A] **26,** 352–360 (1949).

[2] J. Bhimasenschar, Elastic constants of corundum, Proc. Natl. Inst. Sci. India, Pt. A **16,** 241–243 (1950); Elastic constants of corundum, Current Sci. (India) **18,** 372–373 (1949).

[3] W. G. Mayer and E. A. Hiedemann, Optical methods for the ultrasonic determination of the elastic constants of sapphire, J. Acoust. Soc. Am. **30,** 756–760 (1958); Ultrasonic determination of elastic constants and structural irregularities in transparent single crystals (measurements in sapphire), Acta Cryst. **12,** 1–6 (1959).

[4] N. Joel and W. A. Wooster, On the validity of the classical theory of elasticity as applied to ammonium di-hydrogen phosphate, Acta Cryst. **11,** 575–578 (1958).

[5] C. V. Raman and K. S. Viswanathan, On the theory of the elasticity of crystals, Proc. Indian Acad. Sci. [A] **42,** 51–70 (1955).

[6] C. Palache, H. Berman, and C. Frondel, Dana's system of mineralogy, p. 520 (John Wiley & Sons, New York, N.Y., 1944).

[7] J. F. Nye, Physical properties of crystals (Oxford Univ. Press, London, England, 1957).

[8] Horace Winchell, Navigation in crystallography, ull. Geol. Soc. Am. **57,** 295–308 (1946).

[9] H. E. Swanson and R. K. Fuyat, Standard X-ray diffraction powder patterns, NBS Circ. 539, vol. II (1953).

[10] M. L. Kronberg, Plastic deformation of single crystals of sapphire: basal slip and twinning, Acta Met. **5,** 507–524 (1957).

[11] Standards on piezoelectric crystals, Proc. I.R.E. **37,** 1378–1395 (1949).

[12] F. C. Phillips, An introduction to crystallography (Longmans, Green and Co., New York, N.Y., 1955).

[13] R. W. Kebler and R. G. Rudness, Development memorandum No. 44, Orientation of single crystal sapphire, Speedway Develop. Lab., Linde Co., Indianapolis, Ind. (1958).

[14] R. F. S. Hearmon, The elastic constants of anisotropic materials, Rev. Mod. Phys. **18,** 409–440 (1946); The elastic constants of anisotropic materials II, Adv. in Phys. **5,** 323–382 (1956).

[15] W. F. Brown, Jr., Interpretation of torsional frequencies of crystal specimens, Phys. Rev. **58,** 998–1001 (1940).
[16] W. G. Cady, Piezoelectricity (McGraw-Hill Book Co., Inc., New York, N.Y., 1946).
[17] Lord Rayleigh, The theory of sound, **1,** 251 (Dover Publications, New York, N.Y., 1945).
[18] Dennison Bancroft, The velocity of longitudinal waves in cylindrical bars, Phys. Rev. **59,** 588–593 (1941).
[19] S. P. Timoshenko, On the correction for shear of the differential equation for transverse vibrations of prismatic bars, Phil. Mag. **41,** 744–746 (1921); On the transverse vibrations of bars of uniform cross-section, Phil. Mag. **43,** 125–131 (1922).
[20] E. Goens, Über die Bestimmung des Elastizitatsmoduls von Staben mit Hilfe von Biegungsschwingungen, Ann. Physik **11,** 649–678 (1931).
[21] Gerald Pickett, Equations for computing elastic constants from flexural and torsional resonant frequencies of vibration of prisms and cylinders, Proc. ASTM **45,** 846–865 (1945). (Also available as Bull. 7 of the Research Lab. of Portland Cement Assoc.).
[22] Tentative method of test for fundamental transverse, longitudinal, and torsional frequencies of concrete specimens, ASTM designation C215–58T, pp. 701–705, pt. 4, ASTM Standards (1958).
[23] L. Y. Tu, J. N. Brennan, and J. A. Sauer, Dispersion of ultrasonic pulse velocity in cylindrical rods, J. Acoust. Soc. Am. **27,** 550–555 (1955).
[24] H. Kolsky, Stress waves in solids (Oxford Univ. Press, London, England, 1953).
[25] M. F. Markham, Measurements of elastic constants by the ultrasonic pulse method, British J. Appl. Phys., Suppl. 6, pp. S56–S63 (1957).
[26] M. J. P. Musgrave, On the propagation of elastic waves in acolotropic media. I. General principles, Proc. Roy. Soc. [A] **226,** 339–355 (1954).
[27] J. Bhimasenachar, Elastic constants of calcite and sodium nitrate, Proc. Indian Acad. Sci. [A] **22,** 199–207 (1945).
[28] J. R. Neighbours, An approximation method for the determination of the elastic constants of single crystals, J. Acoust. Soc. Am. **26,** 865–869 (1954).
[29] C. S. Barrett, Structure of metals (McGraw-Hill Book Co., Inc., New York, N.Y., 1943).
[30] J. B. Wachtman, Jr., and L. H. Maxwell, Factors controlling resistance to deformation and mechanical failure in polycrystalline (glass-free) ceramics, WADC Tech. Rept. 57/526.
[31] J. P. Buchanan, Handbook of piezoelectric crystals for radio equipment designers, WADC Tech. Rept. 56/156, ASTIA Document No. AD 110448.
[32] H. B. Huntington, The elastic constants of crystals, Solid State Phys. **7,** 213–351 (Academic Press, New York, N.Y., 1958).
[33] W. C. Overton, Jr., and John Gaffney, Temperature variation of the elastic constants of cubic elements. I. Copper, Phys. Rev. **98,** 969–977 (1955).
[34] S. M. Lang, Properties of high-temperature ceramics and cermets, Elasticity and density at room temperature, NBS Monograph 6 (1960)
[35] P. W. Bridgman, Compressibilities and pressure coefficients of resistance of elements, compounds, and alloys, many of them anomalous, Proc. Am. Acad. Arts Sci. **68,** 27–93 (1932).
[36] E. Madelung and R. Fuchs, Kompressibilitäts messungen an festen Körpern, Ann. Physik **65,** 289–302 (1921).

Washington, D.C. (Paper 64A3–45)

JOURNAL OF RESEARCH of the National Bureau of Standards—A. Physics and Chemistry
Vol. 64A, No. 3, May–June 1960

Radial Distribution Study of Vitreous Barium Borate[1]

Arthur Bienenstock,[2] Aaron S. Posner,[3] and Stanley Block

(January 6, 1960)

X-ray diffraction, radial distribution studies of a 20 percent barium oxide, 80 percent B_2O_3 glass have been performed using both the atomic and electronic distribution functions. From these distributions, the average barium-barium distance has been determined as 6.76 A. This distance is in good agreement with that predicted by Levin and Block on the basis of a structural interpretation of immiscibility data.

1. Introduction

Levin and Block [1] have attempted to explain immiscibility of alkali and alkali-earth metal oxides in borate and silicate glasses by means of crystal chemical principles. They considered two short-range structures proposed by Warren and Pincus [2] for the system at the limit of miscibility. For the particular system investigated here, $BaO–B_2O_3$, the type A structure, shown in figure 1, has the boron coordinated either triangularly or tetrahedrally by oxygen. Two bariums are bonded to the same oxygen with approximately a 180° bond angle. Using ionic radii, they calculate a separation of barium atoms of 5.50 A.

The type B structure is shown in figure 2. Here, each boron is tetrahedrally coordinated by oxygen. The boron tetrahedron shares edges with a distorted barium cube. The predicted barium–barium separation in this case is 6.67 A.

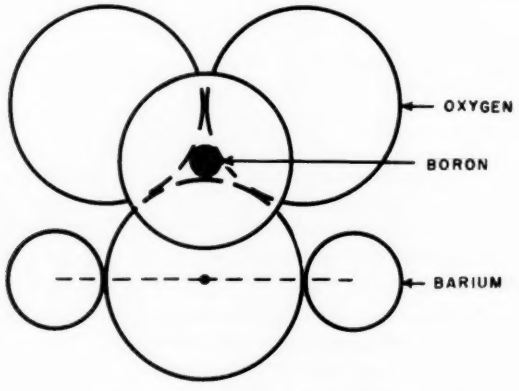

FIGURE 1. *Type A coordination.*

Boron can be either in tetrahedral or triangular coordination. The Ba-Ba distance is the sum of the Ba–O distances.

With a simple model of the barium atoms forming a cubic lattice and a knowledge of the density and composition at the limit of miscibility, Levin and Block found that the average separation of barium atoms is 6.82 A. Hence, they predicted that the structure is type B.

This paper describes the determination of the Ba-Ba distance by means of X-ray diffraction radial distribution techniques. It will be shown that the structure cannot be type A and agrees with type B.

2. Experimental Procedures

Measurements were made with a North American Philips X-ray diffractometer, modified so that the volume defined by the cylindrical scatter shield could be evacuated. Intensities were determined at

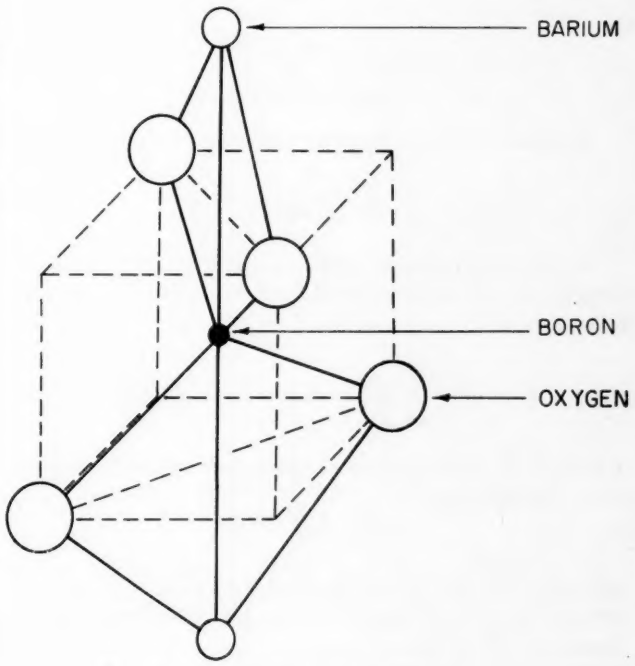

FIGURE 2. *Type B coordination.*

Boron must be in tetrahedral configuration. The boron and barium polyhedra share edges.

[1] This investigation was supported in part by Research Grant D-572, U.S. Public Health Service.
[2] National Science Foundation Predoctoral Fellow, Division of Engineering and Applied Physics, Harvard University, Cambridge, Mass.
[3] American Dental Association Research Associate.

each angular position by the average of two consecutive measurements of the time taken for 6,400 counts. The maximum difference between the two measurements was 3.5 percent. Readings were taken at intervals of 0.05 in $s=4\pi \sin \theta/\lambda$ in the range 0.3 to 3.5 and intervals of 0.1 in the range 3.6 to 7.9 using CuKα radiation with an argon filled Geiger counter, and intervals of 0.1 in the range 6.1 to 10.0 using MoKα radiation and a krypton filled Geiger counter.

A warmup time of 24 hr was allowed, after which the unit was kept running until all the data for each radiation were obtained. The intensity at a standard position was checked periodically to guard against fluctuations in the incident intensity.

Monochromatization of the reflected X-ray beam was accomplished by means of balanced filters [3].

The sample, supplied by G. W. Cleek and E. H. Hamilton of NBS, contained 20 mole percent BaO and 80 mole percent B_2O_3. The observed intensities are shown in figure 3.

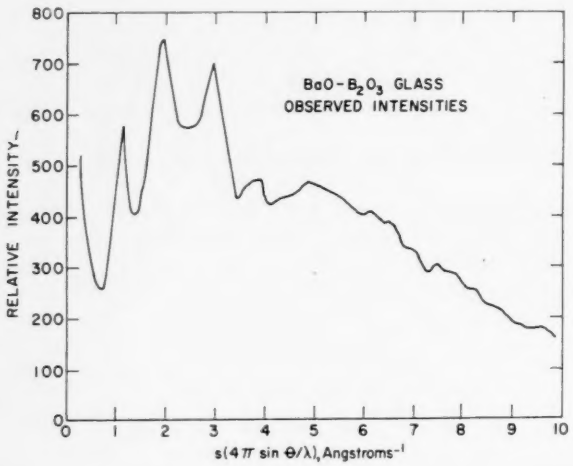

FIGURE 3. *Diffraction pattern of vitreous barium borate.*

3. Theory

Neglecting polarization and atomic constants, the amplitude of X-rays scattered from an electron distribution $\rho(\vec{R})$ is given by

$$F(\vec{k})=\int \rho(\vec{R}) \exp(-2\pi i\vec{k}\cdot\vec{R})d\vec{R} \qquad (1)$$

where $\vec{k}$ is the reciprocal space vector. The intensity is given by

$$I(\vec{k})=F(\vec{k})F^*(\vec{k}),$$

where $F^*(\vec{k})$ is the complex conjugate of $F(\vec{k})$. Then, using the convolution theorem [4], the Fourier transform of $I(\vec{k})$ is given by

$$P(\vec{R})=\int \rho(\vec{r})\rho(\overrightarrow{r+R})\,d\vec{r}=\int I(\vec{k})\exp(2\pi i\vec{k}\cdot\vec{R})d\vec{K} \qquad (2)$$

where, as in most X-ray diffraction transform techniques, we have assumed that the sample is of infinite extent.

If the sample is such that $I(\vec{k})$ is spherically symmetric in k-space, e.g., a powder or an amorphous material, the integral over the angular portions, expressing $\vec{k}$ in a spherical polar coordinate system with the k_z axis parallel to $\vec{R}$, can be performed directly. In this case,

$$P(\vec{R})=\int_0^\infty\int_0^\pi\int_0^{2\pi} I(k)\exp(2\pi i kR\cos\alpha)k^2\sin\alpha\,d\phi\,d\alpha\,dk$$

$$=2\pi\int_0^\infty\int_0^\pi I(k)\exp(2\pi i kR\cos\alpha)k^2\sin\alpha\,d\alpha\,dk$$

$$=(2/R)\int_0^\infty I(k)\sin(2\pi kR)\,k\,dk$$

$$P(\vec{R})=(2/4R\pi^2)\int_0^\infty s\,I(s)\,\sin(sR)\,ds \qquad (3)$$

where $s=2\pi k=4\pi \sin\theta\lambda$.

Here, $P(\vec{R})$ is the three-dimensional Patterson function. Since, for a powder or an amorphous material, it is spherically symmetric, it may be written as $P(R)/4\pi R^2$, where $P(R)$ is the relative probability of finding two electrons separated by a distance R, and is called the electron radial distribution function. Then

$$P(R)=(2R/\pi)\int_0^\infty s\,I(s)\sin(sR)\,ds. \qquad (4)$$

With the usual [5] considerations about the inability to make measurements of I for small s, and the subtraction of the contribution of each atom convoluted with itself to $P(R)$, this can be written

$$P(R)-P_0(R)=(2R/\pi)\int_{s_{min}}^\infty s\{I(s)-\Sigma_m f_m^2\}\sin(sR)\,ds \qquad (5)$$

where $\Sigma_m f_m^2$ is the weighted sum of the squares of the atomic scattering factors of the atoms in the sample and $P_0(R)$ is the distribution obtained from a homogeneous array of electrons with the same average electron density as the sample.

If the usual assumption is made that the different atomic scattering factors can be expressed as multiples of a normalized average scattering factor, f_e, where normalization implies $f_e(s=0)=1$, then division of the integrand by the square of the normalized average scattering factor reduces the distribution to that of point atoms and yields the atomic radial distribution function commonly used [6]. This can be written

$$\sum_m \lambda_m 4\pi R^2(\rho_m-\rho_0)=(2R/\pi)\int_{s_{min}}^\infty si(s)\sin(Rs)ds \qquad (6)$$

where $i(s)=(I(s)-\Sigma_m f_m^2)/f_e^2$, $\Sigma_m \lambda_m$ is the effective number of electrons of atom m summed over atoms m, and $4\pi R^2\rho_m dR$ is the number of atoms, each multiplied by its effective number of electrons, between R and $R+dR$, from atom m.

4. Calculations

The coherent scattered intensity is obtained from the experimentally measured intensity by correction for polarization and incoherent scattering. The incoherent scattering factor for barium was calculated using the equation [7]

$$I_{\text{inc}}=Z-f^2/Z. \tag{7}$$

The coherent scattering factors for barium, oxygen, and boron as well as the incoherent scattering factors for boron and oxygen were obtained from standard references [8]. The incoherent scattering factors were corrected with the Breit-Dirac factor [7].

The density of the sample was 2.83 g/cm^3 and from this value and the molecular weight, the average electron density was calculated to be 0.79 electrons/A^3.

The data were placed on an absolute scale by setting

$$\sum_s sI(s)_{\text{obs}}\Delta s=\sum_s\{\sum_m sf_m^2+sI_{\text{calc inc}}\}\Delta s. \tag{8}$$

After corrections for polarization and incoherent scattering had been applied, the functions $s\{I(s)-\Sigma_m f_m^2\}$ and $si(s)$ were computed from the experimental data. The integrals were replaced by sums of the form

$$\sum_{s=0.3}^{10.0} s\ i(s)\ \sin(sR)\Delta s$$

which were performed on a high speed digital computer for 0.1 A spacings in R from $R=0$ to $R=9.9$. Multiplication by $2R/\pi$ gave the right-hand sides of (5) and (6), and from these the radial distribution functions were calculated.

5. Conclusions

Figure 4 shows the electron radial distribution $P(R)$–$P_0(R)$ obtained. The most significant features for the purpose of this study are the absence of a peak at 5.5 A and the large peak at 6.8 A. The peak at 6.8 A corresponds to the type B barium–barium separation prediction by Levin and Block. 5.5 A is the barium–barium separation for the type A structure.

Figure 5 shows the electron radial distribution $P(R)$. The poor resolution does not allow for a calculation of the area under each peak. However, the areas may be calculated by determining the area between minimums of the peaks of the $P(R)$–$P_0(R)$ distribution and adding to this area the integral of $P_0(R)$ over the range between the minimums. This

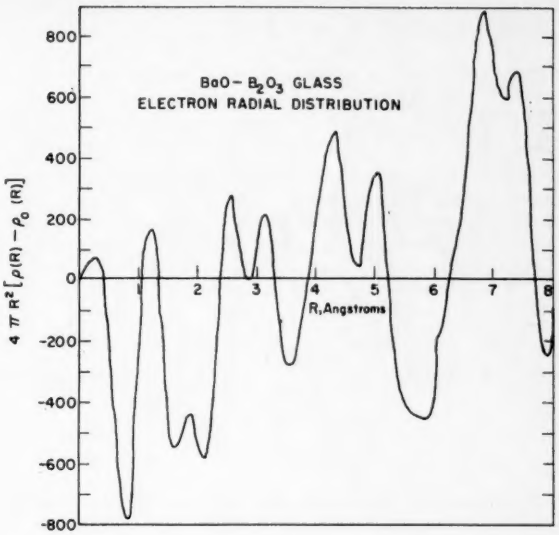

FIGURE 4. *Electron radial distribution function,* $4\pi R^2[\rho(R)-\rho_0(R)]=P(R)-P_0(R)$, *calculated from the data of figure 3.*

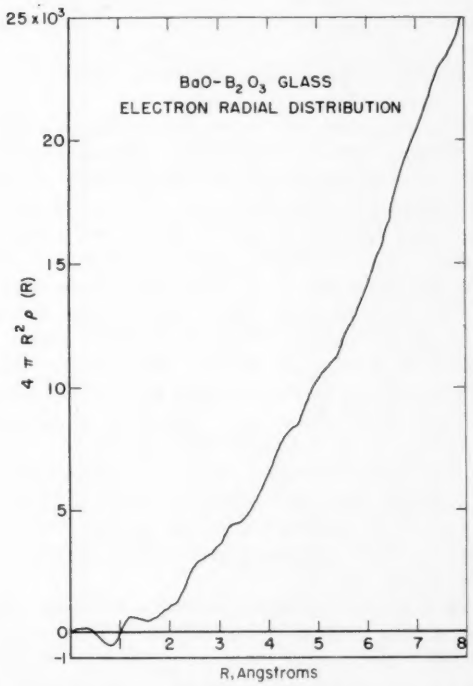

FIGURE 5. *Electron radial distribution function,* $4\pi R^2\rho(R)=P(R)$, *calculated from the data of figure 3.*

method suffers considerably in accuracy due to overlap, but offers some means of calculating areas. For this reason, the areas of the first three peaks only were calculated. The results were 322 (electrons)^2 for the 1.2 A peak, 1750 (electrons)^2 for the 2.55 A peak, and 2779 (electrons)^2 for the 3.1 A peak.

A more complete picture of the type B structure is shown in figure 6. On the basis of this model, the

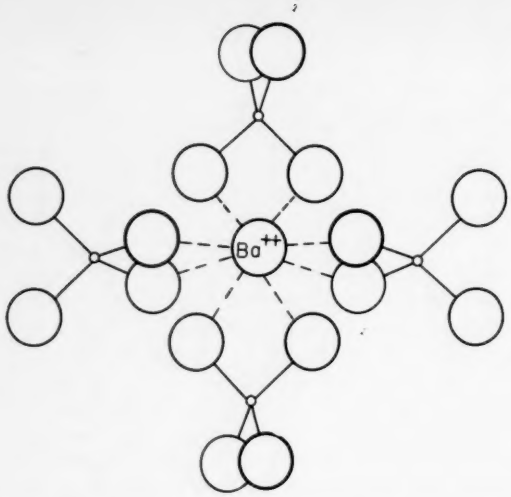

FIGURE 6. *Schematic representation showing the coordination of oxygen atoms about the barium.*

The boron and barium configurations share edges.

peaks in the radial distribution can be explained readily. The 1.2 A peak corresponds to the boron–oxygen distance. The predicted area of this peak is

$$4\times1.6\times10\times2\times2=256(\text{electrons})^2$$

Here 4 is the expected number of oxygens surrounding each boron, 1.6 is the number of borons in the basic unit used for scaling the intensities, 10 and 2 are the number of electrons per ion associated with the oxygen and boron, respectively (these values are used throughout the paper), and the last factor of 2 takes into account the fact that each peak appears twice in the distribution function. The observed area of the peak is more consistent with an oxygen coordination of 5 around boron. However, this coordination would be quite unusual and is inconsistent with the short B–O distance. Hence it seems likely that some error in the distribution function obtained from the data has changed both the area and position of the peak. In the region of small R this function is most susceptible to such errors and these errors will be most significant because of the small area of the peak.

The 2.55 A peak corresponds to the oxygen–oxygen separation in the boron tetrahedron. The predicted area is 1560 (electrons)^2 which agrees to within 15 percent with the observed area of 1750 (electrons)^2.

The 3.1 A peak appears to be a superposition of Ba–O, O–O, and Ba–B peaks. The Ba–O distance predicted on the basis of ionic radii is 2.8 A. Considering the distortion of the Ba cube, however, a larger distance is not unreasonable. The predicted area of the Ba–O peak is 1698 (electrons)^2. This figure is based on a value of 54 scattering electrons for barium. The O–O distance predicted is 3.1 A. This distance is the longer of the edges of the distorted barium cube. The predicted area of this O–O peak is 1040 (electrons)^2. The predicted Ba–B distance is one-half the Ba–Ba distance, or 3.4 A. The predicted area of this peak is only 173 (electrons)^2. Thus, the peak makes no observable contribution to the radial distribution beyond its contribution to the area of the 3.1 A peak. The predicted total area of the 3.1 A peak is 2811 (electrons)^2, in good agreement with the observed value of 2779 (electrons)^2.

The 4.3 A peak corresponds to the distance between a barium and the closest oxygens which are not nearest neighbors. These oxygens are the parts of the boron tetrahedron which are not involved in the edge sharing with the polyhedron of the barium under consideration.

The 5.0 A peak corresponds to the distance across a face diagonal of the distorted barium cube. In addition, there should be a peak at 5.6 A corresponding to a body diagonal in the barium polyhedron. The area of this peak would be only 520 (electron)^2. It is not observed.

Figure 7 shows the atomic radial distribution function obtained from the data. The most interesting feature of the peak is the clearly visible 6.8 A peak. Peaks at this distance are not usually observed in glasses. It seems reasonable to assume either that the introduction of barium into the glass has increased the range of ordering or that because of barium's great scattering power it allowed the determination to be extended to this region.

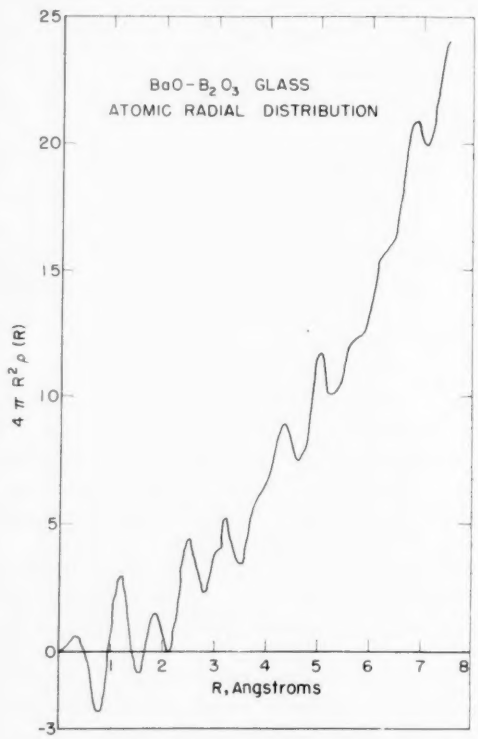

FIGURE 7. *Atomic radial distribution function,* $4\pi R^2\rho(R)$, *calculated from the data of figure 3.*

Because of the agreement between the position of peaks on the radial distribution and the distances predicted on the basis of structure type B, it seems likely that the structure is type B and is definitely not type A. The good agreement between predicted and observed areas adds validity to this conclusion.

6. References

[1] E. M. Levin and S. Block, Structural interpretation of immiscibility in oxide systems, J. Am. Ceram. Soc. **40,** 95 (1957).

[2] B. E. Warren and A. G. Pincus, Atomic considerations of immiscibility in glass systems, J. Am. Ceram. Soc. **23,** 301 (1940).

[3] P. Kirkpatrick, On the theory and use of Ross filters, Rev. Sci. Inst. **10,** 186 (1938); **15,** 223 (1944).

[4] J. Waser and V. Schoemaker, The Fourier inversion of diffraction data, Rev. Mod. Phys. **25,** 671 (1953).

[5] N. S. Gingrich, The diffraction of X-rays by liquid elements, Rev. Mod. Phys. **15,** 90 (1943).

[6] B. E. Warren and N. S. Gingrich, Fourier analysis of X-ray powder patterns, Phys. Rev. **46,** 368 (1934).

[7] R. W. James, The optical principles of the diffraction of X-rays, p. 462 (Macmillan and Company, Ltd., London, England, 1950).

[8] A. H. Compton and S. K. Allison, X-rays in theory and experiment, 2d ed. (D. Van Nostrand Company, New York, N.Y., 1935); W. L. Bragg, The crystalline state (The Macmillan Company, New York, N.Y., 1934); H. Viervoll and O. Ogrim, An extended table of atomic scattering factors, Acta Cryst. **8,** 277 (1949).

Washington, D.C.

(Paper 64A3–46)

JOURNAL OF RESEARCH of the National Bureau of Standards—A. Physics and Chemistry
Vol. 64A, No. 3, May–June 1960

Separation and Determination of Small Quantities of Aluminum in Steel

Bruce B. Bendigo and Rosemond K. Bell

(December 21, 1959)

A method is described for determining small amounts of aluminum (0.01 to 0.3 percent) in stainless and carbon steels. A perchloric-sulfuric acid solution of the steel is electrolyzed in a mercury cathode cell to remove most of the iron, and an extraction with chloroform is made to remove elements such as aluminum, residual iron, and titanium as cupferrates from a solution buffered at *p*H 3.5. These elements are converted from cupferrates to perchlorates; all except aluminum are then extracted as cupferrates with chloroform from 4 *N* hydrochloric acid. Aluminum in the acid solution is determined photometrically with aluminon (ammonium aurintricarboxylate) at a wave length of approximately 540 millimicrons. An accuracy of ±0.005 percent aluminum is indicated.

1. Introduction

Steel may contain up to 1 percent or more of aluminum as an alloying agent, or it may contain less than 0.1 percent aluminum introduced either as a final deoxiding agent or from the processing materials.

The determination of aluminum in steel usually requires the separation of this element from major amounts of iron, as well as from certain other elements that would interfere in the final estimation of the aluminum by photometric methods such as the aluminon method [4].[1]

A number of procedures have been used for this initial concentration step, for example, hydrolytic precipitation with sodium bicarbonate or sodium hydroxide, extraction of iron with ether [13], 8-hydroxyquinoline precipitation in cyanide solution [1], electrolysis in a mercury cathode cell [3], extraction of iron cupferrate [2], and separation by ion exchange [6, 7].

Consideration of the relative advantages and limitations of the above-mentioned procedures, as well as preliminary experimental work, led to the selection of the electrolytic separation as best suited for the initial separation step in the procedure described in this paper.

In the method to be described, the sample of steel is dissolved in hydrochloric acid, perchloric acid is added, and the solution is evaporated to fumes of perchloric acid. The acid solution is electrolyzed in a mercury cathode cell to remove most of the iron. Aluminum, residual iron, and certain other elements not removed by electrolysis are extracted as cupferrates from the electrolyte at *p*H 3.5 with chloroform. These elements are converted from cupferrates to perchlorates; all except aluminum are then extracted as cupferrates with chloroform from 4 *N* hydrochloric acid. Aluminum in the aqueous portion is then determined photometrically with aluminon. Two days are usually required to complete a determination.

[1] Figures in brackets indicate the literature references at the end of this paper.

2. Apparatus and Reagents

Mercury Cathode Cell. A Dynacath type of mercury cathode cell was used to electrolyze the solutions.

Colorimeter. An Evelyn photometer, with voltage stabilizer and galvanometer, was used for the quantitative optical measurements. Matched test tubes (22 by 175 mm) were used as absorption cells.

Cupferron Solution (60 g/liter). Dissolve 6 g of cupferron in 100 ml of cold water and filter. Prepare fresh as needed.

Thioglycolic Acid Solution (100 ml/liter). Dilute 10 ml of thioglycolic acid to 100 ml with water and filter, if necessary. This solution is stable for 1 week.

Aluminon-Buffer Composite Solution. Dissolve 125 g of ammonium acetate in 250 ml of water and add 20 ml of glacial acetic acid. Filter through a tight paper. While stirring this filtrate well, add first a solution of 0.250 g of aluminon (ammonium aurintricarboxylate) dissolved in 50 ml of water, followed by a solution of 0.5 g of benzoic acid dissolved in 20 ml of methanol. Dilute the resulting solution to 500 ml, add 250 ml of glycerol, and stir well. Store in a dark glass-stoppered bottle.

Standard Aluminum Solution A (1 ml=1.00 mg aluminum). Transfer 1.000 g of high-purity aluminum to a 1-liter volumetric flask. Add 50 ml of hydrochloric acid (1+1) [2] and heat gently until the metal is completely dissolved. Cool to room temperature, dilute to the mark, and mix.

[2] Hydrochloric acid (1+1) denotes 1 volume of concentrated hydrochloric acid, sp gr 1.18, diluted with 1 volume of water. Nitric acid (1+1) denotes 1 volume of nitric acid, sp gr 1.42, diluted with 1 volume of water. Sulfuric acid (1+1) denotes 1 volume of sulfuric acid, sp gr 1.84, diluted with 1 volume of water. If no dilution is specified, the concentrated reagent is meant.

Standard Aluminum Solution B (1 ml=0.05 mg aluminum). Transfer exactly 50 ml of the standard aluminum solution A to a 1-liter volumetric flask. Add 10 ml of perchloric acid (70 to 72%), dilute to the mark, and mix. This solution should be prepared as needed.

Dinitrophenol Indicator (0.2 g/liter). Dissolve 20 mg of 2,4-dinitrophenol in 100 ml of water.

3. Procedure

Transfer 5 g of the steel sample (0.01 to 0.3 percent aluminum) to a 600-ml beaker and add 75 ml of hydrochloric acid (2+1). Heat gently until the sample is decomposed. Carefully add nitric acid (1+1) to oxidize the iron and add 20 ml in excess. Cool and add 50 ml of perchloric acid (70 to 72%). Evaporate the solution to fumes of perchloric acid, cover the beaker, and continue the heating for 10 min. If the chromium exceeds 5 percent, add hydrochloric acid in small portions to the hot perchloric acid solution until no more chromyl chloride is volatilized. Cool, add 200 ml of water, and boil for several minutes. Remove from the heat, add paper pulp, and let stand until the precipitate settles. Filter through a close-textured paper containing paper pulp. Wash 10 times with sulfuric acid (1+99) and reserve the filtrate.

Transfer the paper and contents to a 30-ml platinum crucible. Char the paper and ignite under good oxidizing conditions at 500° C until the carbon is destroyed. Cool, add 2 drops of sulfuric acid (1+1), and 5 to 10 ml of hydrofluoric acid (48 percent) to the ignited residue. Heat the crucible in an air bath until the acids are expelled. Cool the crucible, and fuse the residue with 1 g of fused sodium bisulfate. Cool, add 20 ml of sulfuric acid (1+99) to the crucible, and heat gently until the melt is disintegrated. Transfer the contents to a 150-ml beaker with sulfuric acid (1+99). Boil for 5 min to insure complete solution of the aluminum salts and filter through a close-textured paper. Wash 5 times with sulfuric acid (1+99) and discard the paper and contents. Cool the filtrate to room temperature and combine it with the reserved filtrate. Transfer the combined filtrates to a 500-ml volumetric flash, dilute to the mark, and mix.

Transfer a 100-ml aliquot portion of the solution (this portion is equivalent to 1 g of the sample) with a pipet to a mercury cathode cell containing 35 ml of mercury. Add 5 ml of sulfuric acid (1+1) and electrolyze with a current of 15 amp until the solution is colorless. About 15 min are required to remove 1 g of iron. Remove the electrolyte from the cell and wash the electrodes and cell with sulfuric acid (1+99). Filter the electrolyte and washings through a medium-textured paper. Wash 5 times with sulfuric acid (1+99) and discard the paper. Evaporate the filtrate to about 50 ml, then cool.

Neutralize the solution with ammonium hydroxide, using litmus as an indicator. Immediately acidify with hydrochloric acid (1+1) and add 10 ml in excess. Cool to room temperature and add ammonium hydroxide until the *p*H is between 3 and 7, as indicated by a *p*H meter. Immediately add 10 ml of formic acid, and mix. Add ammonium hydroxide until the *p*H is 3.5 ± 0.1.

Transfer the buffered solution to a 250-ml separatory funnel and cool in ice water for 15 min. Disregard any insoluble salts. Add 25 ml of cupferron solution, mix, and allow to stand for 15 min in ice water. Extract the cupferrates with 25-ml portions of chloroform until the chloroform layer remains colorless. Allow the layers to separate while the funnel cools in ice water. Transfer the chloroform layers to a 300-ml Kjeldahl flask containing 10 ml of water. Three or four extractions are usually sufficient. Discard the aqueous layer.

Heat the Kjeldahl flask in a water bath until the chloroform evaporates. Cool and add 10 ml of nitric acid and 6 ml of perchloric acid (70 to 72%). Swirl the solution over a free flame until the perchloric acid condenses at the mouth of the flask. Cool, add 10 ml of hydrochloric acid, and heat as directed before until perchloric acid condenses in the neck of the flask. Cool, add 50 ml of water, and boil for 5 min. Cool to room temperature.

Transfer the solution to a 250-ml separatory funnel, wash the flask with 60 ml of hydrochloric acid (1+1), and add the washings to the funnel. Dilute the resulting solution to 100 ml, mix, and cool the funnel in ice water for 15 min. Add 10 ml of the cupferron solution, mix, and allow to stand in the ice water for 10 min. Extract the cupferrates with one 25-ml portion and several 10-ml portions of chloroform until the chloroform layer remains colorless. Allow the layers to separate while the funnel cools in ice water. Discard the chloroform extracts. Transfer the aqueous portion to the same Kjeldahl flask used before.

Add 10 ml of nitric acid (1+1) and evaporate the solution to about 25 ml. Add 10 ml of nitric acid and continue the evaporation until the perchloric acid condenses at the top of the flask. Cool, add 50 ml of water, and boil for 5 min. Cool to room temperature.

Transfer the solution to a 200-ml volumetric flask, dilute to the mark, and mix. Transfer a 20-ml aliquot portion with a pipet to a 100-ml volumetric flask. Add 3 drops of the dinitrophenol indicator solution to the flask and neutralize the solution by dropwise addition of ammonium hydroxide until the indicator turns yellow. Immediately add hydrochloric acid (1+1) dropwise until the solution is colorless and then add 1 drop in excess. Add 2 ml of the thioglycolic acid solution and exactly 15.0 ml of the aluminon-buffer composite solution. Because the composite solution is rather viscous, the pipet should drain for a minute or two. Place the flask in a 400-ml beaker containing boiling water and heat for exactly 4 min while maintaining the boiling temperature. Remove from the heat and let stand for 1 min. Cool in running water for 4 min. Dilute to the mark and mix. Transfer a suitable portion of the solution to an absorption

cell and measure the absorbancy or transmittancy at 540 mμ, using water as a reference solution. Obtain from a calibration curve the milligrams of aluminum in the final solution. Correct the value obtained for a reagent blank carried through all steps of the procedure.

4. Preparation of the Calibration Curve

To eight 100-ml volumetric flasks transfer 0.0, 0.5, 1.0, 2.0, 3.0, 4.0, 5.0, and 6.0 ml of the standard aluminum solution B. Add 5 drops of perchloric acid (70 to 72%) to each and dilute to 20 ml. Add 3 drops of dinitrophenol indicator to each flask, and follow with dropwise addition of ammonium hydroxide until the indicator turns yellow. Immediately add hydrochloric acid (1+1) dropwise until the solution is colorless and add 1 drop in excess. Add 2 ml of the thioglycolic acid solution and 15.0 ml of the aluminon-buffer composite solution. Place each flask in a 400-ml beaker containing boiling water. Heat for exactly 4 min while maintaining the boiling temperature. Remove from the heat and let stand for 1 min. Cool in running water for 4 min, dilute to the mark, and mix. Measure the absorbancy or transmittancy of each solution as directed for the analysis sample. Plot the values obtained against milligrams of aluminum per 100 ml of solution.

5. Results

The data in table 1 show the results obtained when the recommended procedure is used to determine aluminum in solutions of 1 g of stainless steel (having less than 0.001 percent aluminum) containing known additions of aluminum. The data in table 2 indicate the results obtained by applying the recommended procedure to various NBS standard samples.

TABLE 1. *Results obtained for aluminum by applying the recommended procedure to solutions of one gram of a stainless steel* (Al <0.001%) *containing known additions of aluminum*

Added	Found [a]	Difference
mg	*mg*	*mg*
0.02	0.02	0.0
.04	.04	.0
.06	.06	.0
.10	.09	−.01
.10	.09	−.01
.10	.10	.0
.10	.11	+.01
.20	.21	+.01
.20	.21	+.01
.30	.29	−.01
.30	.32	+.02
.50	.47	−.03
.80	.77	−.03
1.10	1.08	−.02

[a] Corrected for blank on reagents plus the steel.

TABLE 2. *Results obtained for aluminum by applying the recommended procedure to various National Bureau of Standards standard steels*

NBS standard steel	Found	Certificate value	Type of steel
	%	%	
1164	0.0043 .0048	[a] 0.005	Si 0.5, V 0.3.
1166	.014 .015	[a] .015	Open-Hearth Iron (Ti 0.06).
1162	.022 .021	[a] .023	Ni 0.7, Cr 0.7, Sn 0.07, Ti 0.04, Nb 0.1, Zr 0.06.
111b	.042 .044	.042	Ni 1.8, Mo 0.3.
65d	.056 .056 .055 .057 .058	.059	Basic Electric Steel (C 0.3).
22c	.110 .114	.116	Bessemer Steel.
1167	.156 .150	[a] .16	Ti 0.3, W 0.2, Zr 0.1, Nb 0.3, Ta 0.2.
1165	.185 .187	[a] .19	Open-Hearth Iron (Ti 0.2).

[a] Provisional value.

6. Discussion

After electrolysis in the mercury cathode cell, the electrolyte contains all of the aluminum, titanium, vanadium, zirconium, phosphorus, alkaline earths, and residual iron and chromium. It will also contain the earth acids and tungsten which have escaped filtration, as well as relatively large amounts of perchloric acid. Further separations of aluminum are based on the fact that aluminum cupferrate is extracted by chloroform from a solution buffered between *p*H 2 and 5 [5], but not from a solution 4 *N* in acid [11, 14].

There are several advantages gained by an extraction of cupferrates from the electrolyte buffered at *p*H 3.5. At this *p*H, aluminum is separated from phosphate. This is of possible utility when aluminum is determined as the oxide after precipitation as the hydroxide. At *p*H 3.5, the cupferron separation of aluminum removes the relatively large amounts of perchloric and sulfuric acids which would interfere by forming ammonium salts later in the photometric determination of the aluminum. Most of the residual chromium in the electrolyte is also removed in the aqueous phase. Aluminum cupferrate is completely extracted by chloroform from a solution that is buffered with formic acid to *p*H 3.5. Measured quantities of aluminum were added to and extracted from this buffered solution, and very little, if any, of the added aluminum was lost, as can be seen from the results shown in table 3.

The chloroform extraction of cupferrates from a 4 *N* hydrochloric acid separates interfering elements from the aluminum, which remains in the aqueous portion. Very small amounts of chromium may accompany the aluminum. However, tests showed that 0.15 mg of chromium did not interfere in the

TABLE 3. *Results obtained for aluminum when aluminum cupferrate is extracted with chloroform from a solution buffered at pH 3.5 with formic acid*

Added	Found	Difference
mg	*mg*	*mg*
0.27	0.26	−0.01
.50	.49	−.01
.73	.73	.00
1.03	1.01	−.02

photometric determination of the aluminum with aluminon. After the small amount of unextracted cupferron has been destroyed, the aluminum can be determined by any suitable method. When aluminum is present in small quantities, it is determined conveniently by the aluminon-photometric method. When larger amounts of aluminum are present, it can be determined gravimetrically, if desired. Tests were made for aluminum remaining in the aqueous solution after extraction with chloroform from a 4 *N* acid solution to which cupferron and known quantities of aluminum had been added. These results are given in table 4.

TABLE 4. *Results obtained for aluminum in the aqueous solution after a 4 N* HCl-$HClO_4$ *solution containing aluminum and excess cupferron is extracted with chloroform*

Added	Found	Difference
mg	*mg*	*mg*
0.02	0.03	+0.01
.04	.04	.00
.06	.06	.00
.08	.08	.00

It is well established that iron can be separated from aluminum by electrolysis in a mercury cathode cell [8, 9]. Wiberley and Bassett [16] suggests a one-normal mixture of perchloric-sulfuric acids as the electrolyte. It is not necessary to completely remove the iron because small remaining quantities are separated later in the recommended procedure. Because chromium is removed slowly by electrolysis, it is advantageous, with steels containing more than 5 percent chromium, to remove most of the chromium as chromyl chloride prior to electrolysis. No significant errors occur if less than 50 mg of chromium remain before electrolysis. No aluminum is lost during electrolysis, according to Scherrer and Mogerman [12]. When known quantities of aluminum were added to solutions representative of those present after electrolysis, and the recommended procedure followed, quantitative results were obtained, as shown by the data in table 5.

The recommended aluminon photometric procedure has been described by Pellowe and Hardy [10]. The optimum amount of aluminum in the final aliquot is between 0.02 and 0.30 mg. It should be noted that the color of the solution has a significant temperature coefficient [15]. Therefore, when absorbancy measurements are made, the temperature of test solutions and standards should not differ by more than 5° C.

TABLE 5. *Results obtained for aluminum in synthetic solutions representative of the electrolyte remaining after electrolysis with a mercury cathode cell*

Aluminum			Composition of solutions			
Added	Found	Difference	Iron	Chromium	Titanium	Vanadium
mg	*mg*	*mg*	*mg*	*mg*	*mg*	*mg*
0.25	0.26	+0.01	1	1	0.5	0.5
.50	.50	.00	1	1	.5	.5
.75	.72	−.03	1	1	.5	.5

As described, the method recommended in this paper is used to determine *total* aluminum. If desired, however, the acid-insoluble aluminum can be separated from that which is soluble by filtering the hydrochloric acid solution of the sample; each can then be determined separately in the solution and residue.

The recommended sample size of 5 g will minimize the error due to the segregation of aluminum in the alloy. In the procedure described, an aliquot equivalent to 1 g of steel is taken for electrolysis.

7. References

[1] ASTM Methods for chemical analysis of metals, p. 213 (American Society for Testing Materials, Philadelphia, Pa., 1956).
[2] ibid, p. 251.
[3] ibid, p. 282.
[4] C. H. Craft and C. R. Makepeace, Ind. Eng. Chem. Anal. Ed. **17,** 206 (1945).
[5] N. H. Furman, W. B. Mason, and J. S. Pekola, Anal. Chem. **21,** 1325 (1949).
[6] J. V. Gilfrich, Anal. Chem. **29,** 978 (1957).
[7] A. D. Horton and P. F. Thomason, Anal. Chem. **25,** 1326 (1956).
[8] G. E. F. Lundell and J. I. Hoffman, Outlines of methods of chemical analysis, p. 94 (J. Wiley and Sons, Inc., New York, N.Y., 1938).
[9] J. A. Maxwell and R. P. Graham, Chem. Rev. **46,** 482 (1950).
[10] E. F. Pellowe and F. R. F. Hardy, Analyst **79,** 225 (1954).
[11] E. B. Sandell, Colorimetric determination of traces of metals, 3d ed., p. 221. (Interscience Pub., Inc., New York, N.Y., 1959).
[12] J. A. Scherrer and W. D. Mogerman, J. Research NBS **21,** 105 (1938) RP1117.
[13] H. G. Short, Analyst **75,** 420 (1950).
[14] N. Strafford and P. F. Wyatt, Analyst **72,** 54 (1947).
[15] W. Werz and A. Neuberger, Arch. Eisenhuttenw. **26,** 205 (1955).
[16] S. E. Wiberley and L. G. Bassett, Anal. Chem. **21,** 609 (1949).

WASHINGTON, D.C.

(Paper 64A3–47)

JOURNAL OF RESEARCH of the National Bureau of Standards—A. Physics and Chemistry
Vol. 64A, No. 3, May–June 1960

Conformations of the Pyranoid Sugars. II. Infrared Absorption Spectra of Some Aldopyranosides

R. Stuart Tipson and Horace S. Isbell

(January 29, 1960)

The conformations of twenty-four aldopyranosides have been studied by analysis of their infrared absorption spectra. The most stable conformations of twelve of the glycosides had previously been assigned by Reeves from a study of their instability factors; these conformations were assumed to apply to the crystalline state, for which the spectra had been recorded. The compounds were classified into (a) configurationally and (b) structurally related groups, and the spectra were intercompared. The analysis revealed groups of absorption bands which showed a concerted shift on change of anomeric disposition.

With these groups of absorption bands thus identified, intercomparison with nine of the remaining spectra afforded evidence that the anomeric group (1) is axial in methyl D-*glycero*-α-L-*gluco*-heptopyranoside, methyl D-*glycero*-α-L-*manno*-heptopyranoside, and methyl D-*glycero*-α-D-*gulo*-heptopyranoside; (2) is equatorial in methyl 6-deoxy-β-L-mannopyranoside, methyl D-*glycero*-β-D-*gulo*-heptopyranoside, and cyclohexyl D-*glycero*-β-D-*gulo*-heptopyranoside; and (3) either is quasi or occurs as different (or mixed) axial and equatorial forms in methyl α-D-lyxopranoside, methyl β-D-lyxopranoside, and (possibly) α-D-methylgulopyranoside.

Three of the glycosides were available as their crystalline complexes with calcium chloride. The spectra of these complexes were also examined, and the effect of co-crystallization with calcium chloride is pointed out.

1. Scope and Purpose of the Project

The shape or conformation of a molecule greatly influences its rates of reaction and other properties. For this reason, detailed knowledge of the conformations of pyranoid derivatives is desirable. Our prior publications on this subject have presented a system for naming the conformations of pyranoid compounds [1,2].[1]

The conformations of numerous methyl glycosides and other pyranoid derivatives have been determined by Reeves from (a) a study of stereomeric factors and (b) the type of complex formed in cuprammonia solution. Reaction of cuprammonia with an aldopyranoside may sometimes cause alteration in the conformation. Hence, assignments of conformation based on the formation of copper complexes need confirmation by measurement of at least one relevant physical characteristic.

The work herein reported was primarily undertaken to provide infrared spectrograms of aldosides having the pyranoid ring, with the object of discovering correlations that might be of value in conformational analysis. It seemed possible that the axial or equatorial disposition of reference groups in the various molecules of glycopyranosides should give rise to different vibrations, and that it should, accordingly, be feasible to identify certain bands in their spectra as being characteristic of the different ways of arranging the reference groups. The infrared spectra for a group of aldopyranosides have, therefore, been recorded, and the bands have been compiled and then studied by statistical and comparative methods.

Prior publications from our laboratory on related topics have dealt with the infrared absorption spectra of sugar acetates [3] and of some cyclic acetals of sugars [4], and with a system for classifying carbohydrate derivatives for comparative purposes [5]. The acetals previously studied are polycyclic and have fused or bridged rings; the conformations of such molecules are "locked." On the other hand, the pyranoid ring of some unsubstituted glycopyranosides is flexible, and the conformation adopted may depend on the physical conditions; thus, the conformation of the molecules in solution, particularly in the presence of a complexing agent, may be different from that of the molecules in the crystalline material. In the present study, the infrared absorption spectra of compounds *in the solid phase* have been recorded, and a method has been developed for assignment of conformation from analysis of the infrared absorption spectra and comparison with the spectra of glycosides of known conformation.[2]

2. Compounds Investigated

Table 1 gives a list of the compounds, their code numbers [5],[3] predicted stable conformations, and an index to the spectrograms; the serial number of a compound is the same as the number of its spectro-

[1] Figures in brackets indicate the literature references at the end of this paper. The references for table 1 are given at the end of the table.

[2] The method of comparison is being applied to other groups of structurally related pyranoid sugar derivatives.

[3] Code numbers are assigned according to a previously published classification system [5], for use with punched-card techniques.

gram. The spectra were measured in the region of 5000 to 667 cm^{-1} (sodium chloride optics) and in the region of 667 to 250 cm^{-1} (cesium bromide optics). The spectrograms are given together with a discussion of (a) the structure of the compounds and (b) some of the outstanding features of their spectra.

All of the compounds listed in table 1 are glycosides of aldoses, and all have the pyranoid ring. As a common structural feature, all but one of the glycosides have a glycosidic methoxyl group; one has a glycosidic cyclohexyloxy group. The glycosides differ in regard to one or more of the following features: (a) the α or β anomeric configuration at carbon atom 1, (b) the configurations of the other carbon atoms of the pyranoid ring, (c) the nature and configuration of the substituent, if any, at carbon atom 5 of the pyranoid ring, and (d) the configuration of carbon atom 5 in those glycosides in which this atom is asymmetric.

The conformation selected by Reeves as probably the most stable is shown in table 1 for each of those glycosides mentioned that he studied. The conformations are indicated by the system devised by Isbell and Tipson [1, 2]; the symbol CA means "that chair conformation for which the α anomeric group is axial," and the symbol CE means "that chair conformation for which the α anomeric group is equatorial." The chair forms and nomenclature for the anomers of the methyl aldopyranosides are shown in figures 1 and 2. The infrared absorption spectra of the same polymorphic modification of two members of an enantiomorphic pair are indistinguishable Hence, in the present study, the spectrum of whichever member was available was examined, and was considered to apply to the other enantiomorph.

3. Reference Aldopyranosides of Known Conformation

Each methyl aldopyranoside is theoretically capable of assuming at least one of a variety of different conformations, depending on the conditions. From studies made by Reeves [6 to 8], it would appear that two groups (A and B) of methyl aldopyranosides can be distinguished. Glycosides in group A have one of the two chair-forms. The members of group B exist either (a) as a mixture of the two chair-forms or (b) as some other conformation.

It seemed likely that, in the solid state, each individual aldopyranoside would exist in only one conformation; and this conformation would presumably be the one it took as it crystallized from solution. As a working hypothesis, it was assumed that the conformation of an aldopyranoside in the crystalline state is the same as the stable form predicted by Reeves. It would then be reasonable to expect that examination of the infrared absorption spectra of the solid phase of those glycopyranosides of group A (each believed to assume a *single* chair-conformation), followed by a comparison with the spectra of the *other* group (B) of aldopyranosides, might provide evidence regarding the conformations (in the solid phase) of the members of the latter group (B).

TABLE 1. *Compounds measured, stable conformations, and index to spectrograms*

Code [a]	Compound	Reference	Stable conformation [b]					Spectrogram
			Reeves' assignment [c]	Anomeric disposition [c]	Reference	Present assignment [d]	Anomeric disposition [d]	
10.11111	Methyl α-D-xylopyranoside	1, 2	CA	a	13	CA	a	1
10.11211	Methyl β-D-xylopyranoside	1, 2	CA	e	13	CA	e	2
10.21111	Methyl α-D-glucopyranoside	3	CA	a	14	CA	a	3
10.21211	Methyl β-D-glucopyranoside	3	CA	e	14	CA	e	4
10.41111	Methyl D-*glycero*-α-L-*gluco*-heptopyranoside	4				CA	a	5
10.12511	Methyl α-D-lyxopyranoside	5	CA,CE [e]	a,e [e]	13	CA+CE; non-chair.	a+e; a, e, or q	6
10.12511	Methyl β-D-lyxopyranoside	4	CA,CE [e]	e,a [e]	13	CA+CE; non-chair.	a+e; a, e or q	7
10.22111	Methyl α-D-mannopyranoside	6	CA	a	13	CA	a	8
10.22111(6)80	Methyl 6-deoxy-α-L-mannopyranoside	1	CA	a	13	CA	a	9
10.22211(6)80	Methyl 6-deoxy-β-L-mannopyranoside	7				CA	e	10
10.42111	Methyl D-*glycero*-α-L-*manno*-heptopyranoside	8				CA	a	11
10.2651199	Methyl α-D-gulopyranoside, monohydrate	9	CA,CE	a,e	13	CA+CE; non-chair.	a+e; a,e, or q	12
10.26?119899	Methyl α-D-gulopyranoside · ½ ($CaCl_2$ · $3H_2O$).	9						13
10.26211	Methyl β-D-gulopyranoside	9	CA	e	15	CA	e	14
10.36111	Methyl D-*glycero*-α-D-*gulo*-heptopyranoside	4				CA	a	15
10.36?119899	Methyl D-glycero-α-D-*gulo*-heptopyranoside · $CaCl_2$ · H_2O.	4						16
10.36211	Methyl D-*glycero*-β-D-*gulo*-heptopyranoside	1, 4				CA	e	17
10.36?119899	Methyl D-*glycero*-β-D-*gulo*-heptopyranoside · ½ $CaCl_2$ · H_2O.	4						18
10.36213	Cyclohexyl D-*glycero*-β-D-*gulo*-heptopyranoside	10				CA	e	19
10.13411	Methyl α-L-arabinopyranoside	2	CE	e	16	CE	e	20
10.13311	Methyl β-L-arabinopyranoside	2	CE	a	16	CE	a	21
10.2311199	Methyl α-D-galactopyranoside, monohydrate	1, 11	CA	a	16	CA	a	22
10.23211	Methyl β-D-galactopyranoside	1	CA	e	16	CA	e	23
10.23111(6)80	Methyl 6-deoxy-α-L-galactopyranoside	12	CA	a	16	CA	a	24

[a] The third figure after the point was inserted after the present conclusions as to conformation had been reached.

[b] Named by the system of H. S. Isbell and R. S. Tipson, Science **130**, 793 (1959); J. Research NBS **64A**, 171 (1960).

[c] Assignment made by Reeves [13 to 16] from consideration of instability factors.

[d] After accepting several of Reeves' assignments (see text).

[e] Reeves later suggested [Ann. Rev. Biochem. **27**, 15 (1958)] that the stable conformation may be a member of the boat-skew cycle.

1. E. Fischer, Ber. deut. chem. Ges. **28,** 1145 (1895).
2. C. S. Hudson, J. Am. Chem. Soc. **47,** 265 (1925).
3. C. N. Riiber, Ber. deut. chem. Ges. **57,** 1797 (1924).
4. H. S. Isbell and H. L. Frush, J. Research NBS **24,** 125 (1940) RP1274.
5. F. P. Phelps and C. S. Hudson, J. Am. Chem. Soc. **48,** 503 (1926).
6. E. Fischer and L. Beensch, Ber. deut. chem. Ges. **29,** 2927 (1896).
7. E. Fischer, M. Bergmann, and A. Rabe, Ber. deut. chem. Ges. **53,** 2362 (1920).
8. R. M. Hann, A. T. Merrill, and C. S. Hudson, J. Am. Chem. Soc. **57,** 2100 (1935).
9. H. S. Isbell, BS J. Research **8,** 1 (1932) RP396.
10. E. Glaser and N. Zuckermann, Z. physiol. Chem. **166,** 103 (1927).
11. E. Fischer and L. Beensch, Ber. deut. chem. Ges. **27,** 2478 (1894).
12. J. Minsaas, Rec. trav. chim. **51,** 475 (1932).
13. R. E. Reeves, J. Am. Chem. Soc. **72,** 1499 (1950).
14. R. E. Reeves, J. Am. Chem. Soc. **71,** 215 (1949).
15. R. E. Reeves, Advances in Carbohydrate Chem. **6,** 107 (1951).
16. R. E. Reeves, J. Am. Chem. Soc. **71,** 1737 (1949).

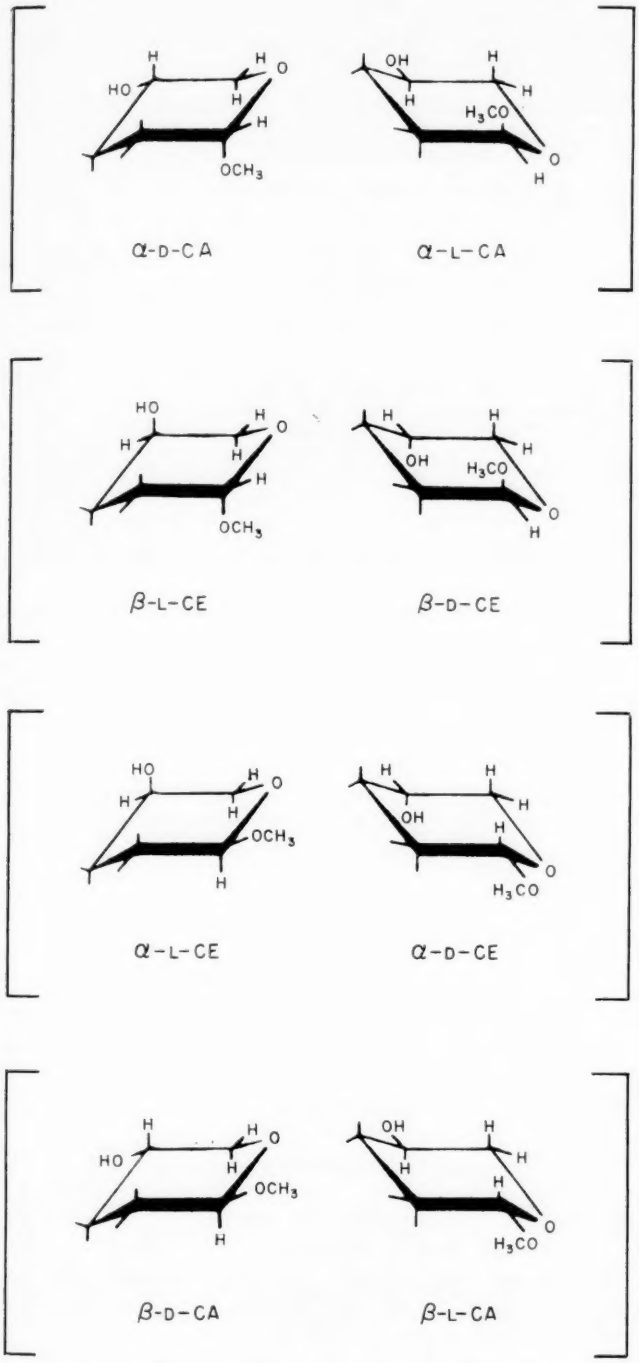

FIGURE 1. *The four general chair-forms of the anomeric methyl aldopentopyranosides, and the enantiomorph of each.*

(The configurations at C2 and C3 are omitted.)

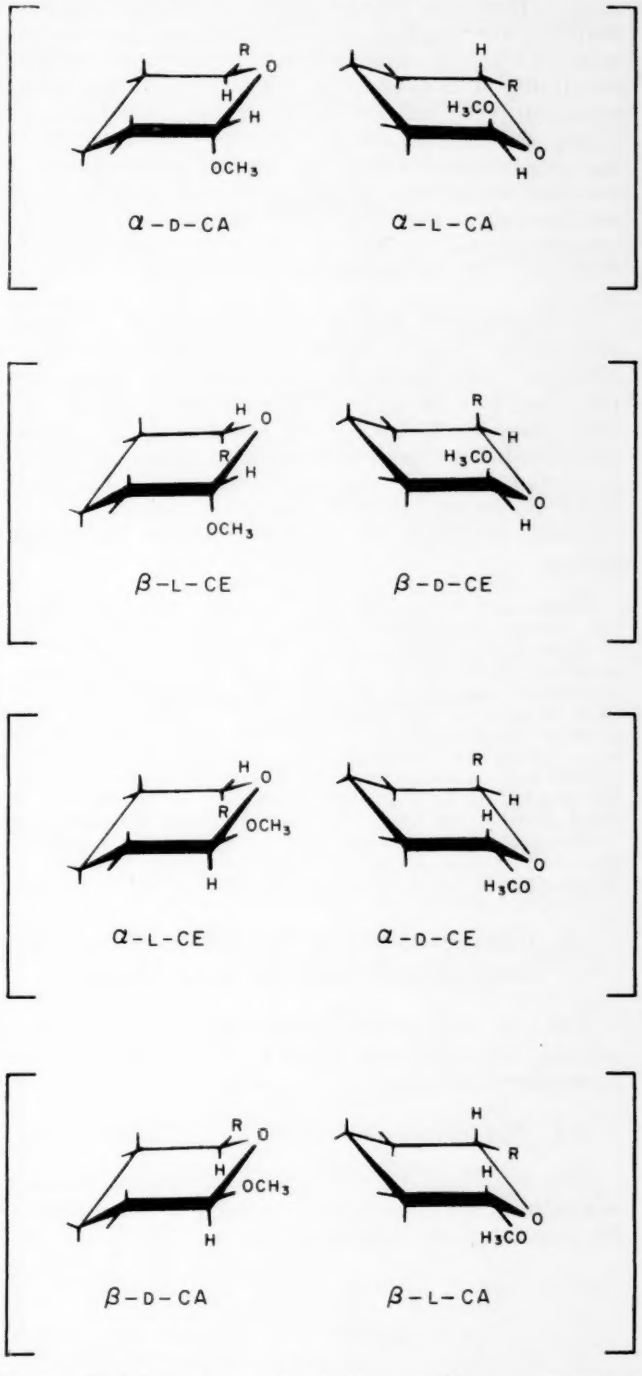

FIGURE 2. *The four general chair-forms of the anomeric methyl 6-deoxyaldohexopyranosides* (R = CH_3), *methyl aldohexopyranosides* (R = CH_2OH), *and methyl aldoheptopyranosides* (R = $CHOH-CH_2OH$), *with the enantiomorph of each.*

(The configurations at C2, C3, and C4 (and at C6, if asymmetric) are omitted.)

For compounds 1, 2, 3, 4, 8, 9, 20, 21, 22, 23, and 24 (see table 1), the conformation predicted for each (by Reeves) as the most stable of all possibilities was found by him to be that actually adopted in cuprammonia; these glycosides comprise group A. Compounds 6, 7, and 12 form group B. For the anomers of methyl D-lyxopyranoside (compounds 6 and 7), Reeves at first predicted approximately equal stability for the CA and CE conformation of each, and his experimental results were in accord with the possibility of a mixture of the two conformations in cuprammonia; but he later suggested [9] that each might actually adopt one of the conformations in the boat-skew cycle. As regards compound 12 (methyl α-D-gulopyranoside), Reeves predicted approximately equal stabilities for the CA and CE conformations, but his experimental results indicated that the CA conformation is adopted in cuprammonia.

In addition to the spectra of these 14 glycosides studied by Reeves, those of 10 aldopyranosides of hitherto undetermined conformation have been recorded and analyzed; conformations have now been assigned to 7 of these glycosides. As regards compound 14 (methyl β-D-gulopyranoside), Reeves predicted that the CA conformation would be the most stable of all conformations, but he did not examine the behavior of this glycoside in cuprammonia.

Barker and Shaw [10] have devised a way of predicting the stable chair-conformation of each pyranose, which involves the assumption "that the degree of distortion in a molecule is determined by the total amount of overlap of non-bonded atoms, overlap between each pair being calculated separately and added together." However, whereas a single, large overlap of x units might prohibit the adoption of a certain ideal conformation, a number of small overlaps (whose sum is equal to, or greater than, x units) might be accommodated by very slight departure of the conformation from ideality, so that, from the practical standpoint, the conformation in question is only slightly distorted. For this reason, the stable chair-conformations predicted by Reeves [6 to 8] have been used in the present study.

4. Classification of the Glycosides into Configurationally Related Groups

The 24 compounds were classified into three groups; the members of each group have like configurational features.

4.1. Aldopyranosides of the *xylo* Configuration

The members of this group of methyl aldopyranosides have the following general formulas (I) for the two chair-conformations.

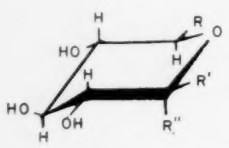

I-CA

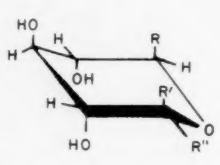

I-CE

Compounds 1 to 5 presumably have one of the above general structures, with the following substituents.

1. Methyl α-D-xylopyranoside, R=H; R′=H; and R″=OCH_3.
2. Methyl β-D-xylopyranoside, R=H; R′=OCH_3; and R″=H.
3. Methyl α-D-glucopyranoside, R=CH_2OH; R′=H; and R″=OCH_3.
4. Methyl β-D-glucopyranoside, R=CH_2OH; R′=OCH_3; and R″=H.
5. Methyl D-*glycero* α-L-*gluco*-heptopyranoside (originally called "methyl α-D-β-galaheptopyranoside"),

R is HCOH

CH_2OH; R′=H; R″=OCH_3; and the molecule is the mirror image of that depicted.

The following names (which have no official status) may be applied to compounds 3 to 5.

3. Methyl D-*glycero*-α-D-*xylo*-hexopyranoside.
4. Methyl D-*glycero*-β-D-*xylo*-hexopyranoside.
5. Methyl D-*threo*-α-L-*xylo*-heptopyranoside.

It should be noted that, in the CA conformation of compounds 2 and 4, all reference groups are equatorial; in the CE conformation of these compounds, all reference groups are axial.

4.2. Aldopyranosides of the *lyxo* Configuration

Three of the members of this group of configurationally related methyl aldopyranosides have the D-*lyxo* or D-*manno* configuration and the following general formulas (II) for the two chair-conformations.

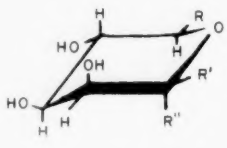

II-CA

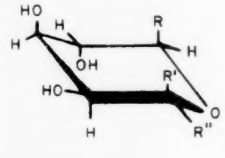

II-CE

Compounds 6 to 8, when in one of the chair conformations, have one of the above general structures, with the following substituents.

6. Methyl α-D-lyxopyranoside, R=H; R′=H; and R″=OCH_3.
7. Methyl β-D-lyxopyranoside, R=H; R′=OCH_3; and R″=H.
8. Methyl α-D-mannopyranoside, R=CH_2OH; R′=H; and R″=OCH_3.

(Purely for comparative purposes, compound 8 can be regarded as methyl D-*glycero*-α-D-*lyxo*-hexopyranoside; the name has no official status.)

Compounds 9 to 11 have the L-*manno* configuration; the following general formulas (III) depict the two chair-conformations, which are essentially the mirror images of formulas II.

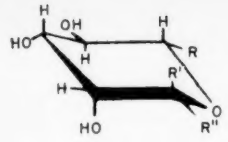

III–CA

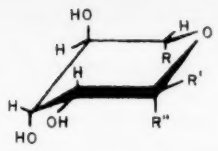

III–CE

When existing in one of the chair conformations, compounds 9 to 11 have one of the above general structures, with the following substituents.

9. Methyl 6-deoxy-α-L-mannopyranoside (methyl α-L-rhamnopyranoside), R=CH_3; R′=OCH_3; and R″=H.

10. Methyl 6-deoxy-β-L-mannopyranoside (methyl β-L-rhamnopyranoside), R=CH_3; R′=H; and R″=OCH_3.

11. Methyl D-*glycero*-α-L-*manno*-heptopyranoside (originally called "methyl α-D-α-galaheptopyranoside"),

R is HCOH
|
CH_2OH; R′=OCH_3; and R″=H.

To emphasize the configurational relationships, the following unofficial names may be temporarily applied:
9. Methyl 6-deoxy-L-*glycero*-α-L-*lyxo*-hexopyranoside.
10. Methyl 6-deoxy-L-*glycero*-β-L-*lyxo*-hexopyranoside.
11. Methyl D-*threo*-α-L-*lyxo*-heptopyranoside.

Compounds 12 to 19 have the D-*gulo* configuration; the following general formulas (IV) depict their chair conformations, which are closely related to formulas III.

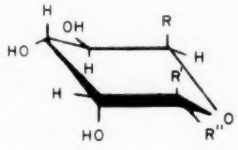

IV–CE

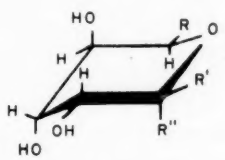

IV–CA

12. Methyl α-D-gulopyranoside monohydrate, R=CH_2OH; R′=H; and R″=OCH_3.

14. Methyl β-D-gulopyranoside, R=CH_2OH; R′=OCH_3; and R″=H.

15. Methyl D-*glycero*-α-D-*gulo*-heptopyranoside (originally called "methyl α-D-α-glucoheptopyranoside"),

R is HCOH
|
CH_2OH; R′=H; and R″=OCH_3.

17. Methyl D-*glycero*-β-D-*gulo*-heptopyranoside (originally called "methyl β-D-α-glucoheptopyranoside"),

R is HCOH
|
CH_2OH; R′=OCH_3; and R″=H.

19. Cyclohexyl D-*glycero*-β-D-*gulo*-heptopyranoside,

R is HCOH
|
CH_2OH; R′=OC_6H_{11}; R″=H.

For comparison with compounds 6 to 8, and 9 to 11, the following unofficial names may be temporarily applied:
12. Methyl D-*glycero*-β-L-*lyxo*-hexopyranoside, monohydrate.
14. Methyl D-*glycero*-α-L-*lyxo*-hexopyranoside.
15. Methyl D-*erythro*-β-L-*lyxo*-heptopyranoside.
17. Methyl D-*erythro*-α-L-*lyxo*-heptopyranoside.
19. Cyclohexyl D-*erythro*-α-L-*lyxo*-heptopyranoside.
Because the α-β names are relative, not absolute, it will be noted that, *whenever C4 and C5 of a sugar have opposite configurations*, the CA conformation for the sugar when named as a substituted L-aldopentopyranose is the CE conformation when it is named as a D-aldohexopyranose.

4.3. Aldopyranosides of the *arabino* Configuration

This group of configurationally related glycosides consists of the methyl L-arabinopyranosides, the methyl D-galactopyranosides, and methyl 6-deoxy-α-L-galactopyranoside. The relationship of the L-arabinopyranosides to the D-galactopyranosides is the same as that of the L-lyxopyranosides to the D-gulopyranosides.

Compounds 20 to 23 may have one of the following structures (V and VI), with the indicated substituents.

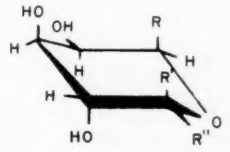

V

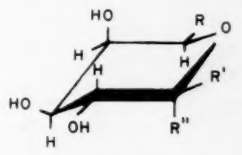

VI

20. Methyl α-L-arabinopyranoside, R=H; R′=OCH_3; and R″=H.

21. Methyl β-L-arabinopyranoside, R=H; R′=H; and R″=OCH_3.

22. Methyl α-D-galactopyranoside, monohydrate, R=CH_2OH; R′=H; and R″=OCH_3.

23. Methyl β-D-galactopyranoside, R=CH_2OH; R′=OCH_3; and R″=H.

For purposes of comparison, compounds 22 and 23 may be temporarily given the following unofficial names:
22. Methyl D-*glycero*-β-L-*arabino*-hexopyranoside, monohydrate.
23. Methyl D-*glycero*-α-L-*arabino*-hexopyranoside.
Named in this way, the CE conformation is the same as the conformation that is called CA when they are named as D-aldohexopyranosides.

For compounds 20 and 21, formula V represents the CA conformation and formula VI represents the CE conformation. For compounds 22 and 23, named as D-aldohexopyranosides, formula V represents the CE conformation and formula VI represents the CA conformation.

The possible chair conformations of compound 24 are the mirror images of those depicted above, with the following substituents.

24. Methyl 6-deoxy-α-L-galactopyranoside (methyl α-L-fucopyranoside), R=CH_3; R′=OCH_3; and R″=H.

The compound may, for purposes of comparison, be unofficially called methyl 6-deoxy-L-*glycero*-β-D-*arabino*-hexopyranoside. Named in this way, the conformation V having an axial (β-D) anomeric group is classified as CE; named as an α-L-hexopyranoside, it is classified as CA.

5. Discussion of the Spectra

In the present investigation, the *positions* of the various absorption bands for each of 24 aldopyranosides have been determined. For reasons discussed later, the relative intensities of absorption were not examined in detail.

The predicted stable conformations of 14 of these glycosides [6 to 8] are listed in table 1; eleven of these were accepted, but three (for compounds 6, 7, and 12) seemed open to question. In order that the conformation of these three and of each of the 10 remaining glycosides might be determined, the problem then resolved itself into a search of the infrared absorption spectra of the 11 "known" glycosides for potentially distinctive bands, followed by attempts to correlate the positions of these bands with such conformational and structural features as axial or equatorial disposition of (a) the glycosidic group at C1 or (b) the reference group (if any) at C5. The resultant findings were then applied in a study of the spectra of the glycosides of unknown conformation, in order to assign a conformation to each (in the solid state).

The spectra were examined in the groups outlined in table 2. However, before proceeding to a detailed analysis (see sections 5.3 and 5.4), some preliminary studies were made (in order to determine which methods of approach were likely to be the most fruitful).

5.1. Effect of Calcium Chloride of Crystallization

Glycosides 12, 15, and 17 lacked the following bands shown by their compounds with calcium chloride (group 1 of table 2): 3226 to 3215 cm^{-1}; 1745 cm^{-1}; 1366 to 1364 cm^{-1}; 1148 to 1130 cm^{-1}; 1117 to 1114 cm^{-1}; 1049 to 1044 cm^{-1}; 772 to 771 cm^{-1}; and 655 to 643 cm^{-1}. Because co-crystallization with calcium chloride alters the spectrum, either by removal or displacement of certain bands, only the spectra of *the 21 compounds lacking calcium chloride* were intercompared with respect to the other structural, configurational, and conformational features (groups 2 to 14 of table 2).

TABLE 2. *Structural groups studied*

Group	Structural feature	Compounds (serial numbers) in group
1	Calcium chloride (of crystallization)	13, 16, 18.
2	*arabino; galacto* configuration	20, 21; 22 to 24.
3	*lyxo; manno; gulo* configuration	6, 7; 8 to 11; 12, 14, 15, 17, 19 [13, 16, 18].
4	*xylo; gluco* configuration	1, 2; 3 to 5.
5	Pentopyranoside	1, 2, 6, 7, 20, 21.
6	5-*C*-Methyl (6-deoxy) group	9, 10, 24.
7	Hexopyranoside; 5-*C*-(hydroxymethyl) group.	3, 4, 8, 12, 14, 22, 23 [13].
8	Heptopyranoside; 5-*C*-(1,2-dihydroxyethyl) group.	5, 11, 15, 17, 19 [16, 18].
9	Hydrate	12, 13, 16, 18, 22.
10	Cyclohexyl group, glycosidic	19.
11	Methoxyl group, glycosidic	1 to 12, 14, 15, 17, 20 to 24 [13, 16, 18].
12	Hydroxyl group, primary	3 to 5, 8, 11, 12, 14, 15, 17, 19, 22, 23 [13, 16, 18].
13	Hydroxyl group, secondary	1 to 12, 14, 15, 17, 19 to 24 [13, 16, 18].
14	Pyranoid ring	

5.2. Preliminary Evaluation of Configurational and Constitutional Effects

Kuhn [11] recorded the spectra (in the range of 1250 to 667 cm^{-1}) for compounds 2, 3, 4, 8, 22, and 23. He noted that "the difference between the anomeric forms shows up very nicely." In table 1 are listed eight anomeric pairs, namely 1, 2; 3, 4; 6, 7; 9, 10; 12, 14; 15, 17; 20, 21; and 22, 23. A cursory inspection of their spectra revealed that Kuhn's remark applies to all of these pairs.

When the two spectra for an anomeric pair are compared, it is seen that (a) they have certain bands "in common" and (b) each shows certain bands that are "absent" from the other. With the information at hand, it was not known whether the absence of a band in one spectrum (and its presence in the other spectrum) is real or is actually due to a shift to some other position. If the "absent" band has actually been shifted to a position matching a band in the other spectrum, it will temporarily be regarded as being a band "common to the two spectra." On the other hand, if a band is shifted to a position not matched in the other spectrum, it will be observed as being "present" as a distinguishing band. Hence, some bands that may actually be ascribable to *different* features may be paired for the two spectra, and some bands (in the two spectra) that are actually ascribable to the *same* feature may appear to differentiate between the two.

Nevertheless, if the bands "differentiating" the two members of *one* anomeric pair are found to bear some relationship to the bands differentiating the two members of a *different* anomeric pair, it is reasonable to ascribe this to some influence that is operative in both instances.

For molecules as complex as those of the aldopyranosides, many of the observed bands cannot yet be assigned to particular vibrational modes. Assignments for some of the bands are given in section 5.5. However, we are not here concerned with (a) which bands, arising from vibrations localized in a functional group, are relatively independent of the remainder of the molecule, or (b) which bands involve other parts of the molecule (and are, therefore, sometimes perturbed in unexpected ways when the molecule is altered). Instead, in the present treatment, a band in two different spectra is regarded as "a band common to the two spectra" if it occupies approximately the same *position* in the spectrum, regardless of (a) whether it is actually contributed by vibrations which are of the same nature in the two molecules, or (b) the relative intensity in the two spectra. In our analysis, all of these bands are given equal weight.

Before proceeding to a detailed study, an examination of effects possibly attributable to configuration and constitution was undertaken. Simultane-

ously, an attempt was made to ascertain whether any of the differentiating bands could be regarded as being indicative of the axial or equatorial disposition of the anomeric group. It was realized that, if the anomeric group of an α anomer is axial, the conclusion that the anomeric group of its β anomer is equatorial might not necessarily follow—the disposition might, for example, be quasi; and *vice versa*. Therefore, to avoid unconscious bias that might arise from the use of the customary α or β names, only the assigned serial numbers of the above eight pairs of glycosides were used when making intercomparisons of their spectral characteristics.

Those of our compounds whose stable conformations had been assigned by Reeves [6 to 8] were all *methyl* glycosides. Consequently, from the total of 24 aldopyranosides listed in table 1, the cyclohexyl glycoside (compound 19) was excluded in this part of the study. Moreover, in view of the effects noted in section 5.1, the three compounds containing calcium chloride of crystallization (group 1 of table 2) were also excluded.

The generalized similarities and differences in the methyl aldopyranosides studied may be summarized as follows.

C1	C2 C3 C4	C5
Disposition of OCH_3	Group-configuration	Substituent
a or *e* or *q*	*xylo* or *lyxo* or *arabino*	H or CH_3 or CH_2OH or $CHOH\text{-}CH_2OH$

No glycoside having the *ribo* group-configuration is included in this investigation.

a. Effect of Change of Group-Configuration on Positions of Bands Common to Spectra (for Each Group-Configuration)

By group-configuration is meant the configuration of the glycoside, regardless of its anomeric form (see groups 2, 3, and 4 of table 2). In this analysis, the infrared spectra were examined for eight anomeric pairs (see above). The bands common to any one pair of anomers were systematically compared with the bands common to each and every other pair of configurationally related anomers. The three pairs of methyl pentopyranosides available for study were not configurationally related; each pair of pentopyranosides was compared with the related 5-*C*-substituted derivatives. For any one anomeric pair of pentopyranosides, these comprised anomeric pairs (and a few single anomers) of one or more of the following derivatives: 5-*C*-methyl, or methyl 6-deoxyaldohexopyranosides; 5-*C*-(hydroxymethyl), or methyl aldohexopyranosides; and 5-*C*-(1,2-dihydroxyethyl), or methyl aldoheptopyranosides. Three such configurational groups were available for study, namely, groups 2, 3, and 4 of table 2. Essentially the same kind of procedure was adopted in examining each group, and so a description of the method used will be exemplified by discussion of its application to group 2.

For group 2, the bands *differentiating* the α from the β anomer of methyl L-arabinopyranoside were tabulated and set aside for later evaluation (see section 5.3), and those bands *common* to the two anomers were tabulated. Similarly, the bands differentiating the α from the β anomer of methyl D-galactopyranoside were tabulated and set aside (see section 5.4), and the bands *common* to these two anomers were tabulated. It was then observed that *introduction of the 5-C-(hydroxymethyl) group in the pentopyranoside*, to afford the hexopyranoside, *had resulted in the display of a different spectrum of bands*. (The fact that the group-configuration was enantiomorphic may be ignored in this connection.) This observation is further developed in section 5.2.c.

In view of this effect of substitution at C5 of the pentopyranoside, a further winnowing of bands was undertaken. Those bands differentiating the pentopyranosides from the hexopyranosides were set aside for later consideration (see sections 5.3 and 5.4), and the bands *common* to the two pentopyranosides *and* the two hexopyranosides were tabulated. Finally, such of these bands as were *also* shown by the sole 6-deoxyaldohexopyranoside in this group (namely, compound 24) were selected and tabulated. This afforded a table recording the bands shown by all the glycosides (in this study) that have the *arabino* or *galacto* configurations.

In a similar manner, a table was compiled of the bands shown by all the members of group 3 (of table 2), and another table of the bands shown by all the members of group 4. These tables recorded, for each group-configuration, the bands that are shown *regardless* of anomeric disposition or of substitution (or nonsubstitution) at C5.

Inspection of these three tables revealed that *a change in group-configuration results in changes in the positions of a number of bands*, common to one configurational group, relative to those common to another configurational group. As a corollary, a set of bands shown by one group-configuration may tentatively be regarded as characteristic of that group-configuration.

Incidentally, on intercomparing the three groups, it was noted that the 21 glycosides comprising groups 2, 3, and 4 have, after application of the winnowing described, only four bands in common, namely, those at 2882 to 2841 cm^{-1}, 1368 to 1330 cm^{-1}, 1153 to 1111 cm^{-1}, and 1109 to 1087 cm^{-1} (see sec. 5.5). These bands are displayed regardless of the anomeric disposition or of substitution (or nonsubstitution) at C5.

b. Effect of Change of Group-Configuration on Positions of Bands Which Differentiate Two Anomers

The bands that differentiate the two members of each anomeric pair were tabulated; they are listed and discussed in sections 5.3 and 5.4. Study of these tables revealed that, for the aldopentopyran-

osides, change from the *xylo* to the *arabino* configuration leaves the majority of the anomer-differentiating bands substantially *unchanged* in position (see sec. 5.3). For the 5-*C*-substituted aldopentopyranosides, change from one configuration to another (e.g., of the aldohexopyranosides) causes *changes* in the positions of bands that differentiate anomers.

c. Effect (on the Spectra) of Various Substitutions at Carbon Atom 5 of Aldopentopyranosides

In this analysis, bands shown by an anomeric pair of aldopentopyranosides (group 5 of table 2) were first compared with those shown by 5-*C*-substituted derivatives (groups 6, 7, and 8). It was found that substitution at C5 of the aldopentopyranosides caused shifts in the anomer-differentiating bands.

However, intercomparison of the spectra of the 5-*C*-substituted derivatives revealed that, for *any one group-configuration*, change in the substituent from the methyl to the hydroxymethyl or to the 1,2-dihydroxyethyl group *did not* cause profound shifts of anomer-differentiating bands.

To summarize the observations in sections 5.2a, b, and c, it is seen that, for the diagnostic purposes under consideration, the spectra of the 5-*C*-substituted aldopentopyranosides of any one group-configuration may be intercompared, but they should not be intercompared with the spectra of their isomers having a different group-configuration, nor with those of the related aldopentopyranosides. On the other hand, intercomparison of the spectra of members of groups 6, 7, and 8 that have the *same* configuration might afford fruitful results.

5.3. Absorption Bands Possibly Indicative of the Axial or Equatorial Anomeric Group of the Methyl Aldopentopyranosides

As the starting point in this series of analyses of spectra, we selected methyl β-D-xylopyranoside (compound 2) because, if this compound adopts a chair conformation, the reference groups will either be all axial (CE) or all equatorial (CA). Its spectrum was compared with that of its α anomer (compound 1), in order to determine the effect (on the spectrum) of changing the anomeric group from equatorial to axial, or vice versa. A similar comparison was now made for the anomers of methyl L-arabinopyranoside (compounds 20 and 21).

Bands that are essentially the same for *both* anomers of (a) the methyl D-xylopyranosides or of (b) the methyl L-arabinopyranosides, or of (c) both configurational groups, are given[4] in table 3. It seemed reasonable to assume tentatively that bands shown by *all* of these glycosides might be independent of total configuration, whereas those shown by one pair of anomers having the same group-configuration might be a reflection, via shifting of bands, of an effect of the total configuration of that pair.

[4] For comparison, bands (in about the same positions) shown by either or both anomers of methyl D-lyxopyranoside are also given in table 3.

TABLE 3. *Bands (cm^{-1}) shown by both anomers of methyl* D-*xylopyranoside or by both anomers of methyl* L-*arabinopyranoside (or by all four compounds); and positionally corresponding bands of the methyl* D-*lyxopyranosides*

Methyl D-xylopyranosides		Methyl L-arabinopyranosides		Methyl D-lyxopyranosides	
2	1	20	21	6	7
Possibly nonconfigurational bands					
2950	2924	2941	2950	2924	2924
2849	2841	2857	2841	2841	2849
1473	1466	1464	1466	1466	1471
1451	1449	1456	1453	1456	1451
1410	1418	1429	1422	1414	1429
1376	1379	1379	1376	1377	1383
1368	1362	1353	1362	1359, 1355	1353
1277	1269	1266	1269	1274	1280
1242	1247	1258	1245	1245, 1241	1235
1192	1195	1205	1192	1199	1211
1161	1147	1166	1145	1151	1160
1119	1119	1116	1119	1106, 1103	1106
1091	1091	1099	1099	1086	1089
898 [a]	[a] 897	877	883	880	885
404 (399?)	400	(396?)	391	401	(398?) 389
Bands possibly affected by configuration and conformation					
3390	3390	3378		3390	3413
2967		2967	3003	2985, 2959	2967
1344	1342	1332	1342		1335
1316		1305	1304	1319, 1311	
1130		1139	1135	1129	1126
1075		1085	1079		1074
1067		1066	1065	1062	
1044	1042		1042		1044, 1034
1015	1007	991	1005	1015	
963	[a] 941	940	944		950
		917	923		
		779, 770	780	778	772
629	(633?)		619	616	
(571?)	(595?)		593		593
551	557	(558?)		541	
528	535	(541?)			
(506?)	(516?) 508		513	(521?)	517
429	426	425	(419?)		
			383	(386?)	(386?)
			(371?)	(376?)	375
358	369 (350?)	360		364 (352?)	351
			342	(337?)	(342?)
325	330		(324?)	332 (325?)	
306	(308?)	(314?)	311 (304?)	(304?)	
	(288?)	293	277	276	283

[a] These bands were mentioned by S. A. Barker, E. J. Bourne, R. Stephens, and D. H. Whiffen, J. Chem. Soc. **1954**, 3468.

In table 4 are given the bands shown by *one* anomer (but not the other) of the methyl D-xylopyranosides and the methyl L-arabinopyranosides. If these "anomer-differentiating" bands have any relationship to the axial or equatorial disposition of the respective glycosidic methoxyl group, the results in table 4 indicate that (a) compounds 2 and 20 have the same anomeric disposition, and (b) compounds 1 and 21 have the same anomeric disposition; that is, in both instances, both are equatorial or both are axial. If the conformation predicted by Reeves [7, 8] as being the most stable *for any one of these four compounds* is accepted for the crystalline state, the conformations of the other three may be deduced from the results in table 4. For example, if the anomeric group of methyl β-D-xylopyranoside is equatorial and that of its α anomer is axial, the results indicate that the anomeric group of methyl

TABLE 4. *Bands (cm^{-1}) shown by only one anomer of the methyl xylopyranosides and methyl arabinopyranosides, compared with bands for both anomers of methyl lyxopyranoside*

Methyl D-xylopyranosides		Methyl L-arabino-pyranosides		Methyl D-lyxo-pyranosides	
2	1	20	21	6	7
3448		3460			
		3279		3289	
3012					
2874				2882	
1433				1445	
1385		1395			1408, 1383
1295		1295		1274	1280
1218		1227			
1060		1058		1062	
976		973		973	975
645		646			
(496?)		487		485	
473				467	463
	3333		3322		3367
			3236	3226	
			2801		
	2710		2695	2717, 2667	2703
			845, 838	848	865
	[a]741		744	744	
			713, 699	685	697
			678	664	
	437		433		

[a] See footnote to table 3.

α-L-arabinopyranoside is equatorial and that that of its β anomer is axial. These conclusions are in complete agreement with Reeves' assignments (see table 1). It may be noted that the sole difference between methyl β-D-xylopyranoside-CA and methyl α-L-arabinopyranoside-CE lies in the configuration of carbon atom 4.

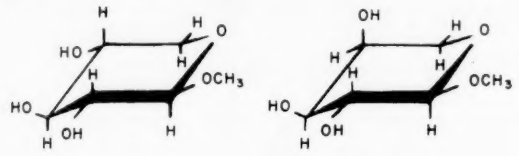

2-CA 20-CE

The corresponding bands of the methyl D-lyxopyranosides are also given in table 4. The results suggest that, for each anomer thereof, either (a) a conformation having a quasi or a different kind of axial or equatorial anomeric group is adopted in the crystalline state, or (b) a mixture of the CA and CE conformations crystallized together. These conclusions *also* agree with Reeves' predictions (see table 1).

It should be noted that, in this series of intercomparisons, there was no possibility of band displacements attributable to the effect of a substituent at carbon atom 5. However, displacements (to lower or higher wavenumbers) caused by the differences in configuration might have been either (a) retained or (b) partially or wholly eliminated by the arbitrary procedure of temporarily ignoring bands that are essentially the same for both anomers of methyl D-xylopyranoside or of methyl L-arabinopyranoside, or both.

5.4. Analysis of the Spectra of Groups of Configurationally Related Aldopyranosides, Excluding the Aldopentopyranosides

In this analysis, two potential sources of misinterpretation were avoided. Firstly, intercomparisons were not made between the aldopentopyranosides and (a) the 6-deoxyaldohexopyranosides, (b) the aldohexopyranosides, and (c) the aldoheptopyranosides, because of the band displacements caused by the various substituents at C5 of the aldopentopyranosides. On the other hand, it was assumed that change from a methyl substituent at C5 to either a hydroxymethyl or a 1,2-dihydroxyethyl substituent would occasion no change in conformation; shifts of bands have already been discussed (see sec. 5.2). Secondly, intercomparisons were confined to intra-group study of groups of glycosides having *the same configuration* for each member of one group. In this way, band shifts attributable to change of configuration did not come into consideration.

First of all, as *a check on the significance* of the results accruing from our method of comparing absorption bands, the spectra of the anomers of methyl D-galactopyranoside (compounds 22 and 23) were compared with that of methyl 6-deoxy-α-L-galactopyranoside (compound 24). The results are given in table 5; column C gives bands shown by the β anomer but not by the two α anomers, and column D records bands shown by the two α anomers but not by the β anomer. It may be concluded that, assuming the validity of the correlations, if the anomeric group of the α anomers is axial, that of the β anomer is equatorial, or vice versa. If the conformation predicted by Reeves [7] as being the most

TABLE 5. *Comparison [a] of absorption bands (cm^{-1}) shown by the methyl D-galactopyranosides (22 and 23) and by methyl 6-deoxy-α-L-galactopyranoside (24)*

A			B		C	D	
22	23	24	22	23	23	22	24
3390	3356	3367	3521	3559	3300	2924	2915
3236	3257	3247	2882	2899	1285	2646	2710
2959	2941	2950	1316	1321	1250	1462	1464
2857(?)	2865	2841	[1274	1261]	981	1355	1348
1449	1445	1433	[b] 1222	[b] 1220	[c] 888	1242	1245
1414	1429	1416	1149	1144	412	1138	1136
1403	1408, 1397	1391	575	585		1074	1079
1372	1383	1364	(505?)	510		1015	1005
1339	1333	1330				964	963
1305	1295	1300				[c] 822	810
1259	1261	1259				673	681
1196 [b]	1182	[d] 1196				532	530
1160	1155	1161				382	382
1120	1124	1120					
1094	1107	1100					
1080 [b]	[b] 1082	[d] 1086					
1064	[b] 1057	[d] 1049					
1034 [b]	1033	1026					
922 [c]	[c] 938	916					
868 [c]	[c] 870	867					
787 [c]	[c] 784	766					
706	727	717, 709					
(629?)	637	639					
458	460	442					
426	426	424					
(367?)	360	355					
314	318	325					
(297?)	(301?)	293					

[a] Key: A. Bands shown by both anomers of methyl D-galactopyranoside and by methyl 6-deoxy-α-L-galactopyranoside. B. Bands shown by both anomers of methyl D-galactopyranoside, but not by compound 24. C. Bands shown by methyl β-D-galactopyranoside, but not by methyl α-D-galactopyranoside or methyl 6-deoxy-α-L-galactopyranoside. D. Bands shown by methyl α-D-galactopyranoside and by methyl 6-deoxy-α-L-galactopyranoside, but not by compound 23. [b] These bands were mentioned by R. L. Whistler and L. R. House, Anal. Chem. **25**, 1463 (1953). [c] See footnote *a* to table 3. [d] These bands were mentioned (see footnote *b*) for the α-D form.

stable for *any one of these three compounds* is accepted for the crystalline state, the deduced conformations for the other two are in complete agreement with Reeves' assignments for them (see table 1).

The anomeric disposition of methyl α-D-gulopyranoside (compound 12) was now studied. Its spectrum was compared with those of methyl α-D-mannopyranoside (compound 8) and methyl β-D-gulopyranoside (compound 14). The results are given in table 6; column C records bands shown by compound 12 that are absent from the spectra of compounds 8 and 14; column D gives the bands common to compounds 8 and 12; and column E gives the bands common to compounds 8 and 14, not shown by compound 12. Thus, the spectrum of compound 12 has some resemblances to that of compound 8 and some to that of compound 14, but it also differs from both. Now, for the most stable conformation of compound 8, Reeves [8] predicted an axial anomeric group; for compound 14, he predicted [12] an equatorial anomeric group. The results in table 6 suggest that, if these assignments are accepted, compound 12 in the crystalline state either (a) assumes a conformation other than the chair form, possibly one having a quasi anomeric group, or (b) consists of a mixture of the CA and CE conformations. These conclusions agree with Reeves' *prediction* for compound 12 (see table 1). It should be noted that compound 12 may be an example of a glycoside whose stable conformation is altered by cuprammonia, because, in this solvent, it adopts the CA conformation [8]. Alternatively, it is possible that, for the purpose under consideration, a sugar derivative having the *manno* configuration should not be compared with related derivatives having the *gulo* configuration.

All of the foregoing deductions are compatible with Reeves' assignments. Consequently, the validity of the deductions (and the reliability of the method of analysis of the spectra) was apparently established. The spectra of the remaining glycosides (compounds 5, 10, 11, 15, 17, and 19) were, therefore, examined in order to assign an anomeric disposition to each. No prediction has been made as to the stable conformation for each of these glycosides.

A comparison of the spectrum of methyl D-*glycero*-α-L-*gluco*-heptopyranoside (compound 5) with those of the anomers of methyl D-glucopyranoside (compounds 3 and 4) indicated its resemblance to the spectrum of methyl α-D-glucopyranoside (compound 3); see column C of table 7. If Reeves' prediction that the most stable conformation for compound 3 is the CA, this observation suggests that compound 5 has the CA conformation in the crystalline state.

The spectrum of methyl 6-deoxy-β-L-mannopyranoside (compound 10) was compared with those of its α anomer (compound 9) and of methyl α-D-mannopyranoside (compound 8). The results are given in table 8; column C records three bands shown by compounds 8 and 10 that are not shown by compound 9. However, column D (table 8) reveals that the two α anomers have some 13 bands in common that are not exhibited by compound 10. Since these two α anomers have the CA conformation as their predicted stable conformation [8], these results suggest that compound 10 has an equatorial anomeric group.

The spectrum of methyl D-*glycero*-α-L-*manno*-heptopyranoside (compound 11) was now compared with the spectra of compounds 8, 9, and 10. The results are given in table 9, except that, to avoid repetition of much of the information in table 8, the bands common to all four of these glycosides are omitted. Column A (table 9) records three bands shared by compound 11 and methyl 6-deoxy-β-L-mannopyranoside (compound 10); column B gives 17 bands that are shown by compound 11 and also by methyl α-D-mannopyranoside (compound 8) or methyl 6-deoxy-α-L-mannopyranoside (compound 9), or both. Since the predicted stable conformation for the latter two compounds is the CA conformation, this evidence indicates that the anomeric group of compound 11 is axial.

The spectra of the anomers of methyl D-*glycero*-D-*gulo*-heptopyranoside [compounds 15 (α) and 17 (β)] were compared with the spectrum of methyl

TABLE 6. *Comparison* [a] *of the absorption bands* (cm^{-1}) *shown by the anomers of methyl* D-*gulopyranoside* (*12 and 14*) *and by methyl* α-D-*mannopyranoside* (*8*)

A			B		C	D		E	
8	12	14	12	14	12	8	12	8	14
3460	3484	3413	3257	3247	3195	2841	2849	1389	1385
3289	3333	3322	2924	2915	1484	1372	1372	1350	1350
3012	3030	2976	2725	2762	1437	1361	1361	1258	1258
2950	2950	2941	1302	1305	1144	(420?)	(421?)	1041	1036
2907	2907	2915	1289	1289	1133	412	(416?)	[b] 916	913
2841	2849	2865	1276	1272		(386?)	378	[b] 848	855
1473	1471	1473	1087	1087				(645?)	(656?)
1451	1451	1449	1018	1016				(329?)	318
1414	1418	1418	468	473				(304?)	296
1399	1406	1393	(360?)	360				286	(277?)
1330	1333	1337	(354?)	(352?)					
1312	1318	1316							
1250	1250	1258, 1238							
1220 [c]	1225	1220							
1199 [c]	1193	1205							
1163	1159	1151							
1119	1121	1126							
1104	1096	1105							
1071 [c]	1078, 1070	1070							
1055 [c]	1053	1056							
1029	1029	1026							
973 [b]	968	994							
890 [b]	873, 872	903							
817 [b]	820	798							
723	739	751							
672	687	675							
608	608	601							
576	548	553							
512	(506?)	506							
483	486	490							
455	458	444							
338	345	333							

[a] Key: A. Bands shown by methyl α-D-mannopyranoside and by both anomers of methyl D-gulopyranoside. B. Bands shown by the methyl D-gulopyranosides, but not by compound 8. C. Bands shown by methyl α-D-gulopyranoside, but not by compounds 8 or 14. D. Bands shown by methyl α-D-mannopyranoside and by methyl α-D-gulopyranoside, but not by compound 14. E. Bands shown by methyl α-D-mannopyranoside and by methyl β-D-gulopyranoside, but not by compound 12.

[b] See footnote *a* to table 3.

[c] See footnote *b* to table 5.

TABLE 7. *Comparison* [a] *of absorption bands* (cm^{-1}) *shown by the anomers of methyl* D-*glucopyranoside* (*3 and 4*) *and by methyl* D-glycero-α-L-gluco-*heptopyranoside* (*5*)

A			B		C	
3	5	4	3	4	3	5
2915	2941	2959	3279	3247	1340	1339
2849	2857	2857	2915	2890	1202	1214
1464	1466	1466	2667(?)	2793(?), 2710	1114	1111
1443	1449	1447	1323	1326	845	864
1401	1410	1403	1135	1129	747	745
1376	1381	1383	(398?)	377	564	553
1366	1353	1364	367	356		
1305	1302	1304	298	300		
1267	1269	1285				
1229	1236	1248				
1229 [b]	1214	[b] 1222				
1188 [b]	1193	[b] 1186				
1159	1153	1161				
1125	1126	1125				
1104	1087	1098				
1075		[b] 1081, 1073				
1053	1053	[b] 1054				
1047 [b]	1040	1037				
1034	1015	1030				
995	997	1002, 993				
899 [c]	892	[c] 885				
794(?)	787	[c] 781				
627(?)	627	631				
598	584	(591?) 580				
539	522	510				
(490?)	501	488				
(442?)	426	420				
(407?)	408	406				
349	344	343				

[a] Key: A. Bands shown by the anomers of methyl D-glucopyranoside and by methyl D-*glycero*-α-L-*gluco*-heptopyranoside. B. Bands shown by the anomers of methyl D-glucopyranoside, but not by compound 5. C. Bands shown by methyl α-D-glucopyranoside and by methyl D-*glycero*-α-L-gluco-heptopyranoside, but not by compound 4.
[b] See footnote *b* to table 5.
[c] See footnote *a* to table 3.

β-D-gulopyranoside (compound 14). Compound 14 showed a band at 751 cm^{-1}; in the same region, compound 15 showed bands at 764 and 738 cm^{-1}. In contrast, compounds 14 and 17 share 17 bands not shown by compound 15 (see column C of table 10). If the CA conformation predicted as being the stable conformation for compound 14 is accepted, these results suggest that the anomeric group is equatorial in compound 17 and nonequatorial (that is, axial or quasi) in compound 15.

Finally, the spectrum of cyclohexyl D-*glycero*-β-D-*gulo*-heptopyranoside (compound 19) was studied in comparison with the spectra of compounds 15 and 17 (the α and β anomers of the corresponding methyl glycoside). To avoid repetition of much of the information in table 10, the bands common to all three of these glycosides are not given here. The spectrum of compound 15 lacked the following bands in the spectra of compound 17 and (in parentheses) of compound 19: 3509 (3484); 3448 (3436); 2732? (2653?); 1330 (1333); 1311 (1304); 1287 (1287); 1212 (1209); 1122 (1129); 1056 (1056); 1006 (1006); 801 (808); 599 (594); and 575 (575) cm^{-1}. If the previous finding is accepted [namely, that the anomeric group of methyl D-*glycero*-β-D-*gulo*-heptopyranoside (compound 17) is equatorial, but that that of the α anomer, compound 15, is not], these results suggest that the anomeric group of cyclohexyl D-*glycero*-β-D-*gulo*-heptopyranoside is equatorial.

For reasons discussed in section 5.1, the spectra of compounds 13, 16, and 18 were not further examined.

5.5. Other Absorption Bands

All of the spectra were studied in regard to the other features listed in table 2. The hydrates (group 9) showed a band at 1664 to 1634 cm^{-1}.

Compound 19, having a cyclohexyloxy group, showed bands at 2933, 2890, and 2857 cm^{-1}, possibly characteristic of $—CH_2—$ (C—H stretching). It also showed bands at 1449 and 1441 cm^{-1}, possibly attributable to $—CH_2—$ (C—H deformation).

All of the compounds showed at least one band in the region of 3413 to 3279 cm^{-1} (associated alcoholic —O—H stretching); at 3012 to 2915 cm^{-1} (C—H stretching); at 1466 to 1441 cm^{-1}, and at 1346 to 1316 cm^{-1} (C—H bending); and at 1267 to 1235 cm^{-1} (C—O). Except for compound 15, all of the compounds showed at least one band in the region of 1247 to 1211 cm^{-1} (C—O stretching). Compounds 3, 6, 8, 13, and 20 showed a band at 3289 to 3279 cm^{-1} (H bonding?).

As previously mentioned, all of the methyl glycopyranosides (group 11 of table 2) show a band in

TABLE 8. *Comparison* [a] *of absorption bands* (cm^{-1}) *shown by methyl* α-D-*mannopyranoside* (*8*) *and by both anomers of methyl 6-deoxy*-L-*mannopyranoside* (*9 and 10*)

A			B		C		D	
8	9	10	9	10	8	10	8	9
3012	2985	2976	3559	3509	3289	3333	2907	2890
2950	2924	2941	3413	3401	1163(?)	1174	1389	1389
2841	2857	2857	1323	1325	723	708	1330	1333
1473	1473	1466	992	1004			1199	1206
1451	1456, 1447	1447	963	959			1119	1114
1414	1420, 1412	1416	534	537			[b] 1055	1058
1372	1376, 1370	1374					973	983
1350	1351	1350					[c] 848	[c] 838
1330	1333, 1323	1325					(645?)	632
1312	1305	1300					576	552
1258	1256	1259					512	(509?)
1220 [b]	1220	1224, 1218					(329?)	328
1199 [b]	1206	1174					286	284
1144	1145	1149						
1133	1125	1127						
1104	1098	1096						
1071 [b]	1083	1088, 1072						
1029	1024	1024						
973 [c]	[c] 963	959						
916 [c]	[c] 909	903						
890 [c]	[c] 877	870						
817 [c]	[c] 803	801, 798						
672	677	699						
608	(610?)	609						
512	534	537						
483	475	(495?)						
455	(467?)444	460						
(420?)412	(420?)	414						
(386?)	380, 368	(376?)						
338	(354?)	352						
(304?)	303	298						

[a] Key: A. Bands shown by methyl α-D-mannopyranoside and by both anomers of methyl 6-deoxy-L-mannopyranoside. B. Bands shown by both anomers of methyl 6-deoxy-L-mannopyranoside, but not by compound 8. C. Bands shown by methyl α-D-mannopyranoside and by methyl 6-deoxy-β-L-mannopyranoside, but not by compound 9. D. Bands shown by methyl α-D-mannopyranoside and by methyl 6-deoxy-α-L-mannopyranoside, but not by compound 10.
[b] See footnote *b* to table 5.
[c] See footnote *a* to table 3.

TABLE 9. *Comparison* [a] *of absorption bands* (cm^{-1}) *shown by methyl* α-D-*mannopyranoside* (*8*), *the anomers of methyl 6-deoxy*-L-*mannopyranoside* (*9 and 10*), *and methyl* D-glycero-α-L-manno-*heptopyranoside* (*11*)

A		B		
10	11	8	9	11
3333	3322	3460		3425
2710	2703(?)	2907	2890	2915
1287	1285	1399, 1389	1389	1395
		1361		1368
			1342	1340
		1250		1241
		[b] 1199	1206	1200
		1119	1114	1115
		[b] 1055	1058	1048
		1041		1036
		[c] 973	983	982
		[c] 848	[c] 838	827
		(645?)	632	654
		576	552	(578?) 562
		512	(509?)	509
		(329?)	328	324
		286	284	277

[a] Key: A. Bands shown by compounds 10 and 11, but not by compounds 8 and 9. B. Bands shown by compounds 8, 9, and 11, but not by compound 10.
[b] See footnote *b* to table 5.
[c] See footnote *a* to table 3.

TABLE 10. *Comparison* [a] *of absorption bands* (cm^{-1}) *shown by methyl* β-D-*gulopyranoside* (*14*) *and by the anomers of methyl* D-glycero-D-gulo-*heptopyranoside* (*15 and 17*)

A			B		C	
14	15	17	15	17	14	17
3413	3401	3448, 3378	948	944	3322	3333
2941	2933	2950	884	880	2762	2732
2865	2849	2882	408	412	1418	1425
1473	1460	1462	(399?)	393	1393	1408
1449	1447	1456			1337	1330
1418	1412	1425			1316	1311
1393		1408			1289	1287
1385	1374	1372			1238	1238
1350	1346	1357			1220	1212
1258	1264	1253			1126	1122
1205	1192	1203			1070	1075, 1064
1151	1153	1151			1056	1056
1105	1106	1099			1026	1025
1087	1089	1082			1016	1006
1036	1042	1036			903	907
994	985	990			798	801
885	844	847			601	599
675	676	683				
(627?)	633	617				
553	559	575, 537				
506	500	502				
473	477	474				
444	(459?) 426	447				
360	(375?)	(359?)				
(352?) 333	342	348				
296	(306?)	306				

[a] Key: A. Bands shown by methyl β-D-gulopyranoside (compound 14) and by both anomers of methyl D-*glycero*-D-*gulo*-heptopyranoside. B. Bands shown by both anomers of methyl D-*glycero*-D-*gulo*-heptopyranoside, but not by compound 14. C. Bands shown by methyl β-D-gulopyranoside and by methyl D-*glycero*-β-D-*gulo*-heptopyranoside, but not by compound 15.

the range of 2882 to 2841 cm^{-1}. This may possibly be attributable to the glycosidic methoxyl group, because Henbest and coworkers [13] have observed that methoxyl groups absorb in the range of 2832 to 2819 cm^{-1}. All of the methyl glycopyranosides also show bands at 1368 to 1330 cm^{-1}, 1285 to 1245 cm^{-1}, 1153 to 1111 cm^{-1}, and 1109 to 1087 cm^{-1}. A band near 1100 cm^{-1} is characteristic [14] of the methoxyl groups in methoxy-steroids.

6. Experimental Procedures

6.1. Preparation and Purification of the Compounds

The compounds listed in table 1 were prepared by the methods given in the references cited. Most of the compounds were prepared in the course of an earlier study on the configuration and conformation of methyl glycosides, with reference to optical rotations and rates of hydrolysis [15]. Each substance was recrystallized from an appropriate solvent until further recrystallization caused no change in its melting point or optical rotation.

6.2. Preparation of the Pellets

Samples for spectrophotometric study were prepared in the solid phase, as pellets of the crystalline glycoside suspended in an alkali-metal halide, exactly as previously described [4]. For the range of 5000 to 667 cm^{-1}, a concentration of 0.4 mg of glycoside per 100 mg of potassium chloride was used. For the range of 667 to 250 cm^{-1}, the following weights of glycoside per 100 mg of potassium iodide were used—compounds 1, 2, and 20: 1.33 mg; compound 5: (A) 0.33 and (B) 2 mg; compound 24: 3 mg; and for the rest of the compounds: 2 mg. In addition, for the range of 667 to 333 cm^{-1}, the spectrum of compound 12 at a concentration of 2 mg per 100 mg of potassium *chloride* was recorded. Comparisons of intensity of absorption, from one compound to another, can only be true and quantitative where the molar concentration is the same.

6.3. Measurement of Infrared Absorption

The spectrograms are shown in figures 3 and 4. They were recorded with a Perkin-Elmer Model 21 (double-beam) spectrophotometer equipped with a prism of sodium chloride (for the range of 5000 to 667 cm^{-1}) and of cesium bromide (for the range of 667 to 250 cm^{-1}), as previously described [4].

Some absorption attributable to water (in the compound, the alkali halide, or both) was observed at 3448 and 1639 cm^{-1} and, attributable to atmospheric water vapor, in the far-infrared curves. These regions are drawn on the spectrograms with dashed lines which are merely precautionary and are not to be interpreted quantitatively.

6.4. Spectra Measured Under Different Conditions

Because of the possibility of interaction of the various compounds with the pelleting halide under high pressure, the spectra of a few of the glycosides, chosen at random, were also recorded in a Nujol mull (requiring no pressure) for comparison. Since a number of these compounds gave markedly different spectrograms in potassium iodide and in Nujol, respectively, the spectra of all of them were now recorded in Nujol. For 16 of the 24 glycosides, the spectra obtained with either medium matched well. However, the following compounds gave spectrograms that were different in Nujol and in potassium iodide: compounds 1, 5, 7, 10, 11, 12, 15, and 20.

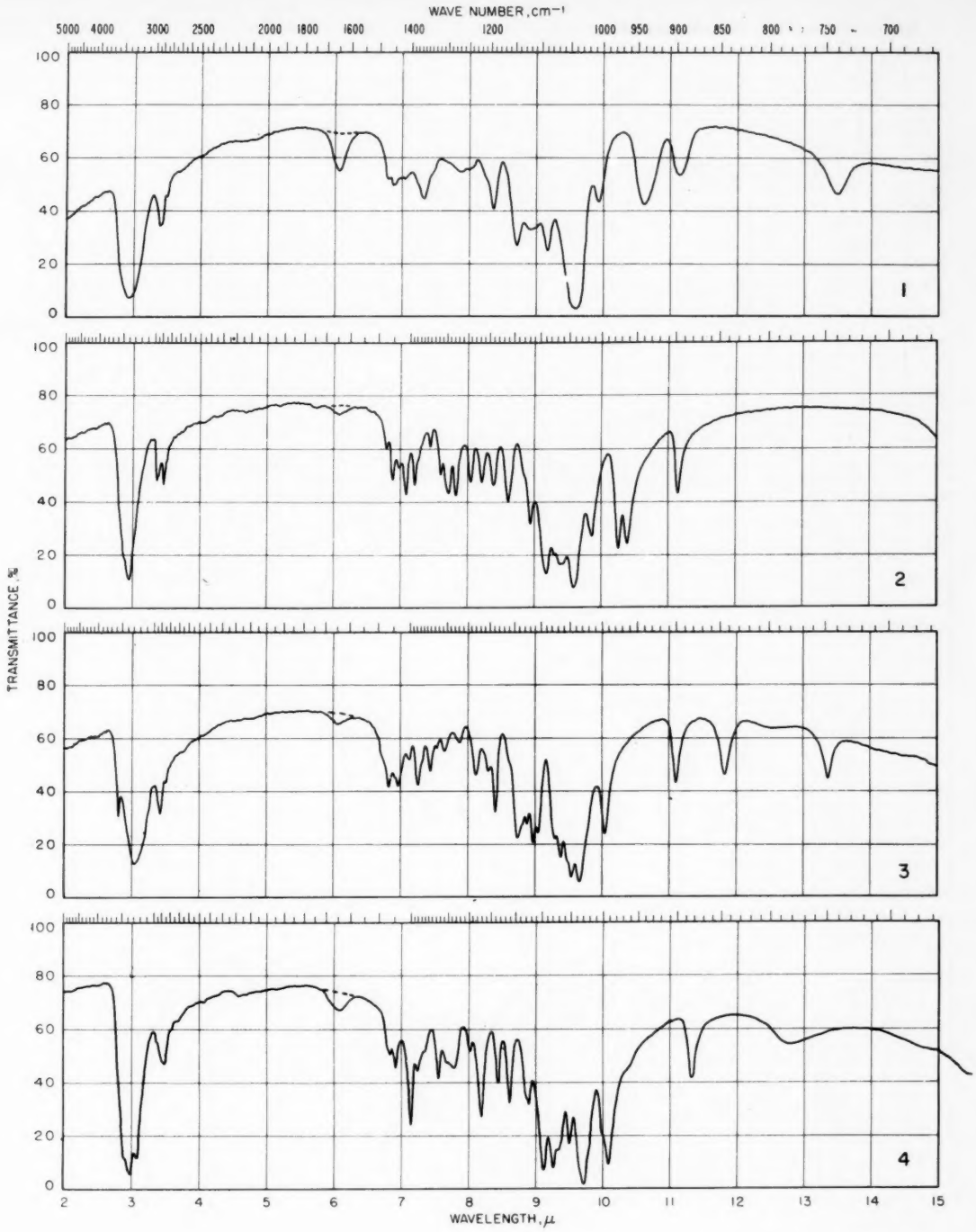

FIGURE 3. *Spectrograms of materials in potassium chloride pellets.*

1, Methyl α-D-xylopyranoside; 2, methyl β-D-xylopyranoside; 3, methyl α-D-glucopyranoside; 4, methyl β-D-glucopyranoside.

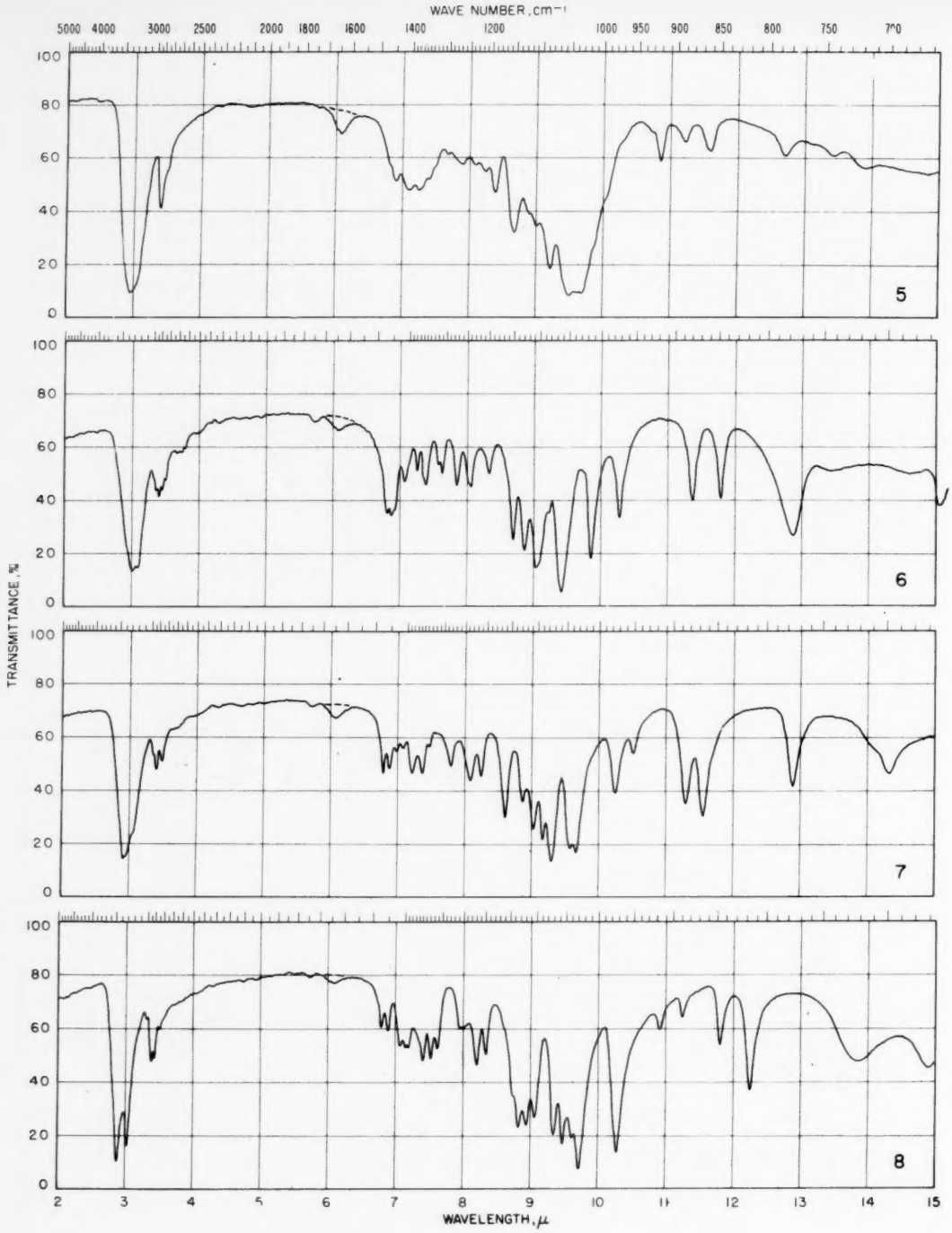

FIGURE 3. *Spectrograms of materials in potassium chloride pellets.*—Continued

5, methyl D-*glycero*-α-L-*gluco*-heptopyranoside; 6, methyl α-D-lyxopyranoside; 7, methyl β-D-lyxopyranoside; 8, methyl α-D-mannopyranoside.

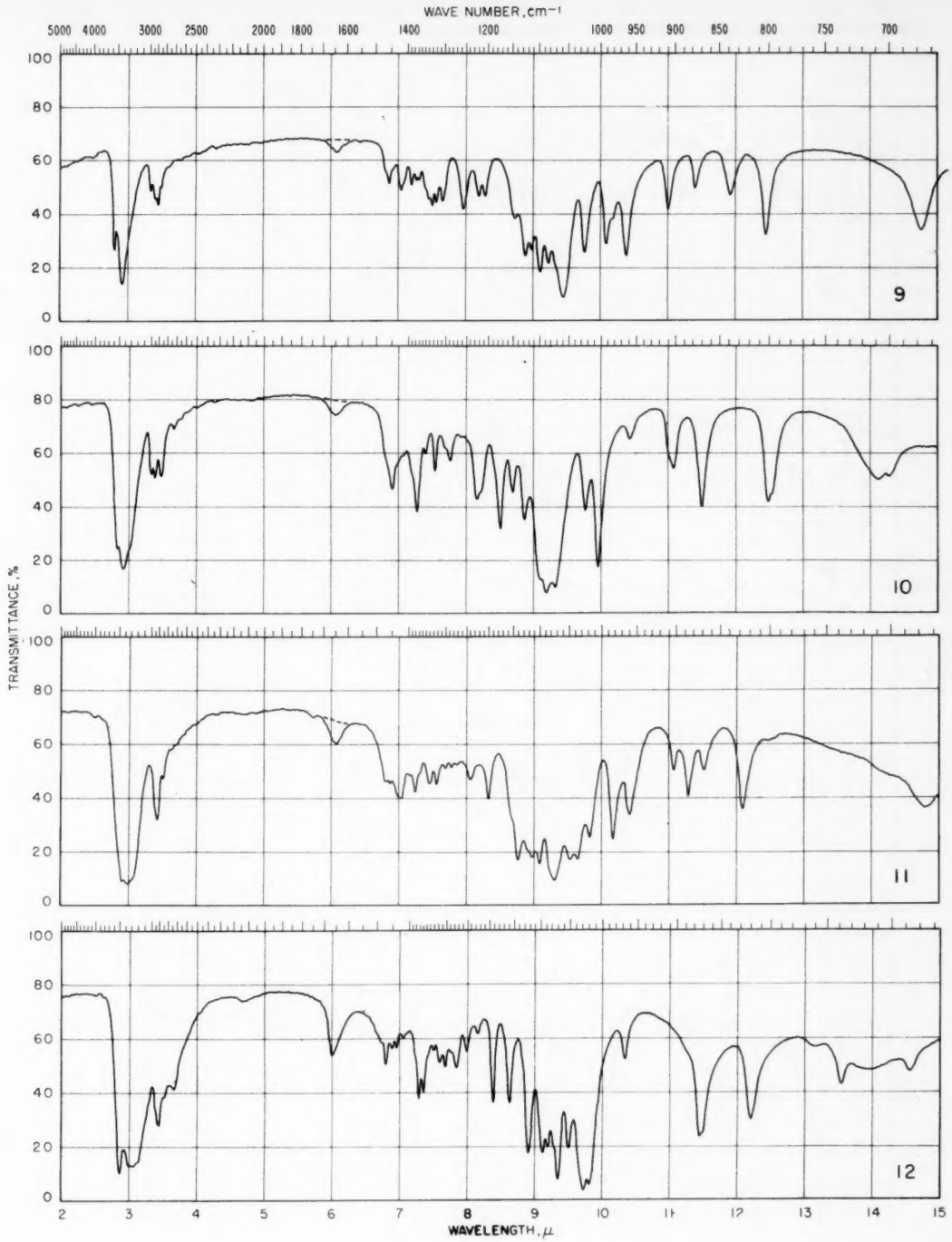

FIGURE 3. *Spectrograms of materials in potassium chloride pellets.*—Continued

9, methyl 6-deoxy-α-L-mannopyranoside; **10,** methyl 6-deoxy-β-L-mannopyranoside; **11,** methyl D-*glycero*-α-L-*manno*-heptopyranoside; **12,** methyl α-D-gulopyranoside monohydrate.

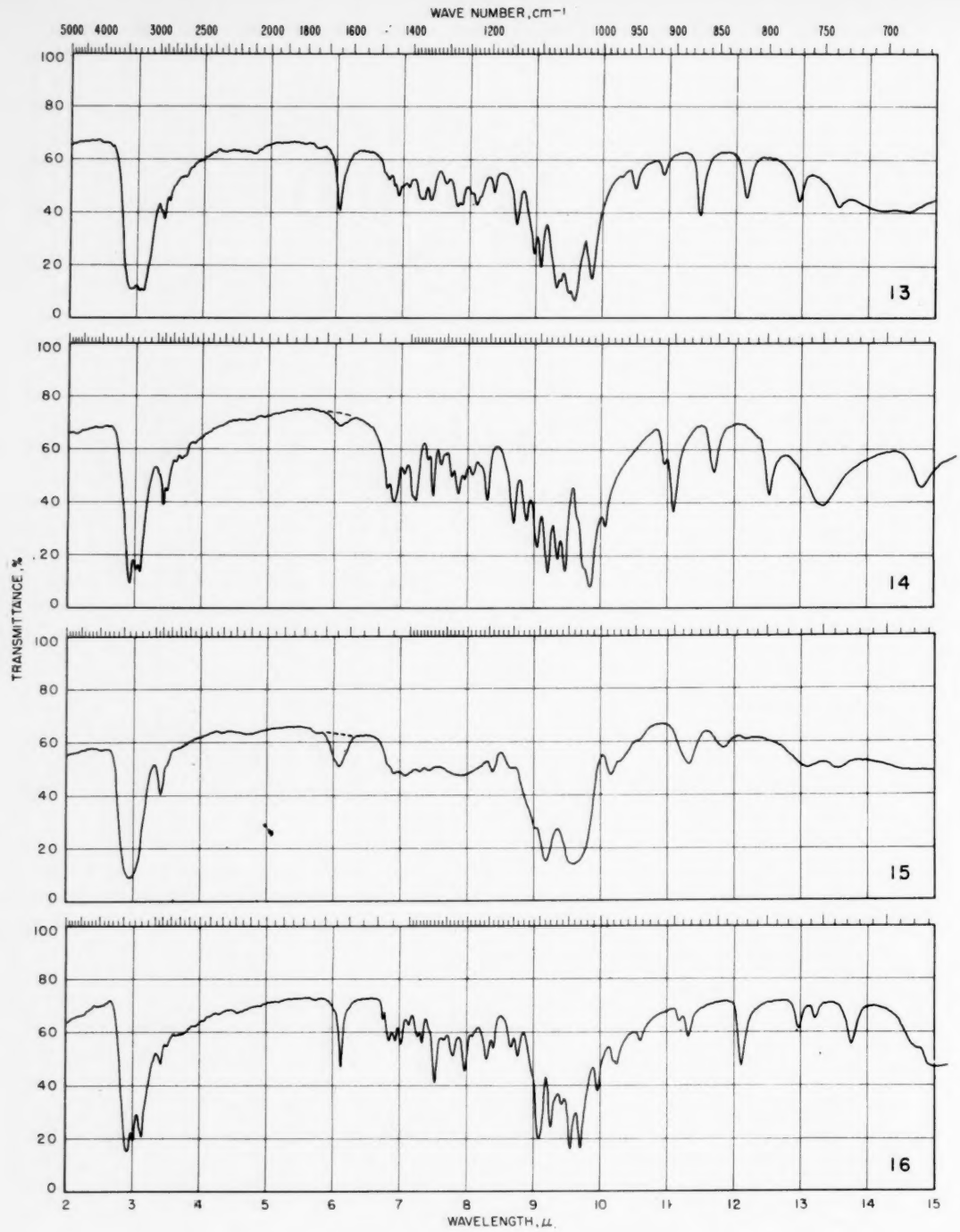

FIGURE 3. *Spectrograms of materials in potassium chloride pellets.*—Continued

13, methyl α-D-gulopyranoside·½($CaCl_2$·$3H_2O$); **14,** methyl β-D-gulopyranoside; **15,** methyl D-*glycero*-α-D-*gulo*-heptopyranoside; **16,** methyl D-*glycero*-α-D-*gulo*-heptopyranoside·$CaCl_2$·H_2O.

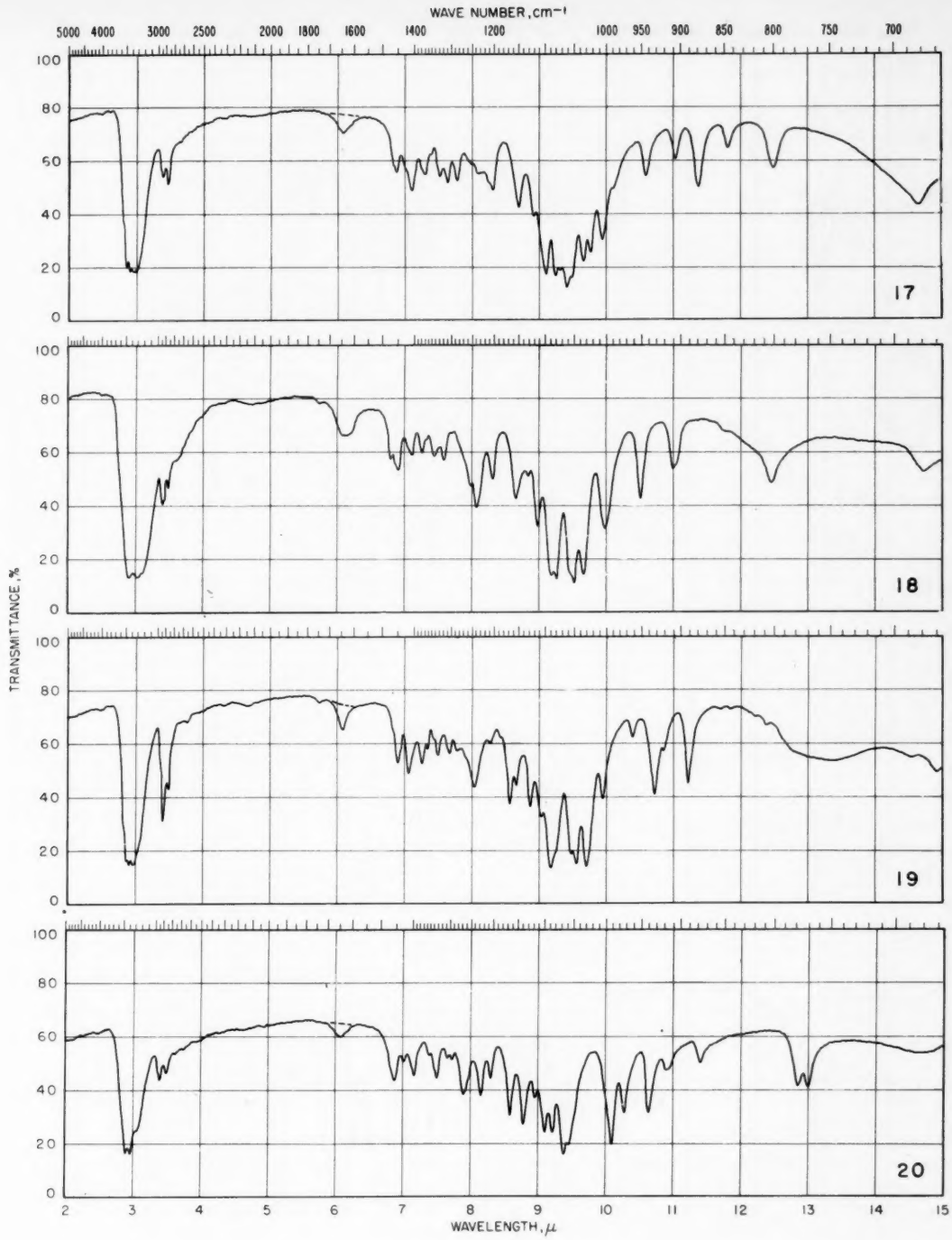

FIGURE 3. *Spectrograms of materials in potassium chloride pellets.*—Continued

17, methyl D-*glycero*-β-D-*gulo*-heptopyranoside; **18**, methyl D-*glycero*-β-D-*gulo*-heptopyranoside ·½$CaCl_2$·H_2O; **19**, cyclohexyl D-*glycero*-β-D-*gulo*-heptopyranoside; **20**, methyl α-L-arabinopyranoside.

543405—60——5

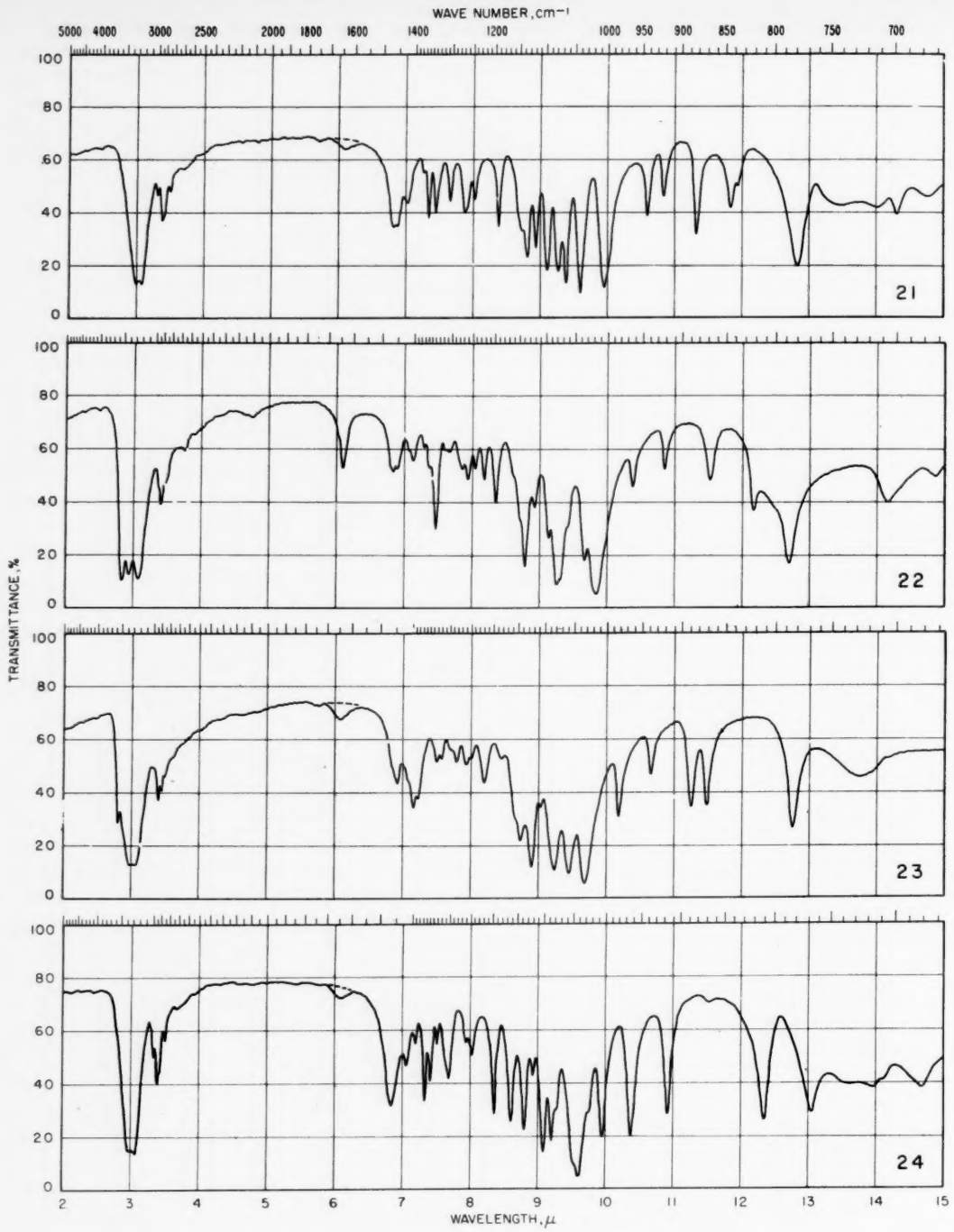

FIGURE 3. *Spectrograms of materials in potassium chloride pellets.*—Continued

21, methyl β-L-arabinopyranoside; **22**, methyl α-D-galactopyranoside monohydrate; **23**, methyl β-D-galactopyranoside; **24**, methyl 6-deoxy-α-L-galactopyranoside.

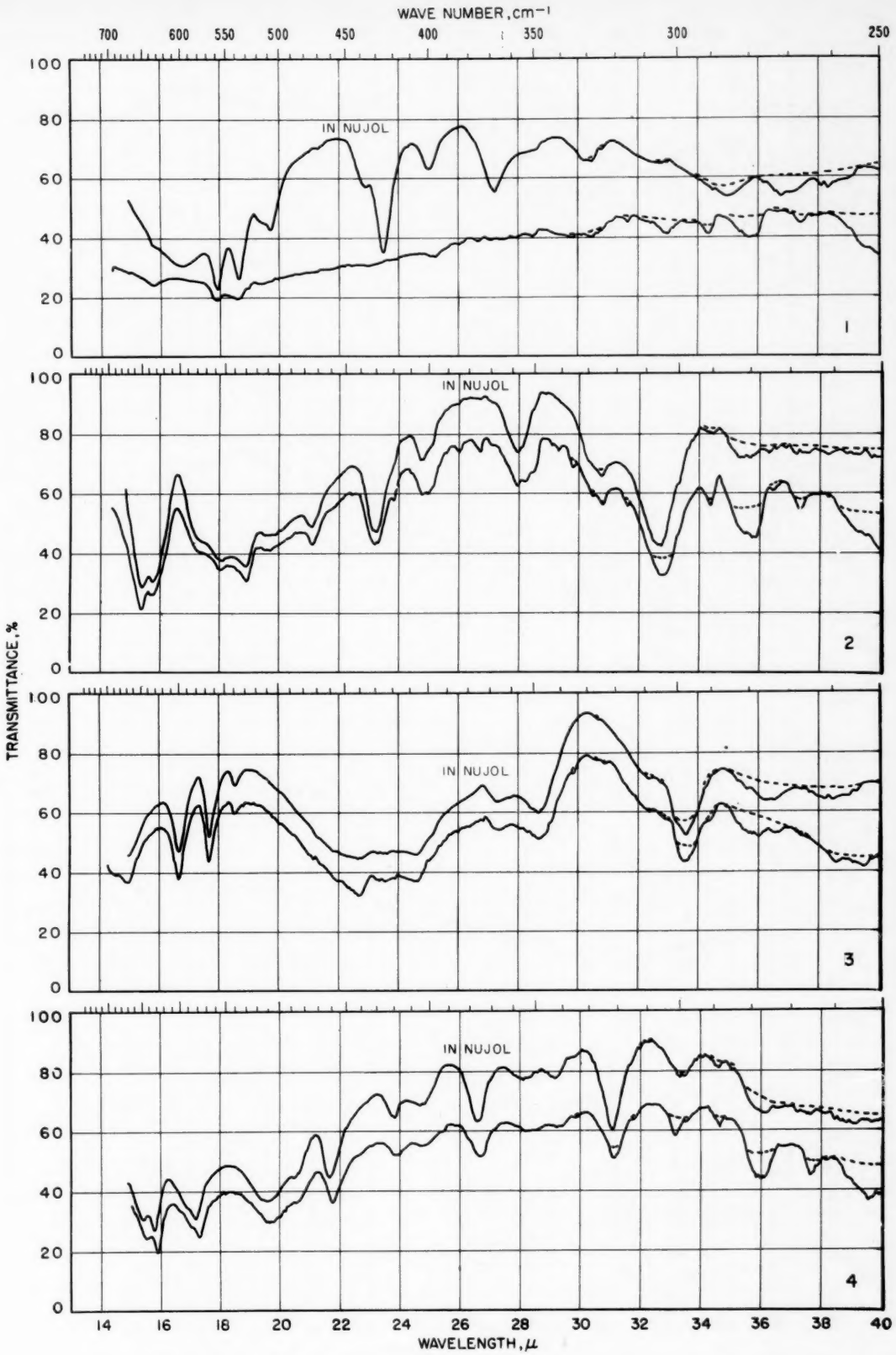

FIGURE 4. *Spectrograms of materials in Nujol mulls and in potassium iodide pellets.*

1, Methyl α-D-xylopyranoside; **2**, methyl β-D-xylopyranoside; **3**, methyl α-D-glucopyranoside; **4**, methyl β-D-glucopyranoside.

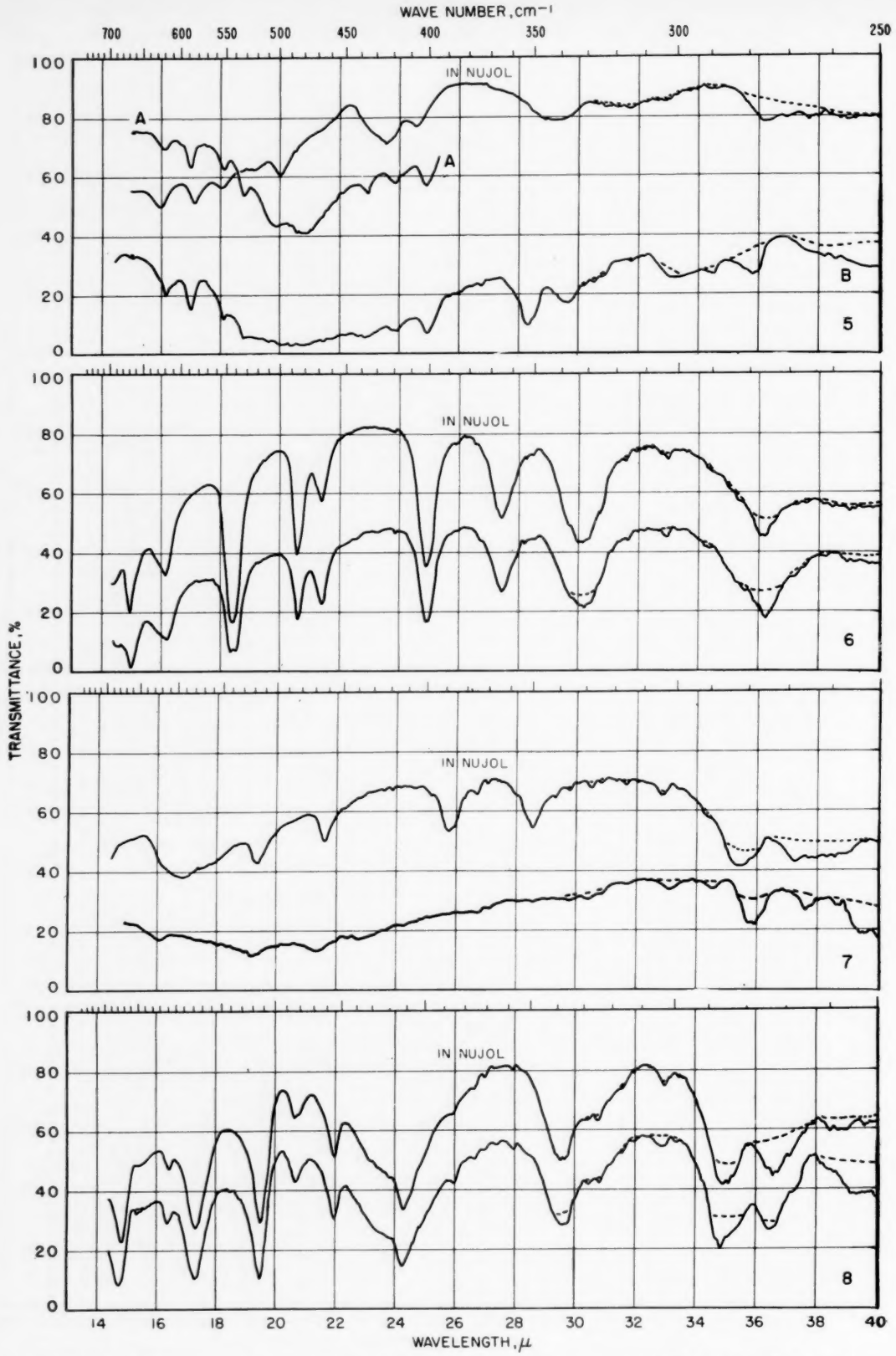

FIGURE 4. *Spectrograms of materials in Nujol mulls and in potassium iodide pellets.*—Continued

5, methyl D-*glycero*-α-L-*gluco*-heptopyranoside; **6**, methyl α-D-lyxopyranoside; **7**, methyl β-D-lyxopyranoside; **8**, methyl α-D-mannopyranoside.

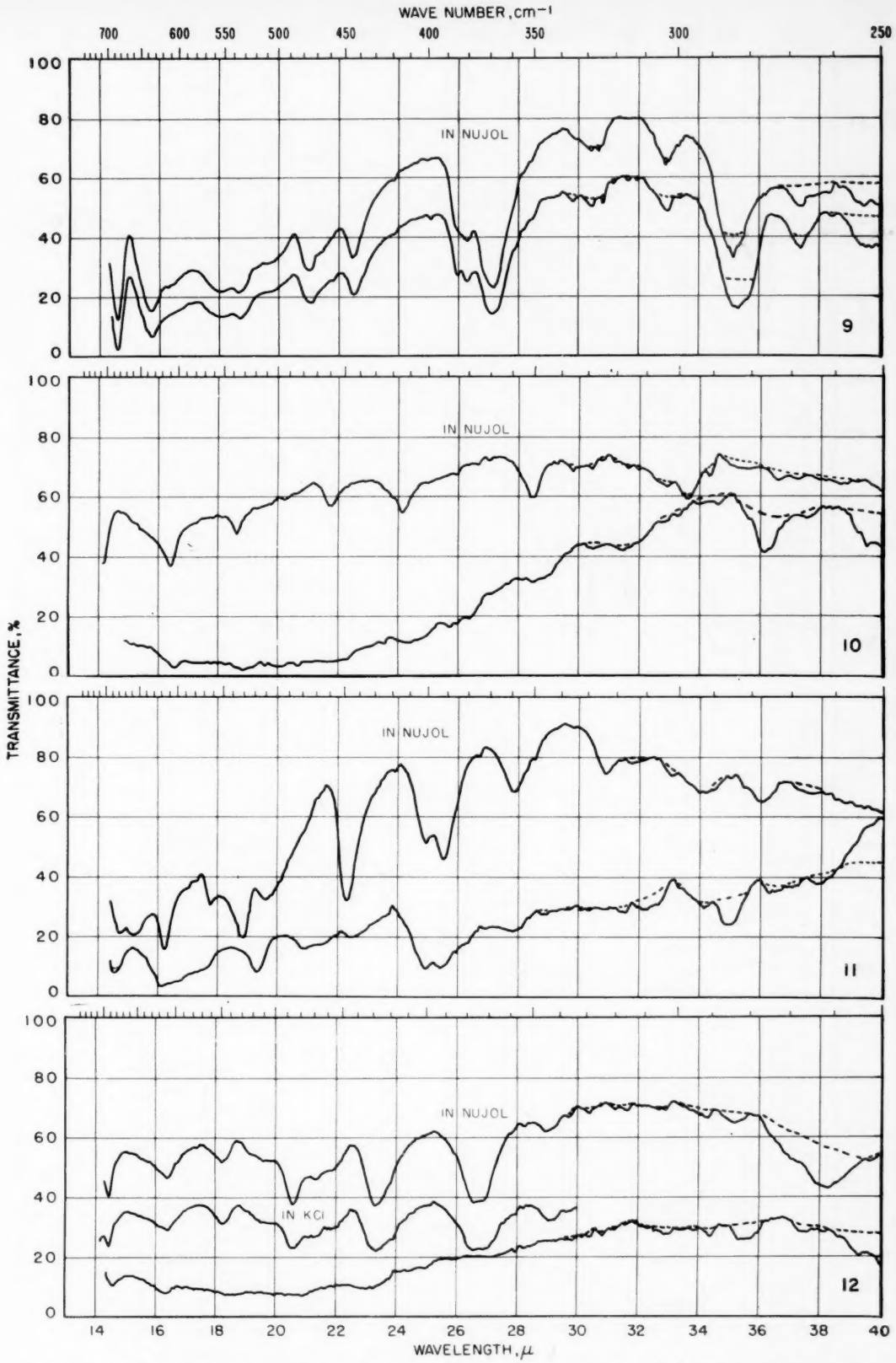

FIGURE 4. *Spectrograms of materials in Nujol mulls and in potassium iodide pellets.*—Continued

9, methyl 6-deoxy-α-L-mannopyranoside; **10,** methyl 6-deoxy-β-L-mannopyranoside; **11,** methyl D-*glycero*-α-L-*manno*-heptopyranoside; **12,** methyl α-D-gulopyranoside monohydrate.

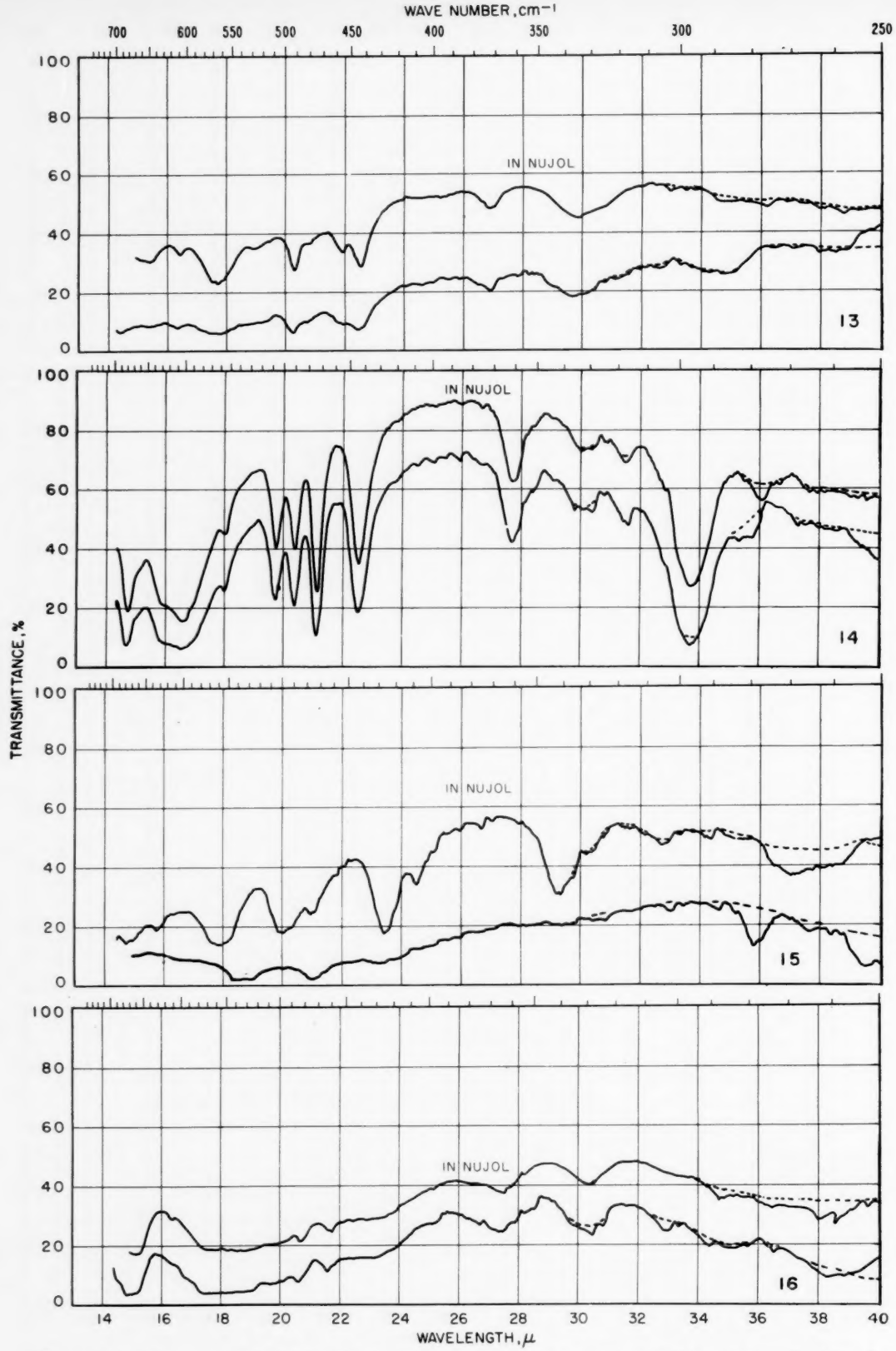

FIGURE 4. *Spectrograms of materials in Nujol mulls and in potassium iodide pellets.*—Continued

13, methyl α-D-gulopyranoside ·½($CaCl_2$·3H_2O); **14,** methyl β-D-gulopyranoside; **15,** methyl D-*glycero*-α-D-*gulo*-heptopyranoside; **16,** methyl D-*glycero*-α-D-*gulo*-heptopyranoside ·$CaCl_2$·H_2O.

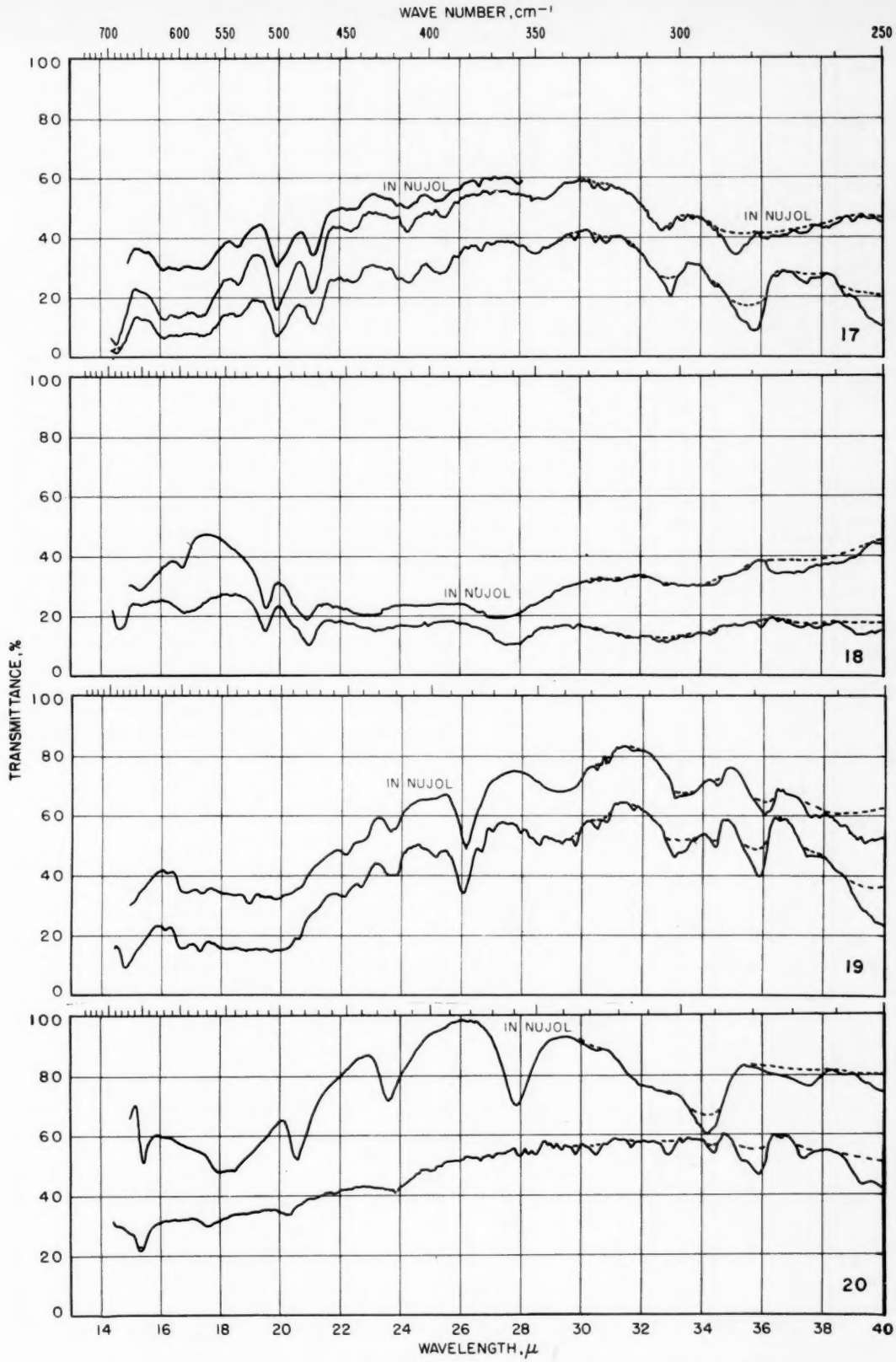

FIGURE 4. *Spectrograms of materials in Nujol mulls and in potassium iodide pellets.*—Continued

17, methyl D-*glycero*-β-D-*gulo*-heptopyranoside; **18,** methyl D-*glycero*-β-D-*gulo*-heptopyranoside ·½$CaCl_2$·H_2O; **19,** cyclohexyl D-*glycero*-β-D-*gulo*-heptopyranoside; **20,** methyl α-L-arabinopyranoside.

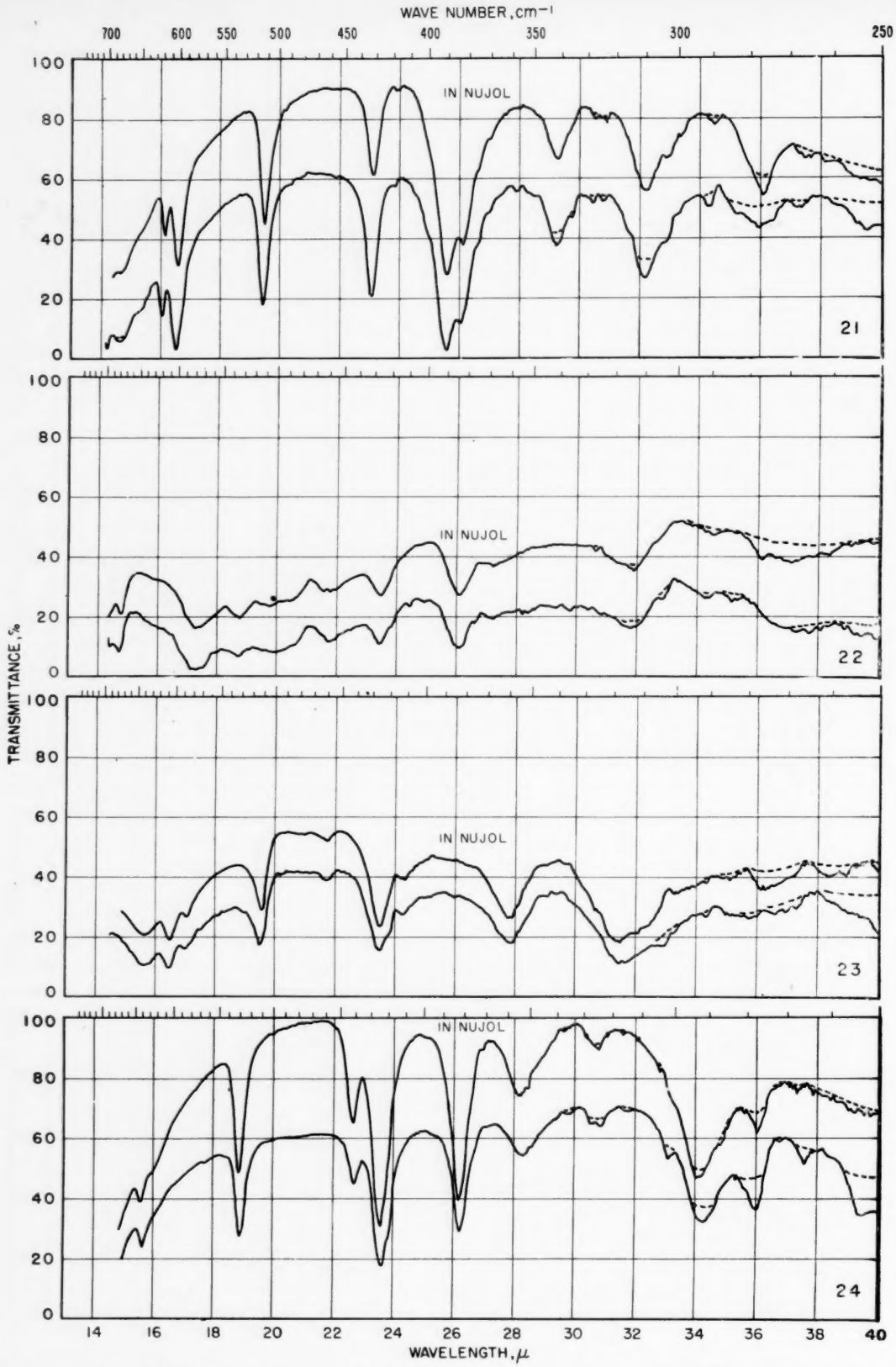

FIGURE 4. *Spectrograms of materials in Nujol mulls and in potassium iodide pellets.*—Continued

21, methyl β-L-arabinopyranoside; **22,** methyl α-D-galactopyranoside monohydrate; **23,** methyl β-D-galactopyranoside; **24,** methyl 6-deoxy-α-L-galactopyranoside.

Of these, compounds 12 and 15 are known to give a molecular complex with calcium chloride, affording compounds 13 and 16, respectively; both compound 13 and compound 16 give essentially the same spectrum in the two media. This observation might suggest a relationship between the ability to form a complex with calcium chloride and the behavior observed in potassium iodide. However, compound 17, which also forms a complex with calcium chloride (namely, compound 18), gives, like compound 18, essentially the same spectrum in the two media. A possible explanation is that some glycosides may react with both calcium chloride and potassium iodide, whereas others may react with only one of these salts.

It is not known whether compounds 1, 5, 7, 10, 11, and 20 form complexes with calcium chloride, nor whether any of the eight glycosides that give an unsatisfactory spectrum in potassium iodide do actually react chemically with this iodide.

In view of these observations, the spectra obtained with a Nujol mull were used exclusively for measuring the positions of absorption bands in the range of 667 to 250 cm^{-1}, not only for the eight glycosides that give unsatisfactory spectra in potassium iodide, but also (in order to keep the measurements strictly comparable) for the 16 other glycosides.

Finally, to make sure that compound 12 (typical of the glycosides "reacting" with both calcium chloride and potassium iodide) does not react with potassium chloride, the spectrum in the range of 667 to 333 cm^{-1} was recorded for a pellet of compound 12 in potassium chloride and compared with its spectrum in Nujol; the spectra matched well. Consequently, the spectra in potassium chloride in the range of 5000 to 667 cm^{-1} were accepted as being satisfactory.

The authors express their gratitude to Harriet L. Frush and J. D. Moyer for preparing and purifying many of the compounds used in this study; to Alex Cohen for technical assistance; and to J. E. Stewart, J. J. Comeford, and F. P. Czech for recording the infrared absorption spectra.

7. References

[1] H. S. Isbell and R. S. Tipson, Science **130,** 793 (1959).
[2] H. S. Isbell and R. S. Tipson, J. Research NBS **64A**, 171 (1960).
[3] H. S. Isbell, F. A. Smith, E. C. Creitz, H. L. Frush, J. D. Moyer, and J. E. Stewart, J. Research NBS **59,** 41 (1957) RP2772.
[4] R. S. Tipson, H. S. Isbell, and J. E. Stewart, J. Research NBS **62,** 257 (1959) RP2960.
[5] H. S. Isbell, J. Research NBS **57,** 171 (1956) RP2707.
[6] R. E. Reeves, J. Am. Chem. Soc. **71,** 215 (1949).
[7] R. E. Reeves, J. Am. Chem. Soc. **71,** 1737 (1949).
[8] R. E. Reeves, J. Am. Chem. Soc. **72,** 1499 (1950).
[9] R. E. Reeves, Ann. Rev. Biochem. **27,** 15 (1958).
[10] G. R. Barker and D. F. Shaw, J. Chem. Soc. **1959,** 584.
[11] L. P. Kuhn, Anal. Chem. **22,** 276 (1950).
[12] R. E. Reeves, Advances in Carbohydrate Chem. **6,** 107 (1951).
[13] H. B. Henbest, G. D. Meakins, B. Nicholls, and A. A. Wagland, J. Chem. Soc. **1957,** 1462.
[14] J. E. Page, J. Chem. Soc. **1955,** 2017.
[15] H. S. Isbell and H. L. Frush, J. Research NBS **24,** 125 (1940) RP1274.

WASHINGTON, D.C. (Paper 64A3-48)

Selected Abstracts

Measurement of cobalt-60 and cesium-137 gamma rays with a free-air chamber, H. O. Wyckoff, *J. Research NBS* **64C,** *No. 2, 87 (1960).*

Design data for free-air chambers measuring cobalt-60 and cesium-137 gamma rays in roentgens have been presented. It has been shown that the Jaffee-Zanstra method of obtaining the saturation current is adequate for air pressures of about 4 to 12 atmospheres. Also, radiation measurements of the gamma rays from cobalt-60 and cesium-137 made by a cavity chamber and a free-air chamber agree to within the experimental errors.

Radiation field from a rectangular source, J. H. Hubbell, R. L. Bach, and J. C. Lamkin, *J. Research NBS* **64C,** *No. 2, 121 (1960).*

Many radiation shielding problems involve calculations of the response of an isotropic detector to radiation of arbitrary angular distribution from uniform rectangular sources. In calculations of this type the family of integrals $\int_S(\cos\theta dS/r^2)P_l(\cos\theta)$ and the integral $\int_S(dS/r^2)\exp(-\mu t/\cos\theta)$ are frequently encountered, where θ is obliquity with respect to an axis perpendicular to the plane containing the rectangular radiant surface, S, r is the distance from an element of source area, dS, to the detector, μ is the attenuation coefficient, and t is the barrier thickness. The first type of integral facilitates use of Legendre expansion representations of radiation directional distributions, and may also have application in other radiant surface studies, such as illumination and heat exchange engineering. The second integral relates to unscattered gamma rays from a monoenergetic, plane isotropic, rectangular source separated from the detector by a layer of material of thickness t. Formulas, expansions, and numerical results are presented.

Response of a loaded electric dipole in an imperfectly conducting cylinder of finite length, C. W. Harrison, Jr., and R. W. P. King, *J. Research NBS* **64D,** *No. 3, 289 (1960).*

Analytical relationships are developed which permit calculation of the power of the load impedance of an electric probe, symmetrically located within an imperfectly conducting cylinder of small radius compared to the wavelength, in terms of the electric field incident upon the cylinder.

Basic theorems in matrix theory, M. Marcus, *NBS Applied Math. Series 57 (1960) 15 cents.*

This is a survey of the basic identities and inequalities of matrix theory. Included are results dealing with elementary properties, canonical forms, invariance, congruence, commutativity, orthogonalization, eigenvalues, determinants, submatrices, rank, determinant and rank inequalities, numerical methods for inversion and eigenvalues, condition numbers.

Paramagnetic resonance in the free hydroxyl radical, H. E. Radford, *Nuovo cimento, Serie X* **14,** *245 (1959).*

Paramagnetic resonance has been observed in electrically discharged water vapor. A calculation of the microwave Zeeman effect for the free OH radical allows a consistent interpretation of the spectrum as arising from electric dipole transitions within the low-lying rotational levels of OH. The spectrum permits accurate measurements of g-factors, Λ-doubling intervals, and hyperfine structure. Higher order effects of Λ-doubling on the Zeeman and hyperfine interactions are detectable. Corresponding OD spectra have been observed in discharged D_2O.

Relaxation processes in multistate systems, K. E. Shuler, *Phys. of Fluids* **2,** *No. 4, 442 (1959).*

An analysis is made of the relaxation of "multistate" systems, i.e., systems with more than two quantum states or two different chemical species, for linearized processes described by the "Master Equation" of the theory of transport processes. These results are compared with those obtained from the analysis of two-state relaxation processes and the concept of "relaxation time" is discussed in this framework. A discussion is presented of the transformation of microscopic to macroscopic relaxation equations. The existence of periodic and/or aperiodic oscillatory solution of the linear multistate relaxation equation is investigated. It is shown that the multistate relaxation equations admit of aperiodic oscillatory solutions.

Optical measurements on thin films of condensed gases at low temperatures, J. Kruger and W. J. Ambs, *J. Opt. Soc. Am.* **44,** *1195 (1959).*

A determination of the retractive indices of thin films of oxygen, nitrogen, carbon dioxide, water, argon, neon, and krypton condensed at 4.2°K using the 5461 A line of Hg was made with an ellipsometer. Similar measurements were also made on films of these gases condensed after passage through a microwave discharge. With the exception O_2, CO_2, and H_2O no measurable differences in refractive indices were observed between films condensed from discharged and undischarged gases.

Invariant and complete stress functions for general continua, C. Truesdell, *Arch. Rational Mech. Anal.* **1,** *No. 4, 1 (1959).*

This paper presents an organized survey of results, with proofs, concerning exact general solution of the underdetermined equations of motion of a continuous medium. Special attention is given to a flat space of n dimensions, to an n-dimensional space of constant curvature, and to a 2-dimensional surface. Two methods are used: (1) the representation of a solenoidal vector as the curl of a vector potential, and (2) a variational formulation, essentially the converse of the principle of virtual work.

Wavelength definition of the meter, I. C. Gardner, *Syst. of Units, Natl. and Intern. Aspects, Publ. Am. Assoc. Advance. Sci., No. 57, p. 53 (1959).*

The different applications of the national prototype meter to the calibration of line standards, of end standards, and of wavelengths are presented. The advantages of a wavelength standard are considered and the progress of international conferences for redefining the meter in terms of a wavelength standard is set forth. One may expect final and conclusive action at the Conference (General) of Weights and Measures in 1960. The advantages to be anticipated from the development of an atomic beam source are discussed.

Ethane carbon-carbon distance obtained from infrared spectra, H. C. Allen and E. K. Plyler, *J. Chem. Phys.* **31,** *No. 4, 1062 (1959).*

The parallel band of ethane at 2753 cm^{-1} and the parallel band of ethane-d_6 at 2816 cm^{-1} have been observed and analyzed. The resultant values of B for C_2H_6 and C_2D_6 are 0.6637 cm^{-1} and 0.4598 cm^{-1}, respectively. From these B values the C–C distance is found to be 1.534 A and the quantity

$(\gamma_{CC/2}+\gamma_{CH}\cos\theta)^2+\gamma_{CH/2}{}^2\sin^2\theta=1.866$ A where $\theta=180-\angle_{HCC}$.

If the γ_{CH} value of methane (1.093 A) is assumed, the $\angle_{HCC}$ is 109° 45′.

Young's modulus of various refractory materials as a function of temperature, J. B. Wachtman, Jr., and D. G. Lam, Jr., *J. Am. Ceram. Soc.* **42,** *No. 5, 254 (1959).*

Young's modulus as a function of temperature was determined by a dynamic method for single-crystal sapphire and ruby and for polycrystalline aluminum oxide, magnesium oxide, thorium oxide, mullite, spinel, stabilized zirconium oxide, silicon carbide, and nickel-bonded titanium carbide. For the single crystals, Young's modulus was found to decrease linearly with increasing temperature from 100° C. to the highest temperature of measurement. For all the polycrystalline materials, except silicon carbide, stabilized zirconium oxide, and spinel, Young's modulus was found to decrease approximately linearly with increasing temperature until some temperature range characteristic of the material was reached in which Young's modulus decreased very rapidly and in a nonlinear manner with increasing temperature. This rapid decrease at high temperature is attributed to grain-boundary slip. Stabilized zirconium oxide and spinel were found to have the same rapid decrease in Young's modulus at high temperature, but they also had a decidedly nonlinear temperature dependence at low temperature.

Branched-chain higher sugars. III. A 4-*C*-(hydroxymethyl)-pentose, R. Schaffer, *J. Am. Chem. Soc.* **81,** *5452 (1959).*

The applicability of a mixed aldol reaction for carbohydrate synthesis is demonstrated by the reaction of 5-aldo-1,2-*O*-isopropylidene-D-*xylo*-pentofuranose (I) with formaldehyde. 4-*C*-(Hydroxymethyl)-1,2-*O*-isopropylidene-L-*threo*-pentofuranose (II) is isolated in 75% yield, and probably results from reduction of the condensation product by a second molecule of formaldehyde through a crossed-Cannizzaro reaction. Hydrolysis of II gives the new branched-chain hexose. Oxidation of the sugar led to isolation of a crystalline calcium hexonate, and degradation of the latter yields previously unreported L-apiose. An alternative procedure involving I and formaldehyde, co-products of periodate oxidation of 1,2-*O*-isopropylidene-D-glucofuranose and used without intermediate crystallization of I, gives II in an overall yield of 58%.

Vibrational spectrum of cyanate ion in various alkali halide lattices, A. Maki and J. C. Decius, *J. Chem. Phys.* **31,** *No. 3, 772 (1959).*

The infrared absorption spectra of dilute solid solutions of cyanate ion in KI, KBr, KCl, and NaCl single crystals have been examined between 600 and 5000 cm^{-1} at temperatures ranging from 150° to 480° K. Over fifty distinct maxima have been observed and assigned (including numerous isotopic, combination, and hot bands) in the most concentrated sample, for which KBr was the solvent. A strong Fermi resonance between $2\omega_2$ and ω_1 occurs. The vibrational energy has been expressed in terms of the eleven fundamental frequency and anharmonicity constants appropriate to a linear, unsymmetric triatomic molecule. Force constants in the KI solvent lattice are $f_{NC}=15.51$, $f_{CO}=11.03$, $f^1=1.35$, and $(f_a/l_1l_2)=0.506$ mdyne/A, a result which shows very clearly that the NC bond is of higher order than the CO bond in the cyanate ion, and that the latter bond is notably weaker in cyanate ion than in CO_2, where its force constant is 16.0.

In general, the fundamental frequencies increase as the lattice constant decreases. Fairly detailed calculations show that although the induction energy term arising from the dipoles induced in the solvent by the vibrating cyanate ion is not negligible, the observed variation of frequency cannot be explained by the induction term alone and must involve the short-range, repulsive forces.

Use of crystal to display high energy X-ray images, J. S. Pruitt, *Non-Destructive Testing XVII, No. 6, 359 (1959).*

This paper describes an instrument composed of a large thallium activated sodium iodide crystal viewed by a television camera. An optical replica of the image produced by X-rays bombarding the crystal is displayed on a monitor. Evidence on the performance of this instrument, obtained both with radium γ-rays and 180 Mev X-rays, will be described. The image quality obtained with γ-rays is good enough for many radiographic purposes. At 180 Mev, where the quality is much poorer, the instrument has some value because of its ability to see gross detail continuously, even when looking through a thick absorber.

Thermodynamic properties of helium at low temperatures and high pressures, D. B. Mann and R. B. Stewart, *J. Heat Transfer* **81,** *323 (1959).*

The thermodynamic properties of helium have been compiled and correlated for a temperature range from 3.0 to 20° K for pressures to 100 atmospheres and for specific volumes from 5 to 800 liters per kilogram. The properties are presented on both the Temperature-Entropy and the Enthalpy-Entropy coordinate systems and include pressure, temperature, volume, entropy and enthalpy.

Absolute photometry of the aurora—I. The ionized molecular nitrogen emission and the oxygen green line in the dark atmosphere, M. H. Rees, *J. Atmospheric and Terrest. Phys.* **14,** *325 (1959).*

A low latitude aurora was measured photometrically. Three prominent emission features, λ3914 band of 1.N.G. N_2^+, λ5577 of *OI* and λ6300–6364 of *OI*, were isolated with narrow pass band filters and recorded continuously throughout the night in the meridian sweep. Absolute calibration was carried out, and corrections for the scattered light and atmospheric extinction were made.

The absolute emission intensity for λ3914 and λ5577 is given at a selected zenith distance. The ratio of instantaneous intensities $I(O)5577$ to $I(O)3914$ was found to be essentially constant over an intensity range of three powers of ten and to be independent of the type of auroral form.

The intensities and correlations obtained are consistent with the following excitation mechanisms. In the dark atmosphere the N_2^+ is excited from ionizing collisions of incoming particles with atmospheric N_2. It is concluded that the *OI* λ5577 line results from secondary electrons, arising from the primary ionization process above, colliding inelastically with oxygen atoms.

Absolute photometry of the aurora—II. Molecular nitrogen emission in the sunlit atmosphere, M. H. Rees, *J. Atmospheric and Terrest. Phys.* **14,** *338 (1959).*

The absolute emission intensity of a sunlit aurora was determined for the 1.N.G. λ3914 band of N_2^+ by subtracting the emission intensity originating in the dark atmosphere from

the total measured intensity. The method is based on the constancy of the ratio of emission intensity of the oxygen green line *OI* λ5577 to the λ3914 emission in the dark atmosphere. The ion density of N_2^+ is computed as a function of height from the emission rate per unit volume.

Atoms and free radicals by γ–irradiation at 4.2°K, L. A. Wall, D. W. Brown, and R. E. Florin, *J. Phys. Chem.* **63,** *1762 (1959).*

In nitrogen, hydrogen, and deuterium at 4.2°K radiolysis produces atoms which are immobilized. They were identified by electron spin resonance (e.s.r.). In irradiated methane both hydrogen atoms and methyl radicals were found in approximately equal amounts. Repeated irradiation of the same samples in all cases led to more efficient production of active species. Added oxygen (0.07%) reduced the nitrogen atom yield of the initial run. Yields were studied as a function of irradiation dose. The maximum nitrogen atom concentration attained in solid nitrogen was 0.06%, while in irradiated methane 0.15% of hydrogen atoms and 0.14% of methyl radicals were attained. Because of saturation of the e.s.r. spectra, the results with hydrogen and deuterium are low. High-energy radiation at low temperatures in general appears to be a useful and promising method for the production of stabilized free radicals or atoms.

Rotational transfer in the fluorescence spectrum of OH ($^2\Sigma^+$), T. Carrington, *J. Chem. Phys.* **31,** *No. 5, 1418 (1959).*

Fluorescence has been produced in OH molecules by absorption of the bismuth emission line 3067.7 A, which excites a single rotational level in the $^2\Sigma^+$ electronic state. The relative population of this level and of other levels populated from it by collisional transfer are determined by intensity measurements on the fluorescence spectrum. The total probability of collisions producing transfer of rotational quanta from the eleventh level corresponds to a cross section roughly twice the kinetic theory value.

A note on the scattering of electrons from atomic hydrogen, A. Temkin, *Phys. Rev.* **116,** *No. 2, 358 (1959).*

The distortion of atomic hydrogen by a slowly moving electron at a large distance from the center of the atom is examined. The problem is the initial phase of a previously described method for the calculation of electron scattering which takes this distortion into account. The initial (static) problem is solved analytically and extended to include higher order effects of the interaction of the electron with the atomic cloud. The construction of a wave function to describe scattering starting from the solution of the static problem is clarified. This yields as an incidental result a new approximation of the second order perturbation energy associated with the above distortion. A short discussion of the present experimental results for this scattering process is included.

Design of free-air ionization chambers for the soft X-ray region (20–100 kv), V. H. Ritz, *Radiology* **73,** *No. 6, 911 (1959).*

Design criteria for standard free-air ionization chambers have been experimentally determined for the soft X-ray region. A tungsten target X-ray tube with a 2 mm beryllium window has been operated at exciting potentials of 20 to 100 kvcp. Up to 4 mm of aluminum has been added to the inherent filtration of the tube.

The electric field distortion at the collecting electrode due to the proximity of the guard strip system has been studied as a function of the distance between the guard strips and the collecting electrode, the centerline to centerline distance between guard strips, and the thickness of the guard strips.

The radial distributions of the primary electron ionization and scattered photon induced ionization have been measured. Agreement with the work of Attix and DeLaVergne is good. Other correction factors of particular importance in the soft X-ray region are discussed. The data indicate that a measurement of the exposure dose in roentgens can be made with a probable limit of error of ±0.5% in this energy region.

Thermal conductivity of indium antimonide at low temperatures, E. V. Mielczarek and H. P. R. Frederikse, *Phys. Rev.* **115,** *888 (1959).*

Thermal conductivity measurements were made on a monocrystalline sample of indium antimonide from 10 to 50° K. Umklapp, isotope, and boundary scattering contributions to the thermal resistivity were calculated from theoretical expressions and then subtracted from the measured value of thermal resistivity. The subsequent deduction of impurity scattering gives a value for the number of point impurities which is compatible with that given by electrical measurements.

Model for vibrational relaxation of diatomic gases behind shock waves, R. Herman and R. J. Rubin, *Phys. of Fluids* **2,** *No. 5, 547 (1959).*

The problem of the vibrational relaxation of a system of harmonic oscillators is examined for the case in which the oscillators are in contact with a heat bath whose total heat capacity is finite and whose temperature therefore varies during the relaxation process. An analysis is carried out for processes in which the initial distribution of vibrational energy is a Boltzmann distribution. Application is made to the vibrational relaxation of a diatomic gas behind a shock wave.

The dissociation constant of CaOH± from 0° to 40° C, R. G. Bates, V. E. Bower, R. G. Canham, and J. E. Prue, *Trans. Faraday Soc.* **55,** *No. 444, 2062 (1959).*

An attempt has been made to derive the dissociation constant of the base CaOH at eight temperatures from 0° to 40° C from e.m.f. data for cells without liquid junction composed of hydrogen and silver + silver chloride electrodes. Nineteen of the 27 solutions studied contained calcium hydroxide and potassium chloride and the remainder contained calcium hydroxide and calcium chloride. The dissociation constant K_2 obtained from the experimental data is strongly influenced by the arbitrary choice of $\gamma Cl/\gamma OH$ necessary to evaluate the molality of hydroxide ion in the solutions. If the activity coefficients of these two ions are assumed to be equal at ionic strengths up to 0·08, K_2 is found to be 0·071 mole kg^{-1} at 25° C; if $\log(\gamma Cl/\gamma OH) = -0{\cdot}31$ is assumed, a value of 0·054 mole kg^{-1} is obtained. Similar uncertainties are inherent in earlier determinations of this constant by solubility, e.m.f., and kinetic methods.

Other NBS Publications

Journal of Research, Section 64C, No. 2, April–June 1960. 75 cents.

Measurement of cobalt-60 and cesium-137 gamma rays with a free-air chamber. H. O. Wyckoff. (See above abstracts.)

Apparatus for the measurement of the normal spectral emissivity in the infrared. Arthur G. Maki, Ralph Stair, and Russell G. Johnston.

Electrostatic deflection plates for cathode-ray tubes. I. Design of single-bend deflection plates with parallel entrance sections. II. Deflection defocusing distortion of single-bend deflection plates with parallel entrance sections. Lothar Frenkel.

The functional synthesis of linear plots. J. P. Vinti and R. F. Dressler.

Radiation field from a rectangular source. J. H. Hubbell, R. L. Bach, and J. C. Lamkin. (See above abstracts.)

Microwave attenuation measurements with accuracies from 0.0001 to 0.06 decibel over a range of 0.01 to 50 decibels. G. F. Engen and R. W. Beatty.

Effect of oleophobic films on metal fatigue. H. E. Frankel, J. A. Bennett, and W. L. Holshouser.

Ratio-recording spectroradiometer. Harry K. Hammond III, Warren L. Holford, and Milton L. Kuder.

An intermittent-action camera with absolute time calibration. G. Hefley, R. H. Doherty, and E. L. Berger.

Journal of Research, Section 64D, No. 3, May–June 1960. 70 cents.

A theory of radar scattering by the moon. T. B. A. Senior and K. M. Siegel.

A theory of wavelength dependence in ultrahigh frequency transhorizon propagation based on meteorological considerations. Ralph Bolgiano, Jr.

A preliminary study of radiometeorological effects on beyond-horizon propagation. F. Ikegami.

Trade-wind inversion as a transoceanic duct. M. Katzin, H. Pezzner, B. Y.-C. Koo, J. V. Larson, and J. C. Katzin.

An analysis of propagation measurements made at 418 megacycles per second well beyond the radio horizon (a digest). H. B. Janes, J. C. Stroud, and M. T. Decker.

On the calculation of the departures of radio wave bending from normal. B. R. Bean and E. J. Dutton.

On the mode theory of very-low-frequency propagation in the presence of a transverse magnetic field. D. D. Crombie.

On the theory of reflection of low- and very-low-radiofrequency waves from the ionosphere. J. Ralph Johler and Lillie C. Walters.

Focusing, defocusing, and refraction in a circularly stratified atmosphere. K. Toman.

Response of a loaded electric dipole in an imperfectly conducting cylinder of finite length. Charles W. Harrison, Jr., and Ronold W. P. King. (See above abstracts.)

Impedance characteristics of a uniform current loop having a spherical core. Saburo Adachi.

Specification for dry cells and batteries (supersedes Circ. 559). NBS Handb. 71, (1959) 25 cents.

Report of the 44th National Conference on Weights and Measures 1959. NBS Misc. Publ. 228, (1959) 65 cents.

Research Highlights of the National Bureau of Standards Annual Report, Fiscal Year 1959. NBS Misc. Publ. 229 (1959) 55 cents.

An atlas of oblique-incidence ionograms, V. Agy, K. Davies, and R. Salaman, NBS Tech. Note 31 (PB151390) (1959) $2.25.

Service area of an airborne television station, M. T. Decker, NBS Tech. Note 35 (PB151394) (1959) 75 cents.

The following are published in Proc. Intern. Rubber Conf., Nov. 8 to 13, 1959 (Washington, D.C., 1959):

Power loss and operating temperature of tires, R. D. Stiehler, M. N. Steel, G. G. Richey, J. Mandel, and R. H. Hobbs, p. 73.

An indoor tester for measuring tire tread wear, G. G. Richey, J. Mandel, and R. D. Stiehler, p. 104.

Measurement of the aging of rubber vulcanizates, J. Mandel, F. L. Roth, M. N. Steel, and R. D. Stiehler, p. 221.

Standard materials for rubber compounding, F. L. Roth and R. D. Stiehler, p. 232.

On the convergence of Gauss' alternating procedure in the method of least squares, A. M. Ostrowski, Ann. Mat. Pura Appl. (IV) (Bologna, Italy) **48,** 229 (1959).

The anomalous inversion in cristobalite, R. F. Walker, The kinetics of high temperature processes, 228 pages (J. Wiley & Sons, New York, N.Y., 1959).

Digital recording of electrocardiographic data for analysis by a digital computer, L. Taback, E. Marden, H. L. Mason, and H. V. Pipberger, IRE Trans. Med. Electron. **ME–6,** 167 (1959).

Determination of starch in paper. A Comparison of the TAPPI enzymatic, and spectrophotometric methods, J. L. Harvey, B. W. Forshee, and D. G. Fletcher, Tappi **42,** No. 11, 878 (1959).

Glass research at the National Bureau of Standards, C. H. Hahner, Glass Ind., p. 588 (1959).

Applications of the molecular refractivity in radio metrology, B. R. Bean and R. M. Gallet, J. Geophys. Research **64,** No. 10, 1439 (1959).

The measuring process, J. Mandel, Technometrics **1,** No. 3, 251 (1959).

Fire research at the National Bureau of Standards, A. F. Robertson, Fire Research Abstr. Rev. **I,** No. 4, 159 (1959).

Refractive indices and transmittances of several optical glasses in the infrared, G. W. Cleek, J. J. Villa, and C. H. Hahner, J. Opt. Soc. Am. **49,** No. 11, 1090 (1959).

Preliminary assessment of the IGY, A. H. Shapley, Proc. Natl. Electron. Conf., p. 1 (1958).

Factorial experiments i life testing, M. Zelen, Technometrics **1,** No. 3, 269 (1959).

Direction findings on whistlers, J. M. Watts, J. Geophys. Research **64,** No. 11, 2029 (1959).

The construction of Hadamard matrices, E. C. Dade and K. Goldberg, Mich. Math. J. **6,** 247 (1959).

Geomagnetic and ionospheric phenomena associated with nuclear explosions, S. Matsushita, Nature **184,** BA33 (1959.)

Stress corrosion cracking in low carbon steel, H. L. Logan, Proc. Phys. Met. Stress Corrosion Fracture Conf., Pittsburgh, Pa., Apr. 2–3, 1959, reprinted from Met. Soc. Conf., p. 295 (Interscience Publishers, New York, N.Y., 1959).

Higher oxides of silver, H. E. Swanson, J. Electrochem. Soc. **106,** No. 12, 1073 (1959).

Oscillatory behavior of magnetic susceptibility and electronic conductivity, A. H. Kahn and H. P. R. Frederikse, vol. IX, Adv. Solid State Phys., p. 257 (Academic Press Inc., New York, N.Y., 1959).

Geomagnetic activity following large solar flares, C. S. Warwick and R. T. Hansen, J. Atmospheric and Terrest. Phys. **14,** 287 (1959).

Bending and stretching of corrugated diaphragms, R. F. Dressler, ASME Trans. **81D,** No. 4, 651 (1959).

Simplification of systems of units currently evolving in the electrical field, F. B. Silsbee, Systems of Units, Am. Assoc. for Advance. Sci., p. 7 (1959).

Determination of viscosity, J. F. Swindells, ch. XII, Phys. Methods of Organic Chem., pt. I, p. 689 (Interscience Publishers Inc., New York, N.Y., 1959).

Triaxial tension at the head of a rapidly running crack in a plate, J. M. Frankland, Trans. ASME [E] **26,** No. 4, 570 (1959).

Poly(tetrafluoroethylene)—a radiation-resistant polymer, L. A. Wall and R. E. Florin, letter to ed., J. Appl. Polymer Sci. **II,** No. 5, 251 (1959).

On the approximate daytime constancy of the absorption of radio waves in the lower ionosphere, S. Chapman and K. Davies, J. Atmospheric and Terrest. Phys. **13,** No. 1–2, 86 (1958).

An X-ray crystallographic study of Schroeckingerite and its dehydration product, D. K. Smith, Am. Mineralogist **44,** 1020 (1959).

Modular forms whose coefficients possess multiplicative properties, M. Newman, Ann. Math. **70,** 478 (1959).

The analysis of latin squares with a certain type of row-column interaction, J. Mandel, Technometrics **1,** No. 4, 379 (1959).

A note on algebras, A. J. Goldman, Am. Math. Mo. **66,** 795 (1959).

Transistor P–A amplifier, G. F. Montgomery and F. R. Bretemps, Electronic Ind. **19,** No. 1, 196 (1960).

Linear differential equations of the second order with a large parameter, F. W. J. Olver, J. Soc. Indust. Appl. Math. **7,** 306 (1959).

Sorting devices in postal tests. 1: Proposal for an electromagnetic sorter, S. Henig, Automatic Control **11,** No. 6, 6 (1959).

Evaluation of chemical analyses on two rocks, W. J. Youden, Technometrics **1,** No. 4, 409 (1959).

Nuclear electronics, L. Costrell, Nucleonics Mag. **18,** No. 1, 124 (1960).

Microscopical studies of failure in polymers, S. B. Newman, ASTM Spec. Tech. Pub. 257, 132 (1959).

Flare-associated bursts at 18 Mc/s, C. Warwick and J. W. Warwick, Paris Symp. on Radio Astron., p. 203 (IAU Symp. No. 9 and URSI Symp. No. 1, 1959).

**Publications for which a price is indicated (except for NBS Technical Notes) are available only from the Superintendent of Documents, U.S. Government Printing Office, Washington 25, D.C. (foreign postage, one-fourth additional). Technical Notes are available only from the Office of Technical Services, U.S. Department of Commerce, Washington 25, D.C. (order by PB number). Reprints from outside journals and the NBS Journal of Research may often be obtained directly from the author.*

UNITED STATES
GOVERNMENT PRINTING OFFICE
DIVISION OF PUBLIC DOCUMENTS
WASHINGTON 25, D.C.

OFFICIAL BUSINESS

PENALTY FOR PRIVATE USE TO AVOID
PAYMENT OF POSTAGE, $300
(GPO)

JOURNAL OF RESEARCH of the National Bureau of Standards
A. Physics and Chemistry

Vol. 64A, No. 3

May–June 1960

Contents

Page

Phase shift effects in Fabry-Perot interferometry. Charles J. Koester. 191

Infrared absorption spectrum of methane from 2470 to 3200 cm^{-1}. Earle K. Plyler, Eugene D. Tidwell, and Lamdin R. Blaine. 201

Elastic constants of synthetic single crystal corundum at room temperature. J. B. Wachtman, Jr., W. E. Tefft, D. G. Lam, Jr., and R. P. Stinchfield. 213

Radial distribution study of vitreous barium borate. Arthur Bienenstock, Aaron S. Posner, and Stanley Block. 229

Separation and determination of small quantities of aluminum in steel. Bruce B. Bendigo and Rosemond K. Bell. 235

Conformations of the pyranoid sugars. II. Infrared absorption spectra of some aldopyranosides. R. Stuart Tipson and Horace S. Isbell. 239

Publications of the National Bureau of Standards. 265

For sale by the Superintendent of Documents, U.S. Government Printing Office, Washington 25, D.C. Price 70 cents (single copy). Subscription price: $4.00 a year; $0.75 additional for foreign mailing.

UNITED STATES GOVERNMENT PRINTING OFFICE, WASHINGTON : 1960